IN THIS ISSUE

London Journals Press

IMAGE: OBSERVATORY WITH STAR TRAILS ON MOUNTAINS FOR CLEAR SKY

www.journalspress.com

LONDON JOURNAL OF RESEARCH IN SCIENCE: NATURAL AND FORMAL

Print ISSN: 2631-8490
Online ISSN: 2631-8504
DOI: 10.17472/LJRS

Volume 21 | Issue 2 | Compilation 1.0

COMPILED IN UNITED KINGDOM

ENGLISH

London Journal of Research in Science: Natural and Formal

Volume 21 | Issue 2 | Compilation 1.0

PUBLISHER

London Journals Press
1210th, Waterside Dr,Opposite Arlington Building, Theale, Reading
Phone:+444 0118 965 4033 Pin: RG7-4TY United Kingdom

SUBSCRIPTION

Frequency: Quarterly

Print subscription
$280USD for 1 year
$500USD for 2 year
(color copies including taxes and international shipping with TSA approved)

Find more details at https://journalspress.com/journals/subscription

ENVIRONMENT

London Journals Press is intended about protecting the environment. This journal is printed using led free environmental friendly ink and acid-free papers that are 100% recyclable.

London Journals Press Headquaters

1210th, Waterside Dr,
Opposite Arlington
Building, Theale, Reading
Phone:+444 0118 965 4033
Pin: RG7-4TY
United Kingdom

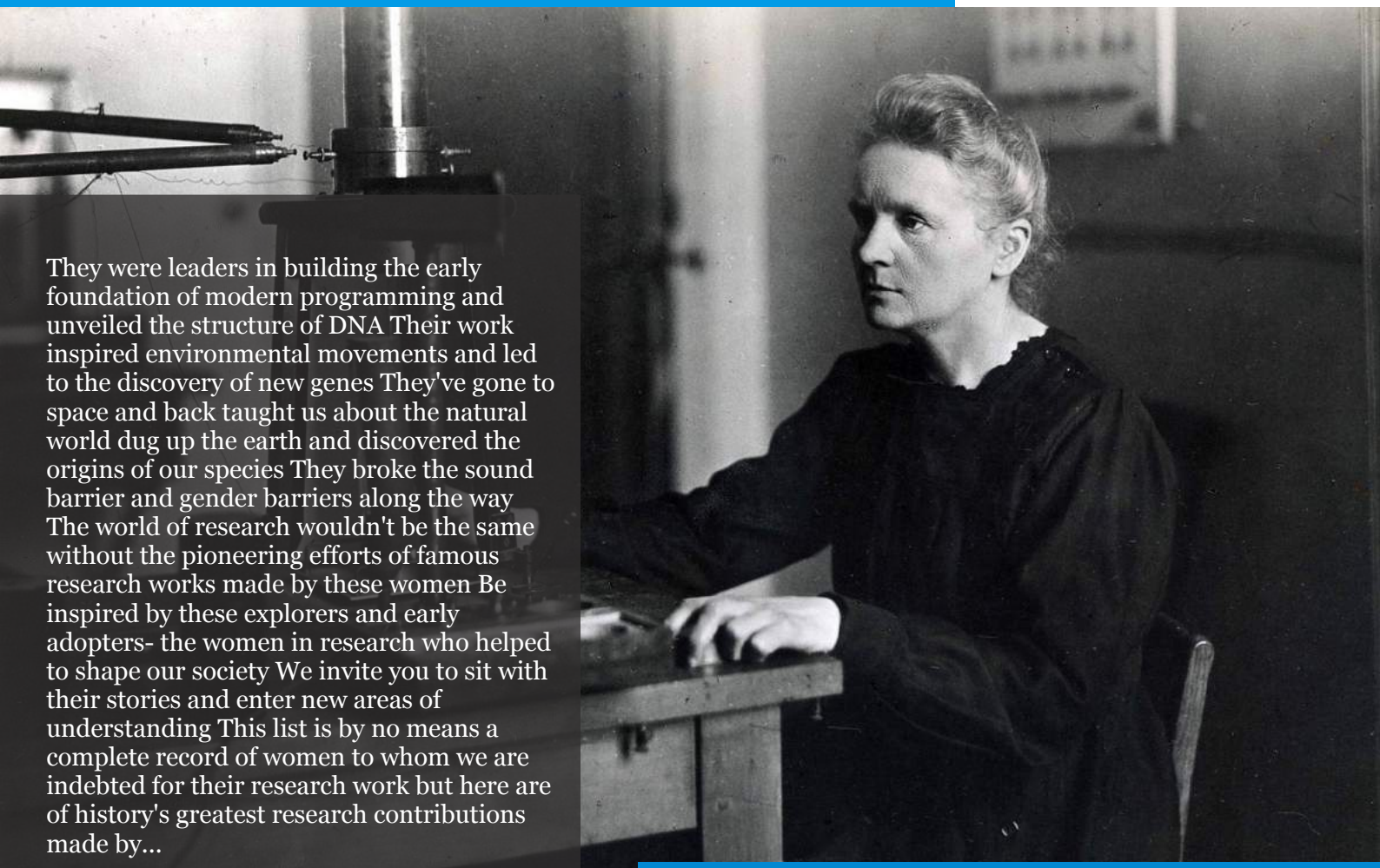

They were leaders in building the early foundation of modern programming and unveiled the structure of DNA Their work inspired environmental movements and led to the discovery of new genes They've gone to space and back taught us about the natural world dug up the earth and discovered the origins of our species They broke the sound barrier and gender barriers along the way The world of research wouldn't be the same without the pioneering efforts of famous research works made by these women Be inspired by these explorers and early adopters- the women in research who helped to shape our society We invite you to sit with their stories and enter new areas of understanding This list is by no means a complete record of women to whom we are indebted for their research work but here are of history's greatest research contributions made by...

Read complete here:
https://goo.gl/1vQ3lS

Women In Research

Computing in the cloud!

Cloud Computing is computing as a Service and not just as a Product Under Cloud Computing...

Read complete here:
https://goo.gl/VvHC72

Writing great research...

Prepare yourself before you start Before you start writing your paper or you start reading other...

Read complete here:
https://goo.gl/np73jP

Journal Content
In this Issue

London Journals Press

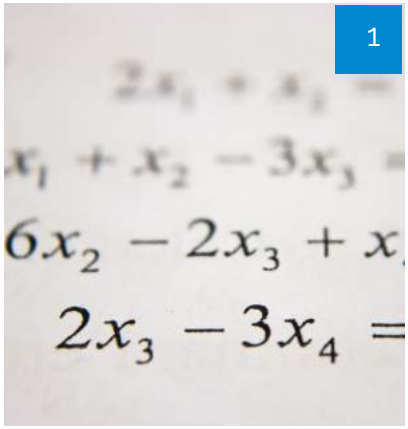

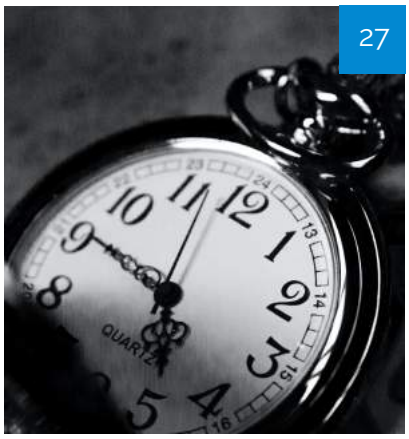

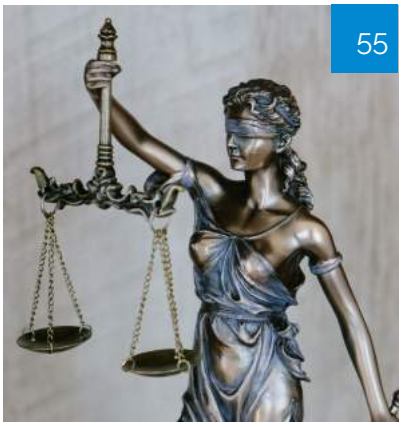

Editorial Board

Curated board members

The Problems Existing in the Complex Continuations of the Gama Function and the Euler Formula of Prime Numbers

Mei Xiaochun

ABSTRACT

The real Gama Function $\Gamma(a)$ is defined in the field of real number with $a>0$. It is infinite and meaningless in the field with $a<0$. However, according to the continuation theory of function at present, except at the points $a=0,\ -1,\ -2,\ -3,\cdots$, $\Gamma(a)$ can be extended to the field of negative number with $a<0$. It is pointed out that this continuation leads to infinite and is meaningless. The reason is that the form of Gama function has no any change in the extended field, so that contradiction is caused. It is proved that the single complex continuation of Gama function does not satisfy the Cauchy-Riemann equation, so it is not an analytic function. But the double complex continuation of the Gama function satisfies the Cauchy-Riemann equation and is an analytic function. Also, it is proved that the complex continuation of the complementary formula of the Gama function is incorrect. The correct result is calculated in the paper. The influences of these results on the Riemann Zeta function equation and the Riemann hypotheses are discussed.

Keywords: gama function, negative continuation of function, complex continuation of gama function, analytic function, residue theorem, euler formula of prime number, riemann hypothesis, riemann zeta function equation, cauchy-riemann equation.

Classification: FOR CODE: 010599

Language: English

London Journals Press

LJP Copyright ID: 925652
Print ISSN: 2631-8490
Online ISSN: 2631-8504

London Journal of Research in Science: Natural and Formal

Volume 21 | Issue 2 | Compilation 1.0

The Problems Existing in the Complex Continuations of the Gama Function and the Euler Formula of Prime Numbers

Mei Xiaochun

ABSTRACT

The real Gama Function $\Gamma(a)$ *is defined in the field of real number with* $a>0$. *It is infinite and meaningless in the field with* $a<0$. *However, according to the continuation theory of function at present, except at the points* $a=0,\ -1,\ -2,\ -3,\cdots$, $\Gamma(a)$ *can be extended to the field of negative number with* $a<0$. *It is pointed out that this continuation leads to infinite and is meaningless. The reason is that the form of Gama function has no any change in the extended field, so that contradiction is caused. It is proved that the single complex continuation of Gama function does not satisfy the Cauchy-Riemann equation, so it is not an analytic function. But the double complex continuation of the Gama function satisfies the Cauchy-Riemann equation and is an analytic function. Also, it is proved that the complex continuation of the complementary formula of the Gama function is incorrect. The correct result is calculated in the paper. The influences of these results on the Riemann Zeta function equation and the Riemann hypotheses are discussed. According to the correct formula, the zeros of Zeta function equation are located on the points* $a=\pm 1/2,\ \pm 3/2,\ \pm 5/2\cdots$, *so the Riemann hypothesis does not hold. The complex continuation of the Euler formula of prime numbers is also discussed. It is proved that the real part of the complex continuation formula is different from the original Euler formula of prime numbers. Because the trigonometric functions are contained in it, which my be irrational numbers, the extended formula does not describe the relation between natural numbers and prime numbers again. Therefore, the complex continuation of the Euler formula of prime numbers is meaningless in number theory. We can not discuss the distribution of prime numbers based on it.*

Keywords: gama function, negative continuation of function, complex continuation of gama function, analytic function, residue theorem, euler formula of prime number, riemann hypothesis, riemann zeta function equation, cauchy-riemann equation.

Author: Department of Theoretical Physics and Pure Mathematics, Institute of Innovative Physics in Fuzhou, Fuzhou, China.

I. INTRODUCTION

It was revealed in the author's first paper [1] that there were several serious mistakes in the Riemann's original paper to deduce the Zeta function equation in 1859.

1. An integral item around the original point of the coordinate system was ignored when Riemann deduced the integral form of the Riemann Zeta function. This item is convergent when $\mathrm{Re}(s)>1$ but divergent when $\mathrm{Re}(s)<1$. The integral form of the Zeta function has not changed the divergence of its series form.

London Journal of Research in Science: Natural and Formal

2. A summation formula was used in the deduction of the integral form of the Zeta function. The applicable condition of this formula is $x>0$. At point $x=0$, the formula is meaningless. However, the lower limit of the Zeta function's integral is $x=0$, so the formula can not be used.
3. The formula $\theta(x)=\sqrt{x}\theta(1/x)$ of Jacobi function was used to prove the symmetry of the Zeta function equation. The applicable condition of this formula is also $x>0$. Because the lower limit of the integral is $x=0$, this formula can not be used too.
4. Due to these mistakes, the inconsistency is caused on the two sides of the Zeta function equation. On the real axis of complex plane, the function equation holds only at point $\mathrm{Re}(s)=1/2$ $(s=a+ib)$. However, at this point, the Zeta function is infinite, rather than zero. At other points of the real axis with $a\neq 0$ and $b=0$, the two sides of the Zeta function equation are contradictory. When one side is finite, another side may be infinite.

Therefore, the Riemann Zeta function equation does not hold, and the Riemann hypothesis is meaningless. This is the fundamental reason why the Riemann hypothesis has not been proved for so many years. At present, the zero calculations of the Zeta function are approximate due to the series with different orders are used. The analytic property of the Zeta function is destroyed so that the so-called zeros are not real ones.

In the author's second paper [2], the Zeta function equation is assumed to be correct, a simple and strict method is proposed to prove that the Riemann Zeta function equation has no trivial zero. The method is to divide the real part and the imaginary part of the Zeta function equation completely. By comparing the real part and the imaginary part individually, an equation set about a and b is obtained.

It is proved that the only solution of this equation set is $a=\pm 2n$ and $b=0$. So $a=1/2$ is not the non-trivial zero of the Zeta function equation. If $a\neq\pm 2n$, four equations are obtained. It is proved that these four equations are not independent of each other. To make them independent, the only way is to let $a=1/2$ and $b=0$. However, in this case, we have $\zeta(1/2,\ 0)\to\infty$, rather than zero. Finally, the comparing method of infinite series is used to prove that the Zeta function itself has no zero. Therefore, the Riemann hypothesis does not hold.

Because the Riemann Zeta function equation is based on the Gama function, the negative and complex continuations of the Gama function are discussed in this paper. To do it, we need to define the continuation of a function clearly at first. Assume that the function $f_1(x)$ has a clear definition in the field L_1 but it is meaningless in the field L_2. To make it meaningful in the field L_2, the function should be extended into $f_2(x)$. The analytic continuation of a function should satisfy the following conditions.

1. After the continuation, the form of the function $f_2(x)$ in the field L_2 should have something different from the function $f_1(x)$. Otherwise, the contradiction would be caused, and the continuation became meaningless.
2. In the original field L_1, the form of function $f_2(x)$ must be completely the same as the form of function $f_1(x)$, otherwise $f_2(x)$ can not be regarded as the continuation of $f_1(x)$.
3. Just for the sake of uniqueness, the continuation of function $f_1(x)$ must be analytic, or the derivative of function $f_2(x)$ exists everywhere. If it is a complex continuation, the Cauchy-Riemann equation must be satisfied.

The Gama function is a very important function with wide applications in pure mathematics and practical problems. Some people think that its importance is only next to the trigonometric function and the exponential function.

For example, based on the Gama function, the integral form of the Riemann Zeta function is introduced. It is the basis of Riemann hypothesis problem. It is proved in this paper that the negative continuation of the Gama function does not satisfy the condition 1 and leads to infinite. The single complex continuation of the Gama function does not satisfy the condition 3, so it is not an analytic function. But the double complex continuation of the Gama function satisfies all three conditions, so it is an analytic continuation.

It is proved that the present complex continuation $\Gamma(s)\Gamma(1-s)=\pi/\sin s\pi$ of the Gama function complementary formula is wrong. It is the result directly let $a\to s$ in $\Gamma(a)\Gamma(1-a)=\pi/\sin a\pi$. The correct calculation result is

$$\Gamma(s)\Gamma(1-s)=\frac{\pi e^{b\pi}}{\sin a\pi} \tag{1}$$

The result is a real number, rather than a complex number. The influences of these results on the Riemann Zeta function equation and Riemann hypotheses are discussed in this paper. It is proved that after Eq.(1) is used, the zeros of the Zeta function equation are located on the points $a=\pm 1/2,\ \pm 3/2,\ \pm 5/2\cdots$, the Riemann hypothesis is proved invalid from another angle.

The complex continuation of the Euler formula of prime numbers is discussed in this paper. It is proved that after the Euler formula of prime numbers is extended into the complex number field, the real part of the formula is different from the original Euler formula of prime numbers. Because it contains the trigonometric functions $\sin(b\ln p_j)$ and $\cos(b\ln p_j)$ which may be irrational numbers, the extended formula does not describe the relation between natural numbers and prime numbers again. Therefore, the complex continuation of the Euler prime number formula is meaningless in number theory. We can not discuss the distribution of prime numbers based on it.

II. THE CONTINUATIONS OF GENERAL FUNCTIONS

2.1 The analytic continuations of real functions

As we knew that a function has its definition field in general. Out of the field, the function may be meaningless. In order to make the function meaningful in the greater field, the continuation is needed. The common example of a real function's continuation is

$$f_1(x)=1+x+x^2+x^3+\cdots \qquad |x|<1 \tag{2}$$

Where $x\in R$ is a real number. Eq. (1) is meaningful and limited in the field $|x|<1$. when $|x|>1$, the function $f_1(x)\to\infty$ and becomes meaningless. On the other hand, we define

$$_*f_2(x)=\frac{1}{1-x} \qquad x\neq 1 \tag{3}$$

London Journal of Research in Science: Natural and Formal

$f_2(x)$ is meaningful on the whole number axis except at the point $x=1$. At all points of the field with $|x|<1$, we always have $f_1(x)=f_2(x)$. By developing $f_2(x)$ into the Taiwan's series when $|x|<1$, we can prove $f_1(x)=f_2(x)$ completely.

However, when $|x|>1$, Eqs. (2) and (3) can not be equal each other. For example, let $x=2$, we have $f_1(2)\to\infty$ and $f_2(2)=-1$. Because the definition field of $f_2(x)$ is greater than that of $f_1(x)$, we consider $f_2(x)$ as the continuation of $f_1(x)$ in the field with $|x|>1$ and write two functions in the unified form as below

$$f(x)=\begin{cases}1+x+x^2+x^3+\cdots & |x|<1\\ \dfrac{1}{1-x} & |x|\neq 1\end{cases} \tag{4}$$

In general, a function can be extended in many different ways, resulting in different results. In order to ensure the uniqueness, the continuation of function needs to meet the continuity condition, so that the function can be differentiated everywhere. The continuation that meets this condition is called as the analytic continuation [3].

It is important to emphasize that at every point in the small field where the original function is meaningful, the value of the extended function should be exactly the same as the value of original function, otherwise it is not the continuation of the original function. Meanwhile, in the extended field, the form of the extended function must be different from the original function, otherwise the extension of the function is meaningless [3].

For example, for Eqs. (2) and (3), in the field $|x|<1$ where the original function makes sense, the values of function $f_2(x)$ and $f_1(x)$ must be the same at every point. Although their forms look different on the surface, they are the same actually. In the field $|x|>1$ after the continuation, the forms of $f_2(x)$ and $f_1(x)$ must be different. Otherwise $f_2(x)$ is still equal to $f_1(x)$, which is no meaning.

It is difficult to find the form of analytic continuation of a function in practical problems. The analytic continuations of some functions in existing mathematics are actually unsuccessful. As we see below, the negative continuation of the Gama function violates the above principles. In the extended field, the form of the function is exactly the same as the original function's form, so it is still infinite and meaningless.

2.2 The analytic continuation of complex function

Let $z=x+iy\in C$ be a complex number, a similar example of analytic continuation of complex function is shown below.

$$F_1(z)=1-z^2+z^4-z^6+\cdots \qquad |z|<1$$

$$F_2(z)=\frac{1}{1+z^2} \qquad z\neq\pm i \tag{5}$$

$F_1(z)$ is an analytic function and convergent inside the unit circle but is divergent outside the unit

circle without meaning. $F_2(z)$ is an analytic function meaningful on the whole complex plane except at points $z \neq \pm i$,

To developing $F_2(z)$ into the Taylor's series of complex functions in the field $|z|<1$, we can obtain $F_1(z)$. That is to say, two functions are completely the same. Since the definition field of $F_2(z)$ is larger than $F_1(z)$, $F_2(z)$can be regarded as an analytic continuation of $F_1(z)$ over the entire complex plane (except at points $z \neq \pm i$). Similar to Eq.(4), we write they in the unified form

$$F(z)=\begin{cases} 1-z^2+z^4-z^6+\cdots & (|z|<1) \\ \dfrac{1}{1+z^2} & (z \neq \pm i) \end{cases} \tag{6}$$

Similarly, within the extended field $|z|>1$ ($z \neq \pm i$), $F_1(z)$and $F_2(z)$ are not the same functions, because $F_1(z)$ is meaningless in this case.

III. THE NEGATIVE CONTINUATION OF THE REAL GAMA FUNCTION

3.1 The definition and character of the real Gama function

The original definition of the real Gama function is

$$\Gamma(a)=\int_0^{\infty} e^{-t}t^{a-1}dt \qquad a>0 \tag{7}$$

Here parameter $a \in R$ is a real number with $a>0$. If $a \leq 0$, the integral of Eq.(7) is infinite and meaningless. The Gama function has the following natures [3]

$$\Gamma(1)=1 \qquad \Gamma(1/2)=\sqrt{\pi} \tag{8}$$

$$\Gamma(a+1)=a\Gamma(a) \quad \text{or} \quad \Gamma(a)=\frac{\Gamma(a+1)}{a} \tag{9}$$

$$\Gamma(n+1)=n! \qquad (n=0,\ 1,\ 2,\ 3,\cdots) \tag{10}$$

$$\Gamma(a)\Gamma(1-a)=\frac{\pi}{\sin a\pi} \tag{11}$$

$$\Gamma(2a)=2^{2a-1}\pi^{-1/2}\Gamma(a)\Gamma(a+1/2) \tag{12}$$

According to the formulas above, the Gama function has no zero with $\Gamma(a)>0$ in the field $a>0$.

3. 2 The negative continuation of the Gama function does not hold.

According to the original definition, the Gama function is meaningless when $a \leq 0$. For example, when $a=0$, Eq. (7) becomes

$$\Gamma(0)=\int_0^\infty e^{-t}t^{-1}dt=-\int_0^\infty t^{-1}de^{-t}=-t^{-1}e^{-t}\Big|_0^\infty+\int_0^\infty e^{-t}dt^{-1}$$

$$=-\frac{1}{e^t t}\Big|_0^\infty-\int_0^\infty e^{-t}t^{-2}dt=\infty-\Gamma(-1)\to\infty \tag{13}$$

By the same method, it can be proved that

$$\Gamma(-1)=\frac{\Gamma(1-1)}{-1}=\frac{\Gamma(0)}{-1}\to-\infty \tag{14}$$

$$\Gamma(-2)=\frac{\Gamma(1-2)}{-2}=\frac{\Gamma(-1)}{-2}\to\infty \tag{15}$$

Therefore, when $a=0,\ -1,\ -2,\ -3,\cdots$, we have $\Gamma(-a)\to\pm\infty$.

However, according to the present theory of the Gama function, as long as $a\neq 0,\ -1,\ -2,\ -3,\cdots$, by using formula (9), Eq.(7) can still be extended from the field $a>0$ to the field $a'=-a<0$, called the negative continuation of the Gama function.We write it as

$$\Gamma(a')=\Gamma(-a)=\frac{\Gamma(1-a)}{-a}\qquad a'\neq 0,\ -1,\ -2,\ -3,\cdots \tag{16}$$

For example, let $a'=-1/2$, according to Eqs. (7), (8) and (16), we have [3]

$$\Gamma(-1/2)=\frac{\Gamma(1-1/2)}{-1/2}=\frac{\Gamma(1/2)}{-1/2}=-2\sqrt{\pi} \tag{17}$$

Let $a'=-3/2$, according to Eqs.(16) and (17), we have

$$\Gamma(-3/2)=\frac{\Gamma(1-3/2)}{-3/2}=\frac{\Gamma(-1/2)}{(-3/2)}=\frac{4\sqrt{\pi}}{3} \tag{18}$$

So, according to the present theory, after negative continuation, as long as $a'=-a\neq 0,\ -1,\ -2,\ -3,\cdots$, the Gama function is still meaningful. The formula (16) appears in various textbooks and literature, and be used widely in mathematics.

However, according to this direct negative continuation, the basic form of the Gama function has no any change. It violates the first condition and is wrong. For example, to take $a'=-0.3$, according to the original definition Eq.(7) and Eq.(16), we have

$$\Gamma(-0.3)=-\frac{1}{0.3}\Gamma(1-0.3)=-\frac{1}{0.3}\Gamma(0.7)$$

$$=-\frac{1}{0.3}\int_0^\infty e^{-t}t^{0.7-1}dt=\frac{1}{0.3}\int_0^\infty t^{-0.3}de^{-t}$$

$$= \frac{1}{0.3}\frac{1}{t^{0.3}e^{t}}\Big|_{0}^{\infty} - \frac{1}{0.3}\int_{0}^{\infty} e^{-t}dt^{-0.3}$$

$$= -\infty + \int_{0}^{\infty} e^{-t}t^{-0.3-1}dt = -\infty + \Gamma(-0.3) \tag{19}$$

So we get the absurd result $\Gamma(-0.3) = -\infty + \Gamma(-0.3)$,the result is meaningless. So Eq.(16) can not hold. Again, to take $a' = -1.5$, according to Eq.(16), we have

$$\Gamma(-3/2) = \Gamma(-1.5) = -\frac{1}{1.5}\Gamma(1-1.5) = -\frac{1}{1.5}\Gamma(-0.5)$$

$$= -\frac{1}{1.5}\int_{0}^{\infty} e^{-t}t^{-0.5-1}dt = \frac{1}{1.5}\int_{0}^{\infty} t^{-1.5}de^{-t}$$

$$= \frac{1}{1.5}\frac{1}{t^{1.5}e^{t}}\Big|_{0}^{\infty} - \frac{1}{1.5}\int_{0}^{\infty} e^{-t}dt^{-1.5}$$

$$= -\infty + \int_{0}^{\infty} e^{-t}t^{-1.5-1}dt = -\infty + \Gamma(-1.5) \tag{20}$$

We still get $\Gamma(-1.5) = -\infty + \Gamma(-1.5)$, which is completely different from Eq.(18). In fact in the general situation, let $a > 0$, we have $-a < 0$. According to Eqs.(7) and (16), the result is

$$\Gamma(a') = \Gamma(-a) = -\frac{1}{a}\Gamma(1-a) = -\frac{1}{a}\int_{0}^{\infty} e^{-t}t^{1-a-1}dt$$

$$= \frac{1}{a}\int_{0}^{\infty} t^{-a}de^{-t} = \frac{1}{ae^{t}t^{a}}\Big|_{0}^{\infty} - \frac{1}{a}\int_{0}^{\infty} e^{-t}dt^{-a}$$

$$= -\frac{1}{ae^{t}t^{a}}\Big|_{t\to 0} + \int_{0}^{\infty} e^{-t}t^{-a-1}dt = -\infty + \Gamma(-a) \tag{21}$$

That is $\Gamma(-a) = -\infty + \Gamma(-a)$. Therefore, the negative continuation formula (16) of the Gama function does not hold. The reason is that in the extend field, the form of the Gama function has not been changed.

IV. THE COMPLEX CONTINUATION OF THE GAMA FUNCTION

4.1 The single complex continuation and the double complex continuation of theGama function.

Let $a \to s = a + ib$ in Eq. (7), the Gama function is extended from real field to complex field with

$$\Gamma(s) = \int_{0}^{\infty} e^{-x}x^{s-1}dx \qquad \mathrm{Re}(s) > 0 \tag{22}$$

We call Eq. (22) the single complex continuation of the Gama function. In the deduction of the integral form of the Riemann Zeta function, the single complex continuation of the Gama function is involved.

According to the definition, the condition that Eq.(22) holds is $\mathrm{Re}(s) = a > 0$. That is to say, Eq.(22) holds only on the right half side of complex plane. On the left half side of complex plane, it does not hold. However, according to the present theory, Eq. (22) is actually considered to be valid on the whole complex plane except at the points of negative integers with $a = 0,\ -1,\ -2,\ -3, \cdots$.. The reason is due to the following relation

$$\Gamma(s+1) = s\Gamma(s) \tag{23}$$

Let $s' = -s$, we re-write Eq.(23) as

$$\Gamma(s') = \frac{\Gamma(s'+1)}{s'} \qquad \mathrm{Re}(s') \neq 0,\ -1,\ -2,\ \cdots \tag{24}$$

In this way, $\Gamma(s)$ is extended into the negative half plane with $\mathrm{Re}(s') < 0$. Similar to the negative continuation of the real Game function as shown in Eq.(16), we call Eq. (24) the negative continuation of the single complex Game function.

By substituting $x^{ib} = e^{ib\ln x}$ in Eq.(22) and separating the real part and the imaginary part, we have

$$\begin{aligned}\Gamma(s) &= \int_0^\infty e^{-x}x^{a-1+ib}dx = \int_0^\infty e^{-x}x^{a-1}e^{ib\ln x}dx \\ &= \int_0^\infty e^{-x}x^{a-1}\cos(b\ln x)dx + i\int_0^\infty e^{-x}x^{a-1}\sin(b\ln x)dx \\ &= \Gamma_1(a,b) + i\,\Gamma_2(a,b)\end{aligned} \tag{25}$$

Here $\Gamma_1(a,b)$ and $\Gamma_2(a,b)$ are the real functions with

$$\Gamma_1(a,b) = \int_0^\infty e^{-x}x^{a-1}\cos(b\ln x)dx \qquad \Gamma_2(a,b) = \int_0^\infty e^{-x}x^{a-1}\sin(b\ln x)dx \tag{26}$$

It can be seen that $\Gamma_1(a,b)$ and $\Gamma_2(a,b)$ are not the originally defined Gama functions due to the existence of the items $\cos(b\ln x)$ and $\sin(b\ln x)$. A new parameter b is increased in Eq. (26), so it becomes the function of double parameters. We can not call them the Gama function again. The formulas (8) ~ (12) can not hold for them. They need to be proved again. Only when $b = 0$, Eq.(25) degenerates to the real Gama function.

If let $x \to z = x + iy \in C$ again in Eq.(22), we call it the double complex continuation of the Gama function with

$$\Gamma_c(s) = \int_C e^{-z}z^{s-1}dz \tag{27}$$

In the deduction of the Riemann Zeta function equation, the double complex continuation of the Gama function is involved. We will discuss them in Section 4.4.

4. 2 The negative continuation of the complex Gama function does not hold.

We now prove that the formula (24) of the negative continuation of the complex Gama function does not hold on the complex half-plane $\mathrm{Re}(s')<0$. Similarly, Eq.(24) can be written as

$$\Gamma(s')=\Gamma(-s)=\frac{\Gamma(1-s)}{-s}=\frac{1}{-s}\int_0^\infty e^{-x}x^{1-s-1}dx$$

$$=\frac{1}{s}\int_0^\infty x^{-s}de^{-x}=\frac{1}{s}e^{-x}x^{-s}\Big|_0^\infty-\frac{1}{s}\int_0^\infty e^{-x}dx^{-s}$$

$$=\frac{1}{se^{x}x^{s}}\Big|_0^\infty+\int_0^\infty e^{-x}x^{-s-1}dx \tag{28}$$

We have

$$x^s=x^{a+ib}=x^a e^{ib\ln x}=x^a\cos(b\ln x)+ix^a\sin(b\ln x) \tag{29}$$

When $x\to 0$, we have $\ln x\to-\infty$, but $\cos(b\ln x)$ and $\sin(b\ln x)$ are limited, so we have

$$\frac{1}{se^{x}x^{s}}\Big|_0^\infty=\frac{1}{(a+ib)e^{x}x^{a}[\cos(b\ln x)+i\sin(\ln x)]}\Big|_0^\infty\to\infty \tag{30}$$

From Eq.(28), we still obtain $\Gamma(-s)=\infty+\Gamma(-s)$, the negative continuation of the complex Gama function is also meaningless.

4. 3 The single complex continuation of the Gama function is not an analytic function

In the theory of complex function, the analytic property of function is very important. There are many theorems which are effective only for analytic functions, such as the Cauchy theorem, the residue theorem, and so on. These theorems do not work if the functions are not analytic ones.

To express the analytic nature, the real part and the imaginary part of complex function $f(s)=f(a+ib)$ should be separated. We write it as

$$f(s)=u(a,b)+iv(a,b) \tag{32}$$

The real part $u(a,b)$ and the imaginary part $v(a,b)$ are not independent, both should satisfy the following Cauchy-Riemann equation [4]

$$\frac{\partial u}{\partial a}=\frac{\partial v}{\partial b}\qquad\frac{\partial u}{\partial b}=-\frac{\partial v}{\partial a} \tag{33}$$

At present, the single complex continuation $\Gamma(s)$ of the real Gama function is considered an analytic function. But it is not true. We prove it below.

Let $u(a,b)=\Gamma_1(a,b)$ and $v(a,b)=\Gamma_2(a,b)$ in Eq.(25). If $\Gamma(\mathrm{s})$ is an analytic function, following relation should be satisfied.

$$\frac{\partial \Gamma_1}{\partial a}=\frac{\partial \Gamma_2}{\partial b} \qquad \frac{\partial \Gamma_2}{\partial a}=-\frac{\partial \Gamma_1}{\partial b} \tag{34}$$

However, according to Eq.(26), we have

$$\frac{\partial \Gamma_1}{\partial a}=(a-1)\int_0^\infty e^{-x}x^{a-2}\cos(b\ln x)dx \qquad \frac{\partial \Gamma_1}{\partial b}=-\int_0^\infty e^{-x}x^{a-1}\ln x\sin(b\ln x)dx \tag{35}$$

$$\frac{\partial \Gamma_2}{\partial a}=(a-1)\int_0^\infty e^{-x}x^{a-2}\sin(b\ln x)dx \qquad \frac{\partial \Gamma_2}{\partial b}=\int_0^\infty e^{-x}x^{a-1}\ln x\cos(b\ln x)dx \tag{36}$$

It is obvious that Eq.(34) can not hold, so the Gama function $\Gamma(s)$ described by Eq.(25) is not an analytic function on the complex plane $s=a+ib$.

4. 4 The double complex continuation of the Gama function is an analytic function.

We prove below that the double complex continuation of the Gama function is an analytic function. We write Eq.(27) as

$$\Gamma(s)=\int_C e^{-z}z^{s-1}dz=u(a,b)+iv(a,b) \tag{37}$$

We have

$$z^{s-1}=(re^{i\theta})^{a+ib-1}=(e^{\ln r}e^{i\theta})^{a-1+ib}=e^{(a-1)\ln r-b\theta}e^{i[b\ln r+(a-1)\theta]} \tag{38}$$

$$e^{-z}z^{s-1}=e^{\boxminus x+iy)}z^{(a+ib)-1}=e^{(a-1)\ln r-b\theta-x}e^{i[b\ln r+(a-1)\theta-y]} \tag{39}$$

$$=e^{(a-1)\ln r-b\theta-x}\left\{\cos\left(b\ln r+(a-1)\theta-y\right)+i\sin\left(b\ln r+(a-1)\theta-y\right)\right\}=A+iB \tag{40}$$

$$A=e^{(a-1)\ln r-b\theta-x}\cos\left(b\ln r+(a-1)\theta-y\right) \tag{41}$$

$$B=e^{(a-1)\ln r-b\theta-x}\sin\left(b\ln r+(a-1)\theta-y\right) \tag{42}$$

Here $x=r\cos\theta$ and $y=r\sin\theta$. Then, we write Eq.(37) as

$$\Gamma(s)=\int_C e^{-z}z^{s-1}dz=\int_C(A+iB)(dx+idy)=\int_C(Adx-Bdy)+i\int_C(Ady+Bdx) \tag{43}$$

and get

$$u(a,b)=\int_0^\infty(Adx-Bdy) \qquad v(a,b)=\int_0^\infty(Ady+Bdx) \tag{44}$$

$$\frac{\partial u}{\partial a}=\int_C\left[\left(\frac{\partial A}{\partial a}\right)dx-\left(\frac{\partial B}{\partial a}\right)dy\right] \qquad \frac{\partial v}{\partial b}=\int_C\left[\left(\frac{\partial A}{\partial b}\right)dy+\left(\frac{\partial B}{\partial b}\right)dx\right] \tag{45}$$

$$\frac{\partial u}{\partial b}=\int_C\left[\left(\frac{\partial A}{\partial b}\right)dx-\left(\frac{\partial B}{\partial b}\right)dy\right] \qquad \frac{\partial v}{\partial a}=\int_C\left[\left(\frac{\partial A}{\partial a}\right)dy+\left(\frac{\partial B}{\partial a}\right)dx\right] \tag{46}$$

From Eq.(41) and (42), we have

$$\frac{\partial A}{\partial a}=\ln r e^{(a-1)\ln r-b\theta-x}\cos\left(b\ln r+(a-1)\theta-y\right)$$
$$-\theta\, e^{(a-1)\ln r-b\theta-x}\sin\left(b\ln r+(a-1)\theta-y\right) \tag{47}$$

$$\frac{\partial B}{\partial a}=\ln r\, e^{(a-1)\ln r-b\theta-x}\sin\left(b\ln r+(a-1)\theta-y\right)$$
$$+\theta\, e^{(a-1)\ln r-b\theta-x}\cos\left(b\ln r+(a-1)\theta-y\right) \tag{48}$$

$$\frac{\partial A}{\partial b}=-\theta\, e^{(a-1)\ln r-b\theta-x}\cos\left(b\ln r+(a-1)\theta-y\right)$$
$$-\ln r\, e^{(a-1)\ln r-b\theta-x}\sin\left(b\ln r+(a-1)\theta-y\right) \tag{49}$$

$$\frac{\partial B}{\partial b}=-\theta\, e^{(a-1)\ln r-b\theta-x}\sin\left(b\ln r+(a-1)\theta-y\right)$$
$$+\ln r\, e^{(a-1)\ln r-b\theta-x}\cos\left(b\ln r+(a-1)\theta-y\right) \tag{50}$$

By considering Eqs.(47) ~ (50), we see that Eq.(33) can be satisfied. So Eq.(44) satisfies the Cauchy-Riemann equation, the double complex continuation of the Gama function is an analytic function.

4.5 The product of the Riemann Zeta function and the Gama function is not an analytic function.

The original definition of the series form of the Riemann Zeta function is

$$\zeta(s)=\sum_{n=1}^{\infty}n^{-s} \qquad \mathrm{Re}(s)>1 \tag{51}$$

It is proved in [2] that Eq.(51) is an analytic function. Riemann obtained the relation between the Riemann Zeta function and the complex continuation of the Gama function in his original paper in 1859.

$$\zeta(s)\Gamma(s)=\int_0^{\infty}\frac{x^{s-1}}{e^x-1}dx=I(s) \tag{52}$$

We prove below that $I(s)$ is not an analytic function about $s=a+ib$. By using $x^{ib}=e^{ib\ln x}$, Eq.(52) can be written as

$$I(s)=\int_0^{\infty}\frac{x^{a-1}e^{ib\ln x}}{e^x-1}dx=\int_0^{\infty}\frac{x^{a-1}}{e^x-1}\Big[\cos(b\ln x)+i\sin(b\ln x)\Big]dx \tag{53}$$

By separating the real part and the imaginary part, we get

$$u(a,b)=\int_0^{\infty}\frac{x^{a-1}}{e^x-1}\cos(b\ln x)dx \qquad v(a,b)=\int_0^{\infty}\frac{x^{a-1}}{e^x-1}\sin(b\ln x)dx \tag{54}$$

So we have

$$\frac{\partial u}{\partial a}=(a-1)\int_0^{\infty}\frac{x^{a-2}}{e^x-1}\cos(b\ln x)dx \qquad \frac{\partial u}{\partial b}=-\int_0^{\infty}\frac{x^{a-1}}{e^x-1}\ln x\sin(b\ln x)dx \tag{55}$$

$$\frac{\partial v}{\partial b}=\int_0^{\infty}\frac{x^{a-1}}{e^x-1}\ln x\cos(b\ln x)dx \qquad \frac{\partial v}{\partial a}=(a-1)\int_0^{\infty}\frac{x^{a-2}}{e^x-1}\sin(b\ln x)dx \tag{56}$$

It is obvious that Eqs.(55) and (56) are similar to Eqs.(35) and (36). The Cauchy-Riemann equation (33) can not be satisfied, so Eq. (52) is not an analytic function.

4. 6 The double complex continuation of $I(s)$ function is an analytic function.

Similar to Eq.(27), let $x\to z=x+iy$ in Eq.(52) for the second complex continuation, we get

$$I(s)\to I_c(s)=\int_C\frac{z^{s-1}}{e^z-1}dz \tag{57}$$

It is proved that the double complex continuation $I_c(s)$ is an analytic function. We have

$$z^{s-1}=e^{(a-1)\ln r-b\theta}e^{i[b\ln r+(a-1)\theta]}$$

$$=e^{(a-1)\ln r-b\theta}\ \{\cos[b\ln r+(a-1)\theta]+i\sin\}e^{i[b\ln r+(a-1)\theta]} \tag{58}$$

$$\frac{1}{e^z-1}=\frac{1}{e^{x+iy}-1}=\frac{1}{e^x\big((\cos y-1)+i\sin y\big)}$$

$$=\frac{\big((\cos y-1)-i\sin y\big)}{e^x\big((\cos y-1)+i\sin y\big)\big((\cos y-1)-i\sin y\big)}$$

$$=\frac{\cos y-1-i\sin y}{2e^x(1-\cos y)}=-\frac{1}{2e^x}+i\frac{\sin y}{2e^x(\cos y-1)} \tag{59}$$

$$\frac{z^{s-1}}{e^z-1}=\left[-\frac{1}{2e^x}+i\frac{\sin y}{2e^x(\cos y-1)}\right]\left(e^{(a-1)\ln r-b\theta}e^{i[b\ln r+(a-1)\theta]}\right)$$

$$e^{-z}z^{s-1}=e^{\boxminus x+iy)}z^{(a+ib)-1}=e^{(a-1)\ln r-b\theta-x}e^{i[b\ln r+(a-1)\theta-y]} \tag{60}$$

$$=e^{(a-1)\ln r-b\theta-x}\left\{\cos\left(b\ln r+(a-1)\theta-y\right)+i\sin\left(b\ln r+(a-1)\theta-y\right)\right\}=A+iB \tag{61}$$

$$A=e^{(a-1)\ln r-b\theta-x}\cos\left(b\ln r+(a-1)\theta-y\right)$$

$$B=e^{(a-1)\ln r-b\theta-x}\sin\left(b\ln r+(a-1)\theta-y\right) \tag{62}$$

Similar to the calculations of Eqs.(47) ~ (50), it can be proved that Eq.(33) can be satisfied, so the function $I_c(\mathrm{s})$ described by Eq.(57) is an analytic function. Riemann used it to calculate and deduce the Zeta function equation.

V. THE COMPLEX CONTINUATION OF COMPLEMENTARY FORMULA OF GAMA FUNCTION

5.1 The complex continuation of complementary formula of the Gama function does not hold

Suppose that a is a real non-integer number with $0<a<1$, it can be proved to exist the following f ormula [4]

$$\int_0^{\infty}\frac{x^{a-1}}{x+1}dx=\frac{\pi}{\sin a\pi} \tag{69}$$

Though the formula is defined in the real field, it needs to use the Residue theorem of complex function to prove. Let $s=a+ib$, the complex continuation of Eq.(69) is considered to directly let $a\to s$ in Eq.(69) at present and get

$$\int_0^{\infty}\frac{x^{s-1}}{x+1}dx=\frac{\pi}{\sin s\pi} \tag{70}$$

Correspondingly, the complex continuation of Eq.(11) is considered to be

$$\Gamma(s)\Gamma(1-s)=\frac{\pi}{\sin s\pi}\qquad 0<\mathrm{Re}(s)<1 \tag{71}$$

Eq. (71) was used when Riemann deduced the integral form of the Zeta function in his original paper in 1859.

It is proved below that Eq. (70) does not hold, so Eq.(71) does not hold too. We write the left side of Eq.(70) as

$$\int\frac{x^{s-1}}{x+1}dx=\int_0^{\infty}\frac{x^{a+ib-1}}{x+1}dx=\int_0^{\infty}\frac{x^{a-1}e^{ib\ln x}}{x+1}dx$$

$$=\int_0^{\infty}\frac{x^{a-1}}{x+1}\cos(b\ln x)dx+i\int_0^{\infty}\frac{x^{a-1}}{x+1}\sin(b\ln x)dx \tag{72}$$

According to the Euler formula, we have

$$e^{is} = e^{ia-b} = e^{-b}\left(\cos a + i\sin a\right) \tag{73}$$

$$\sin(a+ib) = \frac{e^{i(a+ib)} - e^{-i(a+ib)}}{2i} = \frac{e^{-b}(\cos a + i\sin a) - e^{b}(\cos a - i\sin a)}{2i}$$

$$= \frac{-(e^{b} - e^{-b})\cos a + i(e^{b} + e^{-b})\sin a}{2i} \tag{74}$$

$$\frac{\pi}{\sin(a+ib)\pi} = \frac{i2\pi}{-(e^{b\pi} - e^{-b\pi})\cos a\pi + i(e^{b\pi} + e^{-b\pi})\sin a\pi}$$

$$= \frac{2\pi(e^{b\pi} + e^{-b\pi})\sin a\pi}{e^{2b\pi} + e^{-2b\pi} + 2(\sin^2 a\pi - \cos^2 a\pi)} - i\frac{2\pi(e^{b\pi} - e^{-b\pi})\cos a\pi}{e^{2b\pi} + e^{-2b\pi} + 2(\sin^2 a\pi - \cos^2 a\pi)} \tag{75}$$

If Eq.(70) holds, by comparing the real parts and the imaginary parts of Eq.(72) and (75), we have

$$\int_0^{\infty} \frac{x^{a-1}}{x+1}\cos(b\ln x)dx = \frac{2\pi(e^{b\pi} + e^{-b\pi})\sin a\pi}{e^{2b\pi} + e^{-2b\pi} + 2(\sin^2 a\pi - \cos^2 a\pi)} \tag{76}$$

$$\int_0^{\infty} \frac{x^{a-1}}{x+1}\sin(b\ln x)dx = \frac{-2\pi(e^{b\pi} + e^{-b\pi})\cos a\pi}{e^{2b\pi} + e^{-2b\pi} + 2(\sin^2 a\pi - \cos^2 a\pi)} \tag{77}$$

Let $b = 0$ in Eqs.(76) and (77), we get

$$\int_0^{\infty} \frac{x^{a-1}}{x+1}dx = \frac{4\pi\sin a\pi}{2(1+\sin^2 a\pi - \cos^2 a\pi)} = \frac{\pi}{\sin a\pi} \tag{78}$$

$$0 = \frac{-4\pi\cos a\pi}{2(1+\sin^2 a\pi - \cos^2 a\pi)} = -\frac{\pi\cos a\pi}{\sin^2 a\pi} \tag{79}$$

Eq.(78) is completely the same as Eq.(69), but Eq. (79) can not hold when $a \neq (2n+1)/2$. Where is wrong? Let's analyze it below.

5.2 The correct calculation of complex continuation of complementary formula of the Gama function

At present, the Residue theorem is used to calculate Eq.(69). Let's repeat this calculation at first. Suppose that a is a real non-integer, we consider the integral of complex function below with $0 \le \arg z \le 2\pi$ [4]

$$T(a) = \int_C z^{a-1}Q(z)dz \tag{80}$$

Here $Q(z)$ is a single value and analytic function everywhere except at several isolated singularities. There are no singularities on the positive real axis. When $|z| \to 0$ and $|z| \to \infty$, $|z^a Q(z)|$ tends to zero consistently.

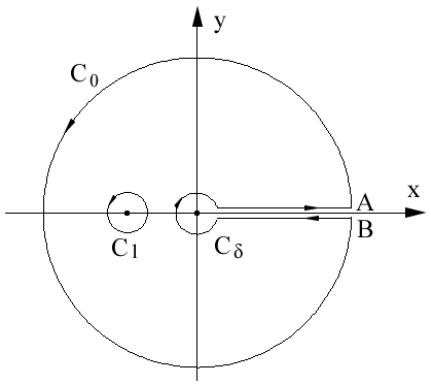

Fig.1: The contour of residue calculation

The integral contour C of residue calculation is shown in Fig.1. It stars off from the point $z = x = \delta$ on the above positive real axis, goes along the positive real axis and arrive at point A with $x = R$. Then goes along a big circle C_0 with radius and comes back to point B on the down positive real axis. Then goes along the negative direction of real axis and arrives at point $x = \delta$. At last, goes around the small circle C_δ and reaches the starting point.

Therefore, the integral of Eq.(80) can be written as

$$\int_C z^{a-1}Q(z)dz = \int_\delta^R z^{a-1}Q(z)dz + \int_{C_0} z^{a-1}Q(z)dz = \int_R^\delta z^{a-1}Q(z)dz + \int_{C_R} z^{a-1}Q(z)dz$$

$$= (1-e^{i2a\pi})\int_\delta^R z^{a-1}Q(z)dz + \int_{C_0} z^{a-1}Q(z)dz + \int_{C_\delta} z^{a-1}Q(z)dz \tag{81}$$

By using the Residue theorem, we have

$$\int_C z^{a-1}Q(z)dz = i2\pi\sum res\left\{z^{a-1}Q(z)\right\} \tag{82}$$

Because of $\left|z^aQ(z)\right| \to 0$ when $|z| = \delta \to 0$ and $|z| = R \to \infty$, we have,

$$\int_{C_0} z^{a-1}Q(z)dz \to 0 \quad \text{and} \quad \int_{C_\delta} z^{a-1}Q(z)dz \to 0 \tag{83}$$

Based on the formula above, we get from Eq. (82)

$$\int_\delta^R z^{a-1}Q(z)dz \to \int_0^\infty x^{a-1}Q(x)dx = \frac{i2\pi}{1-e^{i2a\pi}}\sum res\left\{z^{a-1}Q(z)\right\} \tag{84}$$

Let $Q(z) = 1/(1+z)$, there is an unique singularity $z = -1 = e^{i\pi}$ on the real axis. The residue is

$$\sum res\left\{z^{a-1}Q(z)\right\} = res\left\{\frac{z^{a-1}}{(1+z)'}\right\}\Bigg|_{z=e^{i\pi}} = z^{a-1}\Big|_{z=e^{i\pi}} = e^{i(a-1)\pi} \tag{85}$$

London Journal of Research in Science: Natural and Formal

Substituting it in Eq.(84), we get the current result with

$$\int_0^\infty \frac{x^{a-1}}{1+x}dx = \frac{2\pi i e^{i(a-1)\pi}}{1-e^{i2a\pi}} = \frac{i2\pi e^{-i\pi}}{e^{-ia\pi}-e^{i2a\pi}} = \frac{-i2\pi}{e^{-ia\pi}-e^{ia\pi}} = \frac{\pi}{\sin a\pi} \tag{86}$$

If let $a \to s = a + ib$, it is impossible to let $\sin a\pi \to \sin s\pi$ on the right side of Eq.(86). It needs to be calculated again. Let

$$Q_1(b,z) = \cos(b\ln z)/(1+z) \qquad Q_2(b,z) = \sin(b\ln z)/(1+z) \tag{87}$$

$$T_1(a,b) = \int_C z^{a-1}Q_1(b,z)dz \qquad T_2(a,b) = \int_C z^{a-1}Q_2(b,z)dz \tag{88}$$

When $|z| = \delta \to 0$ and $|z| = R \to \infty$, $\cos(b\ln z)$ and $\sin(b\ln z)$ are uncertain values. But we still have $|\cos(b\ln z)| \le 1$ and $|\cos(b\ln z)| \le 1$, so the conditions $|z^a Q_1(z)| \to 0$ and $|z^a Q_2(z)| \to 0$ still hold. We can still use the Residue theorem. For $T_1(a,b)$, similar to Eq.(85), we have

$$\frac{1}{i2\pi}\int_C z^{a-1}Q_1(b,z)dz = \sum res\{z^{a-1}Q_1(z)\} = z^{a-1}\cos(b\ln z)\Big|_{z=e^{i\pi}}$$

$$= e^{i(a-1)\pi}\cos(b\ln e^{i\pi}) = e^{i(a-1)\pi}\cos(ib\pi) = e^{i(a-1)\pi}\frac{e^{b\pi}+e^{-b\pi}}{2} \tag{89}$$

For $T_2(a,b)$, the result is

$$\frac{1}{i2\pi}\int_C z^{a-1}Q_1(b,z)dz = \sum res\{z^{a-1}Q_2(z)\} = z^{a-1}\sin(b\ln z)\Big|_{z=e^{i\pi}}$$

$$= e^{i(a-1)\pi}\sin(b\ln e^{i\pi}) = e^{i(a-1)\pi}\sin(ib\pi) = e^{i(a-1)\pi}\frac{e^{-b\pi}-e^{b\pi}}{2i} \tag{90}$$

The last result is

$$\int_0^\infty \frac{x^{a-1}}{1+x}\cos(b\ln x)dx = \frac{-i2\pi}{e^{-ia\pi}-e^{ia\pi}}\frac{e^{b\pi}+e^{-b\pi}}{2} = \frac{\pi}{\sin a\pi}\frac{e^{b\pi}+e^{-b\pi}}{2} \tag{91}$$

$$\int_0^\infty \frac{x^{a-1}}{1+x}\sin(b\ln x)dx = \frac{-i2\pi}{e^{-ia\pi}-e^{ia\pi}}\frac{e^{b\pi}+e^{-b\pi}}{2} = \frac{\pi}{\sin a\pi}\frac{e^{b\pi}-e^{-b\pi}}{2i} \tag{92}$$

When $b = 0$, Eq.(91) is consistent with Eq.(78). Eq.(92) is equal to zero. The contradiction shown in Eq.(79) does not exist again. Eq.(70) becomes

$$\int_0^\infty \frac{x^{s-1}}{x+1}dx = \int_0^\infty \frac{x^{a+ib-1}}{x+1}dx = \frac{\pi}{\sin a\pi}\left[\frac{e^{b\pi}+e^{-b\pi}}{2} + i\frac{e^{b\pi}-e^{-b\pi}}{2i}\right] = \frac{\pi e^{b\pi}}{\sin a\pi} \tag{93}$$

The result of integral is a real number, rather than a complex number. The complex continuation formula (71) should be changed as

$$\Gamma(s)\Gamma(1-s)=\frac{\pi e^{b\pi}}{\sin a\pi} \qquad 0<a<1 \tag{94}$$

It is also a real number, rather than a complex number.

It should be noted that Eq. (94) holds only when $0<a<1$. Beyond this condition, Eq. (94) is still invalid. Eq. (71) was used when Riemann derived the Zeta function equation. These two results will have a great influence on the Riemann hypothesis problem.

VI. THE COMPLEX CONTINUATION OF THE GAMMA FUNCTION MULTIPLIER PRODUCT FORMULA.

The multiplier product formula of the Gama function is [4]

$$\Gamma(a)\Gamma(a+1/2)=2^{-2(2a-1)}\Gamma(2a) \qquad a>0 \tag{95}$$

According to the current theory, the complex continuation of Eq.(95) is directly written as

$$\Gamma(s)\Gamma(s+1/2)=2^{-2(2s-1)}\Gamma(2s) \tag{96}$$

Eq.(96) is regarded to be tenable on the whole complex plane. But there is no basis for this result actually. By using the definition of the Gama function, Eq.(95) can be written as

$$\int_0^\infty\int_0^\infty e^{-(x+y)}x^{a-1}y^{a-1/2}dxdy=2^{-(2a-1)}\int_0^\infty e^{-x}x^{2a-1}dx \tag{97}$$

By substituting $s=a+ib$ in Eq.(96) and considering $x^{-ib}=e^{-ib\ln x}=\cos(b\ln x)-i\sin(b\ln x)$, the results are

$$\begin{aligned}&\int_0^\infty\int_0^\infty e^{-(x+y)}x^{a-1}y^{a-1/2}\Big[\cos(b\ln x)\cos(b\ln y)-\sin(b\ln x)\sin(b\ln y)\Big]dxdy\\&+i\int_0^\infty\int_0^\infty e^{-(x+y)}x^{a-1}y^{a-1/2}\Big[\sin(b\ln x)\cos(b\ln y)+\sin(b\ln y)\cos(b\ln x)\Big]dxdy\\&=2^{-(2a-1)}\Big[\cos(2b\ln 2)\int_0^\infty e^{-x}x^{2a-1}\cos(2b\ln x)dx+\sin(2b\ln 2)\int_0^\infty e^{-x}x^{2a-1}\sin(2b\ln x)dx\Big]\\&+i2^{-(2a-1)}\Big[\cos(2b\ln 2)\int_0^\infty e^{-x}x^{2a-1}\sin(2b\ln x)dx-\sin(2b\ln 2)\int_0^\infty e^{-x}x^{2a-1}\cos(2b\ln x)dx\Big]\end{aligned} \tag{98}$$

By separating the real part and the imaginary part, Eq.(98) becomes

$$\begin{aligned}&\int_0^\infty\int_0^\infty e^{-(x+y)}x^{a-1}y^{a-1/2}\Big[\cos(b\ln x)\cos(b\ln y)-\sin(b\ln x)\sin(b\ln y)\Big]dxdy\\&=2^{-(2a-1)}\Big[\cos(2b\ln 2)\int_0^\infty e^{-x}x^{2a-1}\cos(2b\ln x)dx+\sin(2b\ln 2)\int_0^\infty e^{-x}x^{2a-1}\sin(2b\ln x)dx\Big]\end{aligned} \tag{99}$$

$$\int_0^\infty\int_0^\infty e^{-(x+y)}x^{a-1}y^{a-1/2}\left[\sin(b\ln x)\cos(b\ln y)+\sin(b\ln y)\cos(b\ln x)\right]dxdy$$

$$=2^{-(2a-1)}\left[\cos(2b\ln 2)\int_0^\infty e^{-x}x^{2a-1}\sin(2b\ln x)dx-\sin(2b\ln 2)\int_0^\infty e^{-x}x^{2a-1}\cos(2b\ln x)dx\right] \tag{100}$$

The status of Eqs.(99) and (97) are equivalent, but they are different when $b\neq 0$. Eq.(97) needs proof but we have no at present. And so do for Eq.(100). So the complex continuation formula of the gamma function multiplier product is generally incredible. Because the double integrals are involved in the left sides of Eq.(99) and (100), the calculations are complex, they will be discussed in a separated paper.

VII. THE COMPLEX CONTINUATION OF THE EULER FORMULA OF PRIME NUMBERS

The Euler formula of prime numbers is

$$\sum_{n=1}^{\infty}n^{-a}=\prod_{k}\left(1-p_k^{-a}\right)^{-1} \tag{101}$$

Here $a>1$ is a real number, $n=1,\ 2,\ 3,\ 4\cdots$ is nature number and $p_k=2,\ 3,\ 5,\ 7,\cdots$ is prime number. They are all positive integers. By considering $p_k^{-a}=1/p_k^a<1$, we have

$$\frac{1}{1-p_k^{-a}}=1+p_k^{-a}+p_k^{-2a}+p_k^{-3a}+\cdots \tag{102}$$

By developing the multiple products on the right side of Eq.(101) , it can be written as

$$\sum_{n=1}^{\infty}n^{-a}=1+\sum_{k}p_k^{-a}+\sum_{j<k}(p_jp_k)^{-a}+\sum_{j<k<l}(p_jp_kp_l)^{-a}+\cdots$$

$$+\sum_{j<k}(p_j^{-2a}p_k^{-a})+\sum_{j<k}(p_j^{-a}p_k^{-2a})+\sum_{j<k<l}(p_j^{-2a}p_k^{-a}p_l^{-a})$$

$$+\sum_{j<k<l}(p_j^{-a}p_k^{-2a}p_l^{-a})+\sum_{j<k<l}(p_j^{-a}p_k^{-a}p_l^{-2a})+\cdots \tag{103}$$

Riemann extended the Euler formula of primes number into the complex field and write it as

$$\sum_{n=1}^{\infty}n^{-s}=\prod_{p_k}\left(1-p_k^{-s}\right)^{-1} \tag{104}$$

Here $s=a+ib$ is a complex number. It should note that the Riemann's complex continuation is only a hypothesis without strict proof. It is proved below that this complex continuation has no meaning in the theory of prime numbers for it does not describe the relation between prime numbers and natural numbers again.

Let $s=a+ib$ in Eq.(104), we have

$$\sum_{n=1}^{\infty} n^{-(a+ib)} = \prod_{p_k}\left(1 - p_k^{-(a+ib)}\right)^{-1} \tag{105}$$

By using $n^{-ib} = e^{-ib\ln n} = \cos(b\ln n) - i\sin(b\ln n)$, the left side of Eq.(105) can be written as

$$\sum_{n=1}^{\infty} n^{-(a+ib)} = 1 + \frac{1}{2^{a+ib}} + \frac{1}{3^{a+ib}} + \cdots + \frac{1}{n^{a+ib}} + \cdots$$

$$= 1 + 2^{-a}\cos(b\ln 2) + 3^{-a}\cos(b\ln 3) + \cdots + n^{-a}\cos(b\ln n) + \cdots$$

$$- i\left(2^{-a}\sin(b\ln 2) + 3^{-a}\sin(b\ln 3) + \cdots + n^{-a}\sin(b\ln n) + \cdots\right) \tag{106}$$

The right side of Eq.(105) becomes

$$\prod_{p_k}\left(1 - p_k^{-(a+ib)}\right)^{-1} = 1 + \sum_k p_k^{-a}\left[\cos(b\ln p_k) - i\sin(b\ln p_k)\right]$$

$$+ \sum_{j<k}(p_j p_k)^{-a}\left[\cos(b\ln p_j) - i\sin(b\ln p_j)\right]\left[\cos(b\ln p_k) - i\sin(b\ln p_k)\right]$$

$$+ \sum_{j<k<l}(p_j p_k p_l)^{-a}\left[\cos(b\ln p_j) - i\sin(b\ln p_j)\right]\left[\cos(b\ln p_k) - i\sin(b\ln p_k)\right]$$

$$\times\left[\cos(b\ln p_l) - i\sin(b\ln p_l)\right] + \cdots + \sum_{j<k}(p_j^{-2a} p_k^{-a})\left[\cos(2b\ln p_j) - i\sin(2b\ln p_j)\right]$$

$$\times\left[\cos(b\ln p_k) - i\sin(b\ln p_k)\right] + \cdots \tag{107}$$

By separating the real part and the imaginary part of Eq.(105), we get

$$1 + 2^{-a}\cos(b\ln 2) + 3^{-a}\cos(b\ln 3) + \cdots + n^{-a}\cos(b\ln n) + \cdots = 1 + \sum_k p_k^{-a}\cos(b\ln p_k)$$

$$+ \sum_{j<k}(p_j p_k)^{-a}\left[\cos(b\ln p_j)\cos(b\ln p_k) - \sin(b\ln p_j)\sin(b\ln p_k)\right]$$

$$+ \sum_{j<k<l}(p_j p_k p_l)^{-a}\left\{\left[\cos(b\ln p_j)\cos(b\ln p_k) - \sin(b\ln p_j)\sin(b\ln p_k)\right]\cos(b\ln p_l)\right.$$

$$\left. + \left[\cos(b\ln p_j)\sin(b\ln p_k) + \sin(b\ln p_j)\cos(b\ln p_k)\right]\sin(b\ln p_l)\right\} + \cdots$$

$$+ \sum_{j<k}(p_j^{-2a} p_k^{-a})\left[\cos(2b\ln p_j)\cos(b\ln p_k) - \sin(2b\ln p_j)\sin(b\ln p_k)\right] + \cdots \tag{108}$$

$$2^{-a}\sin(b\ln 2)+3^{-a}\sin(b\ln 3)+\cdots+n^{-a}\sin(b\ln n)+\cdots=\sum_k p_k^{-a}\sin(b\ln p_k)$$

$$+\sum_{j<k}(p_j p_k)^{-a}\left[\cos(b\ln p_j)\sin(b\ln p_k)+\sin(b\ln p_j)\cos(b\ln p_k)\right]$$

$$+\sum_{j<k<l}(p_j p_k p_l)^{-a}\left\{\left[\cos(b\ln p_j)\sin(b\ln p_k)+\sin(b\ln p_j)\cos(b\ln p_k)\right]\cos(b\ln p_l)\right.$$

$$\left.+\left[\cos(b\ln p_j)\cos(b\ln p_k)-\sin(b\ln p_j)\sin(b\ln p_k)\right]\sin(b\ln p_l)\right\}+\cdots$$

$$+\sum_{j<k}(p_j^{-2a}p_k^{-a})\left[\cos(2b\ln p_j)\cos(b\ln p_k)-\sin(2b\ln p_j)\sin(b\ln p_k)\right]+\cdots \quad (109)$$

All quantities in Eqs.(108) and (109) are real numbers. But $\sin(b\ln p_j)$ and $\cos(b\ln p_j)$ are not integers in general. They may even be irrational numbers which can not be represented by the addition, subtraction, multiplication and division of two integers. So these two formulas do not describe the relation between nature numbers and prime numbers.

The status of Eq.(108) and (103) are parallel, but they are obviously different. Eq.(101) was proved strictly by Euler. Eq.(108) was based on the complex continuation of Eq.(101) proposed by Riemann without any proof. Because Eq.(108) does not describe the relation between natural numbers and prime numbers, and contradicts with Eq.(103), it is meaningless. Eq.(109) has no basis and proof too. We has no reason to think it is correct.

Therefore, the complex continuation of the Euler formula of prime numbers has no meaning actually. The theory of prime numbers based on this formula can not be correct.

VIII. THE INFLUENCE ON THE PROBLEM OF THE RIEMANN HYPOTHESIS

8.1 The deductions of integral form of the Riemann Zeta function and the Zeta function equation

Based on the complex continuation form of the Gama function, Riemann deduced the integral form of Zeta function [1, 6]. Let $x\to nx$ in Eq.(22), the result is

$$\Gamma(s)=\int_0^\infty e^{-(nx)}(nx)^{s-1}d(nx)$$

$$=n^s\int_0^\infty e^{-nx}x^{s-1}dx \quad (110)$$

Taking the summation of Eq.(110), Riemann get

$$\left(\sum_{n=1}^\infty n^{-s}\right)\Gamma(s)=\sum_{n=1}^\infty\int_0^\infty e^{-nx}x^{s-1}dx=\int_0^\infty\left(\sum_{n=1}^\infty e^{-nx}\right)x^{s-1}dx \quad (111)$$

Then, Riemann used the following summation formula of series (The original paper of Riemann had not provided this formula but used it actually.) [8].

$$\sum_{n=1}^{\infty} e^{-nx} = e^{-x} + e^{-2x} + e^{-3x} + \cdots = e^{-x}\left(1 + e^{-x} + e^{-2x} + e^{-3x} + \cdots\right)$$

$$= \frac{e^{-x}}{1-e^{-x}} = \frac{1}{e^{x}-1} \tag{112}$$

By substituting Eq.(112) in Eq.(111), Riemann obtained

$$\left(\sum_{n=1}^{\infty} n^{-s}\right)\Gamma(s) = \int_0^{\infty} \frac{x^{s-1}}{e^{x}-1} dx \qquad \mathrm{Re}(s) > 1 \tag{113}$$

To calculate Eq.(113), Riemann extended the integral of real number x to the field of complex number with $z = x + iy \in C$ and defined the function $I(z)$

$$I(s) = \int_L \frac{(-z)^{s-1}}{e^{z}-1} dz \qquad \mathrm{Re}(s) \neq 1 \tag{114}$$

Eq. (114) is just the double complex continuation of Gama function. The definition domain of function $I(s)$ was extended into whole complex plane except at the point $\mathrm{Re}(s) = 1$, rather than original $\mathrm{Re}(s) > 1$.

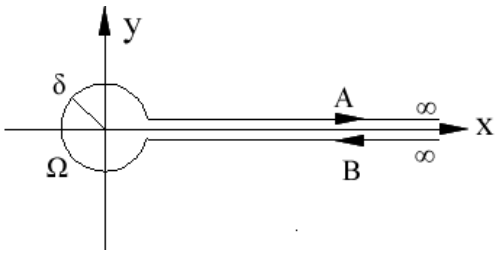

Fig. 2: The integral path of Riemann Zeta function

The path of integral started from $x \to \infty$ to $x = \delta$ along the straight line B under the x-axis. Here δ was a small quantity. Then the path was along the circle Ω with radius $\sqrt{x^2 + y^2} = \delta$ around the original point of the coordinate system. At last, the path was from $x = \delta$ to $x \to \infty$ along the straight line A above the x-axis.

According to Fig. 2, Eq.(114) contains three items.

$$I(s) = \int_{\infty}^{\delta} \frac{(-x)^{s-1}}{e^{x}-1} dx + \int_{\Omega} \frac{(-z)^{s-1}}{e^{z}-1} dz + \int_{\delta}^{\infty} \frac{(-x)^{s-1}}{e^{x}-1} dx \tag{115}$$

Riemann's paper provided the following result without concrete calculation [1]

$$I(s) = (e^{i\pi s} - e^{-i\pi s}) \int_0^{\infty} \frac{x^{s-1}}{e^{x}-1} dx \tag{116}$$

It indicated that Riemann assumed that the medium item on the right side of Eq.(115) was zero

$$\int_{\Omega} \frac{(-z)^{s-1}}{e^{z}-1} dz = 0 \tag{117}$$

By using the Euler's formula

$$\frac{e^{i\pi s}-e^{-i\pi s}}{2i}=\sin(\pi s) \tag{118}$$

and substituting Eqs.(116) and (118) in Eq.(113), the result was

$$I(s)=i2\sin(\pi s)\Gamma(s)\sum_{n=1}^{\infty}n^{-s} \tag{119}$$

By using the complementary formula of the Gama function

$$\Gamma(s)\Gamma(1-s)=\frac{\pi}{\sin(\pi s)} \tag{120}$$

and considering Eq. (114), Eq. (119) can be written as

$$\sum_{n=1}^{\infty}n^{-s}=\frac{I(s)}{i2\sin(\pi s)\Gamma(s)}=\frac{\Gamma(1-s)}{2\pi i}\int_{L}\frac{(-z)^{s-1}}{e^{z}-1}dz \tag{121}$$

Riemann used the method of contour integral and the residue theorem, and obtained the integral

$$\frac{1}{2\pi i}\int_{L}\frac{(-z)^{s-1}}{e^{z}-1}dz=2(2\pi)^{s-1}\sin\frac{\pi s}{2}\sum_{n=1}^{\infty}n^{-(1-s)} \tag{122}$$

Eq.(121) becomes

$$\sum_{n=1}^{\infty}n^{-s}=2(2\pi)^{s-1}\Gamma(1-s)\sin\frac{\pi s}{2}\sum_{n=1}^{\infty}n^{-(1-s)} \tag{123}$$

By considering the original definition of the Riemann Zeta function

$$\zeta(s)=\sum_{n=1}^{\infty}n^{-s}\qquad\zeta(1-s)=\sum_{n=1}^{\infty}n^{-(1-s)} \tag{124}$$

the Riemann Zeta function equation was obtained.

$$\zeta(s)=2(2\pi)^{s-1}\Gamma(1-s)\sin\frac{\pi s}{2}\zeta(1-s) \tag{125}$$

Eq.(125) describes the relation between $\zeta(s)$ and $\zeta(1-s)$. Then, Riemann introduced the transformation [1,4]

$$\xi(s)=\frac{1}{2}s(s-1)\pi^{-s/2}\Gamma\left(\frac{s}{2}\right)\zeta(s) \tag{126}$$

and proved the follow symmetry relation

$$\xi(s)=\xi(1-s) \tag{127}$$

Since the functions $\zeta(s)$ and $\xi(s)$ have the same zero, based on Eq.(126), Riemann proposed the hypothesis that all non-trivial zeros of Zeta function lie on the straight line of $s=1/2+ib$.

At present, it is generally believed that after the Riemann complex continuation, the right side of Equation (125) becomes a new definition of Zeta function, so the left side of Eq.(125) is no longer in the form of Eq. (124). However, this is not the case because to get Eq. (125) from Eq. (123), Eq. (124) must be used. It must be remembered that the prototype of Eq. (125) is Eq. (123). Equation (125) is only a symbolic simplified representation of Eq.(123). This is very important in the discussion of consistency problem of the Zeta function equation.

8.2 The problems existing in the Riemann's deduction of the Zeta function equation

There are many problems in Riemann's original paper in 1859 on the derivation of the Zeta function equation, which the author had discussed in detail in the paper [1]. The most critical one is that the middle term on the right side of Eq.(115) was missing. So Eq.(117) is not equal to zero in general. The calculation result is as follows

$$\int_{\Omega} \frac{(-z)^{s-1}}{e^{z}-1} dz \approx \frac{\delta^{a-1}}{a-1} \cos(\pi(a-1)) = \mathrm{Q}(\delta) \tag{128}$$

If $\mathrm{Re}(s) = a > 1$, when $\delta \to 0$, we have $Q(\delta) \to 0$, which is the result in the Riemann's original paper. However, if $\mathrm{Re}(s) = a \le 1$, when $\delta \to 0$, we have $Q(\delta) \to \infty$. The right side of Eq.(115) becomes infinite.

Therefore, the integral form of the Riemann Zeta function does not change the divergence of its series summation form. The Riemann Zeta function equation is meaningless in the field $\mathrm{Re}(s) = a \le 1$. Since the Riemann hypothesis involved the values at the points $\mathrm{Re}(s) = 1/2 < 1$, the result of Eq. (128) makes the Riemann hypothesis meaningless.

This result also explains why the two sides of the Riemann Zeta function equation (125) are inconsistent [2]. And why the Riemann hypothesis is so hard to be proved, because the Zeta function equation itself doesn't hold.

In the proof of Eq. (127), Riemann also used a formula of Jacobean function $\theta(x) = \sqrt{x}\theta(1/x)$. The formula is also tenable when $x > 0$. If $x = 0$, the formula doesn't make sense. So Eq.(127) is also problematic because the lower limit of integration is $x = 0$ in the calculation process, so this formula cannot be used [1].

In addition, there is another problem that has not been found in the author's paper [1]. Here is a supplement. To derive the formula (111), the order of integral sign and summation sign needs to be exchanged. The condition of interchangeability is that the integrated function is converges uniformly [9]. Since the lower limit of integral is zero, it leads to singularity. The integrated function can not be converges uniformly at point $x = 0$, so the integral sign and the summation sign in Eq. (111) cannot be exchanged. We have

$$\left(\sum_{n=1}^{\infty} n^{-s}\right)\Gamma(s) = \sum_{n=1}^{\infty}\left(\int_{0}^{\infty} e^{-nx} x^{s-1} dx\right) \neq \int_{0}^{\infty}\left(\sum_{n=1}^{\infty} e^{-nx}\right) x^{s-1} dx \tag{129}$$

Therefore, we can not obtain Eq.(113) form Eq.(111).

The key problem is caused by the use of summation formula (112), which is meaningless under

conditions $x=0$. However, the integral lower limit of the Zeta function is zero, which leads to the above problems and makes the Riemann Zeta function equation and the Riemann hypothesis meaningless.

8.3 The influence of the calculation in this paper on the Riemann Zeta function equation

The influences of the calculations in this paper on the Riemann Zeta function equation are below.

1. According to the calculation in Section 4.3, the single complex continuation of the Gama function is not an analytic function. Therefore, Eqs. (110) and (113) are practically meaningless.
2. Because Eq.(120) does not hold, we can not get Eqs.(122) and (123). Eq.(121) becomes

$$\sum_{n=1}^{\infty} n^{-s} = \frac{I(s)}{2i\sin\pi s\Gamma(s)} = \frac{\sin\pi a\Gamma(1-s)}{2i\pi e^{\pi b}\sin\pi s}\int_L \frac{(-z)^{s-1}}{e^z-1}dz$$

$$= \frac{\sin\pi a\Gamma(1-s)}{e^{\pi b}\sin\pi s} 2(2\pi)^{s-1}\sin\frac{\pi s}{2}\sum_{n=1}^{\infty} n^{-(1-s)}$$

$$= \frac{(2\pi)^{s-1}\sin\pi a\Gamma(1-s)}{e^{\pi b}\cos(\pi s/2)}\sum_{n=1}^{\infty} n^{-(1-s)} \tag{130}$$

Correspondingly, Eq.(125) becomes

$$\zeta(s) = \frac{(2\pi)^{s-1}\sin\pi a\Gamma(1-s)}{e^{\pi b}\cos(\pi s/2)}\zeta(1-s) \tag{131}$$

If we still use the transformation (126), the symmetry of formula (127) does not exist, there is no symmetry of formula (127), we have $\xi(s)\neq\xi(1-s)$. Because an infinite item is missing, Eq. (131) is still inconsistent and meaningless.

If the missing of the infinite large terms is not taken into account, we suppose that Eq. (131) is correct. According to the understanding of existing theory, the right side of Eq. (131) is regarded as a redefinition of the Riemann Zeta function, then we discuss its nontrivial zero problems.

According to the standard method proposed in the author's paper [2], the real and the imaginary parts on both sides of Eq.(131) are completely separated, then comparing them. It can be strictly proved with $\zeta(1-s)\neq 0$, so the zeros of Eq.(131) are located at the points satisfying $\sin\pi a=0$. They are $(k=0,\ \pm1,\ \pm2,\cdots)$

$$a=\frac{2k+1}{2}=\pm\frac{1}{2},\pm\frac{3}{2},\pm\frac{5}{2}\cdots \tag{132}$$

No matter whether they are nontrivial zeros or not, the Riemann hypothesis is proved untenable again.

IX. CONCLUSIONS

In this paper, it is proved that the negative continuation of the Gama function in the real number field is still infinite according to the direct continuation method. The reason is that the form of the Gama function has no any change in the extended field. The single complex continuation of the Gama function does not satisfy the Cauchy-Riemann equation, so it is not an analytic function. But the double complex continuation of the Gama function satisfies the Cauchy-Riemann equation, so it is an analytic

function. The complex continuation of the complementary formula of the Gama function is proved to be wrong, and the correct calculation result is given in this paper.

The paper also discusses the complex continuation of the Euler prime formula, and proves that the real part of the formula is different from the original Euler prime formula after the continuation. So it no longer represents the relationship between natural numbers and prime numbers. Therefore, the complex continuation of the Euler prime number formula is meaningless in mathematics. We can not discuss the distribution of prime numbers based on it.

At the end of this paper, we discuss the influence of the calculation results on the Riemann Zeta function equation and the Riemann hypothesis, and prove again that the Riemann hypothesis does not hold from another angle.

REFERENCES

1. Mei Xiaochun, The Inconsistency Problem of Riemann Zeta Function Equation, Mathematics Letters, 2019; 5(2): 13-22., doi: 10.11648/j.ml.20190502.11.
2. Mei Xiaochun, A Standard Method to Prove That the Riemann Zeta Function Equation Has No Non-Trivial Zeros, Advances in Pure Mathematics, 10, 8699. https://doi.org/10.4236/apm.2020.102006.
3. Guo, D.R. Method of Mathematics and Physics, High Education Press, Beijing, 1965, P.109.
4. Liang Kunmiao, Mathematics Physics Method, People's Education Press, 1979, p. 554.
5. Ru Changhai, The Riemann Hypothesis, Qianghua University Publishing Company, 2016, p.61, 52, 192.
6. Bent E. Petersen, Riemann Zeta Function, https://pan.baidu.com/s/1geQsZxL.
7. Mathematics Handbook, Scientific Publishing House, 1980, p. 144.
8. Neukirch, J., Algebraic Number Theory, Springer, Berlin, Heidelberg, 1999 .
9. Fei Liwen, Typical problems and methods in mathematical analysis, High Education Press., 2018, P.563.

This page is intentionally left blank

Einstein's Time Synchronization Versus Special Relativity Postulates

Steven D. Deines

ABSTRACT

One fundamental principle of physics is all observers concurrently measuring the output of an experiment must have identical or equivalent results, especially when the recorded data are transformed to one inertial frame. Einstein claimed that the one-way time interval using light from one end of a uniformly moving rod to the other end was equal to half of the roundtrip for light originating from the rod's end and reflecting from the other end toward the origination, forming Einstein's time synchronization method. For an observer stationary relative to the rod, light traverses one rod length in either direction with equal transmission time intervals between ends. For an external inertial observer monitoring the one-way distances, light traverses a longer distance than the rod length to overtake the receding end and a shorter distance when intercepting the approaching end, making the total roundtrip greater than two rod lengths. The roundtrip distance increases with a faster uniformly moving rod.

Keywords: length contraction, time dilation, time synchronization, light speed, special relativity, Michelson-Morley interferometer, and Kennedy- Thorndike test.

Classification: FOR CODE: 240599

Language: English

London Journals Press

LJP Copyright ID: 925652
Print ISSN: 2631-8490
Online ISSN: 2631-8504

London Journal of Research in Science: Natural and Formal

Volume 21 | Issue 2 | Compilation 1.0

Einstein's Time Synchronization Versus Special Relativity Postulates

Steven D. Deines

ABSTRACT

One fundamental principle of physics is all observers concurrently measuring the output of an experiment must have identical or equivalent results, especially when the recorded data are transformed to one inertial frame. Einstein claimed that the one-way time interval using light from one end of a uniformly moving rod to the other end was equal to half of the roundtrip for light originating from the rod's end and reflecting from the other end toward the origination, forming Einstein's time synchronization method. For an observer stationary relative to the rod, light traverses one rod length in either direction with equal transmission time intervals between ends. For an external inertial observer monitoring the one-way distances, light traverses a longer distance than the rod length to overtake the receding end and a shorter distance when intercepting the approaching end, making the total roundtrip greater than two rod lengths. The roundtrip distance increases with a faster uniformly moving rod. Length contraction from special relativity undercompensates for this extra distance. Assuming a universal speed of light, theory predicts unequal transmission intervals for the external inertial observer witnessing the uniformly moving rod. In all ultraprecise lab measurements, the observed light speed is the same quantity and satisfies Einstein's time synchronization convention when the distance between the light source and detector is always fixed. For the external observer to witness the same output as the observer fixed with the rod, light must obey vector velocity addition for the external observer to have equal transmission time intervals over both directions (as required by Einstein's time synchronization convention) and measure the standard speed of light between the ends of the uniformly moving rod. The Laser Interferometer Gravitational-Wave Observatories (LIGO) consortium verifies these conditions as the ends of each LIGO arm move at different velocities due to Earth's rotation, making all one-way light paths different in inertial space, yet null results are output for all observers, whether accelerated on Earth's surface or in an inertial reference frame.

One key equation in the evaluation corrects a mathematical error in the distance that light traverses toward an approaching object in five previous papers by the author. An appendix in this paper contains the errata to correct the corresponding equations and replaces inaccurate summaries to correct the results and conclusions in those five papers.

Keywords: length contraction, time dilation, time synchronization, light speed, special relativity, Michelson-Morley interferometer, and Kennedy-Thorndike test.

Author: Donatech Corporation, Inc., Fairfield, Iowa USA.

I. EINSTEIN'S TIME SYNCHRONIZATION AND RELATIVITY PRINCIPLE

In his groundbreaking 1905 manuscript on special relativity, Einstein defined his concept of time synchronization in the first section of that paper. He first illustrated the time of an event is always a judgment of simultaneous events. In his example, "The pointing of the small hand of my watch to 7 and the arrival of the train are simultaneous events", meaning "That train arrives here at 7 o'clock." He further emphasized, "It might appear...the definition of 'time' can be overcome by substituting 'the position of the small hand of my watch' for 'time'." [1, §1, lines 15-20]. What he

London Journal of Research in Science: Natural and Formal

meant is that within an acceptable neighborhood encompassing both the train and pocket watch, the train arrived at 7 o'clock, else the train would crush the pocket watch upon arrival. An observer at point A can time events in the immediate vicinity of A by coordinating the positions within the neighborhood of the clock as being simultaneous. If a remote location at point B is far outside of the neighborhood of A, then time recorded by an identical clock near B would indicate for an observer at B the timed events in the immediate neighborhood of B. Einstein stated it is impossible without further definitions to compare 'A time' with 'B time', because there is no master time or common time between A and B. Surprisingly, Einstein made the following claim without evidence, "The latter time can now be defined by requiring that *by definition*[1] the 'time' necessary for light to travel from A to B be identical to the 'time' necessary to travel from B to A. Let a ray of light start at the 'A time' t_A from A toward B, let it at the 'B time' t_B be reflected at B in the direction of A, and arrive again at A at the 'A time' t'_A. The two clocks run in synchronization by definition if

$$t_B - t_A = t'_A - t_B. \qquad (\S1.1)$$

We assume this definition of synchronization to be free of any possible contradictions applicable to arbitrarily many points." [1, §1, lines 41-48]

"In addition, in agreement with experience we further require that the quantity

$$\frac{2AB}{t'_A - t_A} = c \qquad (\S1.2)$$

be a universal constant (the velocity of light in empty space)." [1, §1, lines 61-63]

This is known as the Einstein synchronization convention, which assumes that the one-way time of transmission of light is the average of two transmission intervals from A to B and from B to A. The immediate equation above defines c as a constant, which is also the average roundtrip velocity between A and B. As shown later in this paper, there is a contradiction between an external inertial observer recording light bouncing between points A and B of a rod moving at a constant velocity and another observer stationary relative to that rod. It is important to know that this synchronization process has no verified, empirical data to support this assumed convention. It is simply a stipulation that alludes to one's experience, which often is misleading using casual observations. For example, it has taken millennia to refute the illusion that Earth is the center of the universe, as the cosmos always appears to rotate around us without noticeable vibrations. Equation §1.1 is Einstein's stipulation that light transmission is the same in either direction, but the roundtrip excursion can be the same if light's velocity is $c/2$ in one direction and infinite on the return, or infinite in the initial direction and $c/2$ on the return, or anything between [2]. Einstein chose this option that the transmission interval of light between A and B is identical in either direction with no evidence to justify his choice. He later wrote, "That light requires the same time to traverse the path $A \rightarrow M$ as for the path $B \rightarrow M$ is in reality neither a supposition nor a hypothesis about the physical nature of lights, but a stipulation which I can make of my own freewill in order to arrive at a definition of simultaneity." [3, page 27] So, Einstein's synchronization convention is very subjective and must be scrutinized.

Another problem is Einstein often equated simultaneity and synchronization, which are not identical. The author defines simultaneity as two or more phenomena that either split, divide, separate, etc., or merge, collide, overlap, join, mix, fuse, coalesce, unite, combine, etc. at one point at one instant of time. An observer is effectively a point in space. So, communications of events arriving at the same time instant at the observer's location are simultaneous for that observer. Einstein required that a clock is needed to assign a time at the coordinate position within some acceptable neighborhood for all phenomena in that neighborhood (i.e., coordinate time). To make any meaningful timescale for all such clocks

[1] Original italics implying a convention: Die letztere Zeit kann nun definiert werden, indem man *durch Definition* festsetzt, daß die „Zeit", welche das Licht braucht, um von A nach B zu gelangen, gleich ist der „Zeit" welche es braucht, um von B nach A zu gelangen.

within the domain of a reference frame, those clocks must be synchronized to a master clock, preferably using light to communicate the time tags between clocks. Einstein required that the interval to transmit time from *A* to *B* be the same from *B* to *A* for synchronizing clocks to a master timepiece for a standard timescale. The author defines synchronization as two or more separated events or phenomena as having the same coordinate time at different locations. Much like a team competes in synchronized swimming, the parallel actions do not interfere between team members. Such competitions are not called simultaneous. An example of a simultaneous event is the collision of two cars in an intersection. All observers witness this event as simultaneous, whether they are stationary, move at a uniform velocity, or accelerate relative to the intersection. All such observers saw by way of light and heard by way of sound the simultaneous collision of vehicles. This underscores the most fundamental principle of physics: all observers concurrently measuring the output of an experiment must have identical or equivalent results, especially when the recorded data are transformed to one reference frame. Even in a court of law, all credible witnesses of an event testify to the same outcome. A corollary to this fundamental principle is that any theory failing to predict the same outcome for all observers concurrently witnessing an event is inconsistent and needs revision.

Einstein tried to demonstrate that a simultaneous event in one inertial frame is not necessarily simultaneous in another inertial frame [3]. He considered a thought experiment where two lightning strikes hit points *A* and *B* synchronously on the ground equidistant from a ground observer and a train passenger collocated at a midpoint *M* (i.e., both observers are located on the perpendicular bisector to the line *AB* with the ground observer abreast with the train passenger at the instant of the lightning, but the passenger is moving at a constant velocity). Einstein did not consider the physical limitations of the human eye, because the standard frame rate of movies is 24 per second. One can embellish the thought experiment with ultrahigh speed video cameras and attachments to serve as suitable observers recording the events. All railcars can be equipped with synchronized clocks, lightning rods and cables touching the rails to conduct the lightning into the ground. On the ground, there are synchronized clocks beside tall lightning rods at *A* and *B*. The train is moving at a constant velocity *V* in a direction parallel from *A* to *B*. One lightning bolt branched to strike lightning rods at *A* and *A′* simultaneously (i.e., lightning rod *A* stands on the ground and *A′* is on the railcar, but both are in the same neighborhood), and another bolt hits both lightning rods of *B* and *B′* simultaneously. The times of the ground clocks and train clocks were recorded when current in the cables conducted electricity into the ground, and the comparison reveals that the twin lightning bolts occurred synchronously (i.e., same coordinate time) between *A* and *B* and between *A′* and *B′*. The ground camera at *M* records simultaneous reception of light from *A* and *B*, but in the finite time for light to traverse toward *M*, which would be in microseconds, the camera located at *M′* on the train has moved slightly closer to *B*, causing the moving camera to record light from *B′* sooner than *A′*. Einstein considered the twin bolts to strike simultaneously in the ground frame, not synchronously, because the distances traversed were identical and, with a constant light speed, the ground observer saw simultaneous light from both bolts at *M*. In the train, Einstein considered the train observer still saw light from *B* earlier than *A*, but with equal distances of *A′M′* and *B′M′* and a constant light velocity of c, Einstein inferred the train observer must decide that the bolt struck *B′* sooner than the bolt at *A′*. Thus, Einstein concluded this demonstrated that events may be simultaneous in one inertial frame and not in another inertial frame [3]. He did not have a rigorous definition for simultaneous and overlooked another possibility. His inference that the train observer concludes the bolt struck *B′* sooner than the bolt at *A′* contradicts his initial requirement that both bolts struck synchronously. The alternate explanation is the effective light speed (and sound speed) is faster because the train observer is moving toward the lightning bolt (and thunder) from *B* and receding from the *A* bolt, which creates a slower net velocity. His dual lightning strike illustrates the net velocity of light

obeys vector addition of velocity between the source and observer.

Einstein never explained how this paradox occurs in select frames. In this embellished version, both cameras are identically at the midpoint at the onset of the dual lightning strikes. In the ground frame, the ground camera at M records simultaneous reception of lightning. With still air, the camera also records audio that would register simultaneous sounds of thunder. The train camera at M' moved toward B while light approached the train's camera. This camera will record light from B' sooner than A' as well as thunder from B' before recording thunder from A'. However, in the inertial train frame, the equal distances of $A'M'$ and $B'M'$ are maintained, and an examination of the time logs would show the dual lightning strikes occurred synchronously by the train clocks. Even length contraction of both $A'M'$ and $B'M'$ would still maintain equal distances. Time dilation would only make the train clocks mutually slower than the ground clocks, but it would not disturb the synchronization between the train clocks. With a universal light speed for all inertial frames, theory would predict simultaneous reception for the train camera at M'. This contradiction implies one or more assumed concepts may be incorrect. This thought experiment is a precursor for examining whether Einstein's stipulated clock synchronization procedure and assumed relativity postulate are consistent or contradictory. In any case, physics is the science that explains how nature operates with the goal of combining similar phenomena under one explanation.

II. EINSTEIN'S THOUGHT EXPERIMENT: REFLECTING LIGHT BETWEEN ROD ENDS

Einstein defined his second postulate of relativity, "Any ray of light moves in the 'resting' coordinate system with the definite velocity c, which is independent of whether the ray was emitted by a resting or by a moving body. Consequently, velocity = (light path)/(time interval) where time interval is to be understood in the sense of the definition in §1. Consider a rigid rod at rest whose length is L when measured by a measuring rod which is also at rest. We now imagine the axis of the rod lying along the x-axis of the resting coordinate system, and that a uniform motion of parallel translation with velocity v along the x-axis in the direction of increasing x is then imparted to the rod. [1, §2, lines 10-17]...We imagine further that at the two ends A and B of the rod, clocks are placed which synchronize with the clocks of the resting system—that is, that their indications correspond at any instant to the 'time of the resting system' at the places where they happen to be. Consequently, these clocks are 'synchronous in the resting system'. We imagine further that with each clock there is a moving observer, and that these observers apply to both clocks the criterion established in §1 for the synchronization of two clocks. Let a ray of light depart from A at the time t_A, let it be reflected at B at the time t_B, and reach A again at the time t'_A. Taking into consideration the principle of the constancy of the velocity of light, we find that

$$t_B - t_A = \frac{r_{AB}}{c-v} \text{ and } t'_A - t_B = \frac{r_{AB}}{c+v}$$

where r_{AB} denotes the length of the moving rod—measured in the resting system. Observers moving with the moving rod would thus find that the two clocks were not synchronous, while observers in the resting system would declare the clocks to be synchronous." [1, §2, lines 41-54].

Einstein's formula produces (time interval) = (light path)/c. The following analysis will determine the path length that light with its finite velocity c took to overtake the receding end B of the moving rod and the path length to intercept the approaching end A after reflecting from B. It is emphasized here that simultaneous events in one reference frame transform to equivalent coordinate points and time instants in another reference frame. In Einstein's thought experiment, the light leaving A at the instant t_A is a simultaneous event (i.e., atoms located in the neighborhood of A emit photons at one instant of time, separating a photon from an atom), which is a single point at an instant of time in mutually overlapping reference frames. The reflection of light at B is also simultaneous, as it is the absorption and emission of photons with atoms of

the reflective surface in the neighborhood of B occurring at a point in a virtual instant of time. There are two observers: one fixed relative to the rod moving at a uniform velocity $v < c$ along the positive x-axis of the stationary frame and the other observer fixed in the stationary frame. Let the moving rod be attached to an inertial laboratory frame. The laboratory observer measures a rod of length, L, for the one-way light path, calculates the roundtrip light path is $2L$, and determines that the time interval of $A \rightarrow B$ is the same as $B \rightarrow A$ when light speed has a fixed velocity, which conforms to Einstein's synchronization convention. The transformation between the laboratory frame and the stationary frame is a simple Galilean conversion, which is $x' = x_o + v(t - t_o)$, $y' = y$, $z' = z$, and $t' = t - t_o$ where the primed terms apply to the laboratory frame and unprimed terms apply to the stationary frame.

In the stationary frame, the light paths will be derived for the separate legs of $A \rightarrow B$ and $B \rightarrow A$. This is identical to Zeno's paradox of Achilles and the tortoise, who convinced Achilles that he would always be behind the tortoise after a head start, even after an infinite number of time intervals elapsed, implying Achilles would never catch up to the tortoise and would lose the race. The ancient Greek mathematicians did not understand that a finite time interval could be divided into an infinite number of subintervals, allowing Achilles eventually to overtake the tortoise and win the race. Similarly, a light beam emitted at A in the stationary frame overtakes the receding end of the moving rod, B, at some point B' in the stationary frame. Assume the speed of light is c in the stationary frame. When the emitted beam travels the distance L over the time interval L/c, the receding rod end, B, has traveled a further distance, $\xi(1)$. When that beam travels the extra distance $\xi(1)$, B has moved a further distance $\xi(2)$ over the same time interval of $\xi(1)/c$. Over n repetitions of this, the rod moved a distance of $L + \xi(1) + \xi(2) + \ldots + \xi(n)$ where $\xi(1) = v \times (L/c)$ and $\xi(i+1) = v \times \xi(i)/c$. Substitute the individual terms with $v < c$, and the series is:

$$L + v\frac{L}{c} + v\frac{\frac{Lv}{c}}{c} + \cdots + v\frac{\frac{Lv^{n-1}}{c^{n-1}}}{c} =$$
$$L + L\frac{v}{c} + L\frac{v^2}{c^2} + \cdots + L\frac{v^n}{c^n} = \frac{L(1-v^n/c^n)}{1-v/c}$$

$$L_{\rightarrow} = \lim_{n\to\infty} \frac{L(1-v^n/c^n)}{1-v/c} = \frac{L}{1-v/c} = \frac{cL}{c-v} > L \qquad (1)$$

This is the length of the light path to intercept the receding end of the moving rod, B, at some point B' in the stationary frame. After reflection, the beam travels a shorter distance than L as the rod end, A, approaches it. Note that the velocity of the reflected beam is opposite the direction of the moving rod, so that the ratio of v/c is negative. Substitute this into the series (1) to find the distance from B' to intercept the rod's A end at A' in the stationary frame using v and c as speeds.

$$L - L\frac{v}{c} + L\frac{v^2}{c^2} - \cdots + (-1)^n L\frac{v^n}{c^n} = \frac{L(1-(-1)^n v^n/c^n)}{1+v/c}$$

$$L_{\leftarrow} = \lim_{n\to\infty} \frac{L(1-(-1)^n v^n/c^n)}{1+v/c} = \frac{L}{1+v/c} = \frac{cL}{c+v} < L \qquad (2)$$

The roundtrip light path in the stationary frame is

$$L_{\rightarrow} + L_{\leftarrow} = \frac{cL}{c-v} + \frac{cL}{c+v} = \frac{2L}{1-\frac{v^2}{c^2}} > 2L \qquad (3)$$

Algebra can verify (1) and (2). Solve for D in $D/v = (L+D)/c$ and replace it in $L_{\rightarrow} = L+D$, where D is the distance in the stationary frame that end B of the rod moved until light from end A intercepted B. Similarly, solve d in $d/v = (L-d)/c$ to substitute in $L_{\leftarrow} = L-d$ where d is the distance in the stationary frame that end A of the moving rod advanced toward the light reflected from end B until interception. Define $\gamma = (1-v^2/c^2)^{-0.5}$. Then (3) in the stationary frame has a roundtrip path of $2\gamma^2 L$. If one invokes length contraction from special relativity because the rod is moving, then length contraction replaces L as L'/γ, resulting in the roundtrip path of $2\gamma L'$ for the stationary observer versus $2L$ for the laboratory observer. This still does not resolve the disparity in the magnitude of the light paths predicted in the laboratory or stationary frames. The Lorentz transformation for length converts L in the laboratory frame to L/γ, which predicts equal lengths for light to travel $A \rightarrow B$ and $B \rightarrow A$. However, the stationary observer records that $L_{\rightarrow} > L_{\leftarrow}$, a difference of

$$L_{\rightarrow} - L_{\leftarrow} = \frac{cL}{c-v} - \frac{cL}{c+v} = \frac{2vcL}{c^2-v^2} > 0 \qquad (4)$$

This result is a major discrepancy between observers. These are simultaneous events when the observers concurrently witness the phenomena. Light is emitted from its light source at A, which is common to both laboratory and stationary frames. Light is reflected at B in the laboratory frame and at B' in the stationary frame (i.e., photons are absorbed and then emitted in the opposite direction by the atoms on the reflecting surface at the virtual point in either frame according to Snell's law). Finally, the light beam is absorbed at the rod's end at point A in the laboratory frame, which must be the same point location as A' in the stationary frame. The roundtrip light paths measured precisely in both frames are not equal, especially after all measurements are transformed to a common reference frame. The corollary from the fundamental principle of concurrent observation reveals some theoretical concepts are inconsistent and need updating.

As cited above, Einstein believed his dual lightning test demonstrated simultaneity for the ground observer, but nonsimultaneity for the train observer, who would conclude lightning at B struck earlier than lightning at A. [3, p. 30], which contradicts the test requirement that both strikes occurred synchronously in both frames. For example, a pedestrian standing on the corner of an intersection witnesses two cars collide upon entering an intersection simultaneously, but a moving driver approaching the intersection reports nonsimultaneous entry of the two cars, which results in no collision. This is absurd, and the corollary requires some theoretical concept must be revised. Einstein never included criteria showing which inertial observers concurrently witness synchronized or nonsynchronized events. Einstein's concepts of simultaneity and universal light speed are imprecise or inconsistent, which is unacceptable for rigorous physics experimentation.

The speed of light cannot be the universal value of c, as the transmission intervals along the moving rod are unequal in the stationary frame, but equal in the inertial laboratory frame fixed with the moving rod. Simply divide c into $L_{\rightarrow}$ and $L_{\leftarrow}$, getting unequal results that violate the synchronization convention. On closer examination, two different sets of photons are involved with this thought experiment. One set of photons is emitted from end A, traveling parallel with the moving rod to end B until absorption by the atoms of the reflective surface at end B. The other set of photons are emitted by the reflective atoms at end B, moving antiparallel to the moving rod until absorbed by the atoms at end A. Because two different sets of photons are involved, designate $c_{\rightarrow}$ for the light speed from $A \rightarrow B$ and $c_{\leftarrow}$ for light speed moving $A \leftarrow B$. However, the stationary observer can synchronize identical clocks at points A' and B' to match the master clock A^* before the test (A^* is collocated at the rod's A at $t_o = 0$). Attach two identical clocks to the ends of the rod (i.e., the rod's A and B) and set those two clocks to match the master time t at A^* in the stationary frame (e.g., $t_o = 0$ in the Galilean transformation). Impart a velocity v to the rod and the laboratory fixed with the rod. As required by Einstein's synchronization convention, the transmission intervals for light to travel $A \rightarrow B$ and $B \rightarrow A$ in the laboratory frame must be equal using the clocks at the ends of the rod. The stationary observer compares the times of the clocks when B of the rod is at B' and later when the rod's point A is at A'. As stipulated by Einstein, if a clock at B is synchronized to a clock at A, then the clock at A is synchronized to the clock at B, and if a clock at A is synchronized to clocks at B and at C, then the clocks at both B and C are synchronized with each other [1, §1, lines 50-53]. The stationary observer records equal time intervals of transmission for the two separate legs with $A^* \rightarrow B'$ and $B' \rightarrow A'$, as all five clocks are synchronized. The formula is (time interval) = (light path)/(light speed), and the two legs defined by a moving rod have unequal light paths in the stationary frame, yet the time intervals of transmission are equal.

To resolve this apparent dilemma, rewrite (1) and (2) for the light paths with the generalized light speeds where $c_{\rightarrow}$ is parallel to the rod's velocity in the initial traverse and $c_{\leftarrow}$ is antiparallel in the reflected traverse .

$$L_{\rightarrow} = \frac{c_{\rightarrow} L}{c_{\rightarrow} - v} > L \qquad (1')$$

$$L_{\leftarrow} = \frac{c_{\leftarrow} L}{c_{\leftarrow} + v} < L \qquad (2')$$

Divide by the appropriate light speed for that leg of the roundtrip into the light path and equate the time intervals as required by Einstein's time synchronization equation §1.1.

$$t_B - t_A = \frac{L}{c_{\rightarrow} - v} = \frac{L}{c_{\leftarrow} + v} = t'_A - t_B \qquad (5)$$

Equation (5) is valid only if the denominators are identical, nonzero constants and light speed varies. This means $c_{\rightarrow} = c + v$ and $c_{\leftarrow} = c - v$ with c being a nonzero constant. When the laboratory observer is fixed relative to the light source, then the speed of light is apparently constant in the laboratory frame as $v = 0$. In the stationary frame, the stationary observer records different light paths and different light speeds such that the time of transmission is the same for either leg. Thus, light's speed obeys the magnitude of vector velocity addition.

The speed of light in a vacuum could not be a universal constant for inertial frames by comparing the synchronization convention against an assumed constant light speed. Even special relativity can not transform a measured speed of light in one inertial frame into the same numerical quantity in another inertial frame that has a uniform velocity relative to the first frame. Let the numerical value of c be 299792458 m/s in the stationary frame. Before measuring light, the laboratory is at rest in the stationary frame, so that the laboratory has an identical meter standard and a synchronized clock maintaining the second as the stationary observer's master clock. Accelerate the laboratory to a fixed velocity so that the laboratory observer can concurrently measure light speed with the stationary observer. According to special relativity, the moving observer has a shorter meter for length and a longer second for time (i.e., $\Delta L_S = \gamma \Delta L_{Lab}$ and $\gamma \Delta \tau_S = \Delta \tau_{Lab}$). The Lorentz transformation would cause concurrent measurement of light speed in different inertial frames to be:

$$c_{Stationary} = (c)\frac{meter}{second} = \left(\frac{\#\ length\ units}{1\ time\ unit}\right) \times \frac{\gamma \Delta L_{Lab}}{\Delta \tau_{Lab} / \gamma}$$

$$= (c\,\gamma^2)\frac{\Delta L_{Lab}}{\Delta \tau_{Lab}} = \left(c'\right)\frac{\Delta L_{Lab}}{\Delta \tau_{Lab}} = c_{Lab} \qquad (6)$$

Numerically, $c = c_{Stationary} \neq c_{Lab}$ as $\gamma > 1$. For example, light speed is now defined as 299792458 m/s, which can be converted into yards/minute where yard < meter (illustrating length contraction) and a minute > second (demonstrating time dilation). In this example, the laboratory's numerical number is larger than the standard c number. According to special relativity and with today's high precision in metrology, some variation in the numerical value of light speed should be observed in a laboratory by varying velocity as Earth rotates and revolves about the Sun relative to outer space. Again, light speed appears constant only if the observer is fixed relative to the source of light (i.e., $\gamma = 1$ if $v = 0$) and if light's velocity obeys vector addition of velocity.

The clock synchronization convention is only valid when the distance between remote clocks remains constant during the calibration. Einstein assumed a constant r_{AB} between clocks on the moving rod during the whole synchronization process. In the example of a stationary observer with a master clock at A^* in the stationary frame (i.e., colocation of the moving rod's A at $t = 0$) and the clock at B on the moving rod, it would be impossible to calibrate clock B using the synchronization convention when the distance changes between A^* and B during a light transmission.

III. EXPERIMENTAL EVIDENCE FOR LIGHT'S CHANGING VELOCITY

The previous section theoretically demonstrates that light's speed obeys the magnitude required in vector velocity addition, which also mandates that photons must move in the required direction.

A simple test would demonstrate that emitted photons acquire the added velocity in the direction supplied by the photon emitter. Set a laser to point horizontally at a partially silvered mirror that is angled at 45 degrees relative to the

local plumb line. The reflected beam is aimed vertically to a hemisphere mirror that is a distance, d, of about 10 meters above the partially silvered mirror, so that the hemisphere is centered along the light beam. The vertical beam is reflected from the hemisphere of 2 cm radius, r, to the partially silvered mirror below, and some light is transmitted through it to the floor below. Observe if the impact point varies over time as Earth rotates. If there is a sideway displacement of the vertical light path due to the velocity $\boldsymbol{v}$ of Earth around the Sun, the beam should miss the nadir of the hemisphere mirror by an angle of $\theta \approx sin(\theta) = v\Delta t/r = vd/(cr)$ in radians. The reflected beam from the hemisphere mirror should touch the floor about $d\ \theta$ = 50 cm from the plumb line assuming $v \approx 30000$ m/s for Earth's orbital velocity. Even assuming the orbital speed is 15000 m/s from the cosine projection onto the 10 m arm, this would still cause a 25 cm displacement from the plumb line. If no noticeable displacement from the vertical plumb line over a day is detected within the laboratory frame fixed on Earth, this demonstrates that photon velocity obeys angular vector direction in some stationary frame fixed in outer space. In the elapsed time that photons move from the hemisphere mirror to the floor, Earth's revolution has displaced the floor in a varying direction relative to the initial plumb line in the external inertial frame and imparts a varying distance to the floor (like the moving ends of the rod previously discussed). As multiple photons over hours keep impacting the same point on the floor, this demonstrates that the light source (e.g., the hemisphere mirror) imparts an additional vector velocity to the photons in the external inertial frame while the floor is fixed relative to the hemisphere mirror.

Such a null result has been demonstrated repeatedly with the Michelson-Morley interferometer tests with equal arms and Kennedy-Thorndike interferometer tests with unequal arms. Einstein never published any analysis of the Michelson-Morley experiment, even in his book, which he deferred to Lorentz, who "showed that the result obtained at least does not contradict the theory of an aether at rest". [3, p.168] "Lorentz and FitzGerald rescued the theory from this difficulty by assuming that the motion of the body relative to the aether produces a contraction of the body in the direction of motion, the amount of contraction being just sufficient to compensate for the difference in time mentioned above." [3. p. 59] During any interferometer testing, no one has reported that one beam moved off the reflection mirror or the recombination point.

The problem with the analysis that Lorentz and others ignored is there are two components of velocity, V_x and V_y, parallel respectively to the x-axis and y-axis of an interferometer—not just one component velocity—after combining all velocities of the laboratory relative to the cosmos. Define γ_x using the velocity V_x, and γ_y using V_y, and define L_x for the length of the x-axis arm and L_y for the y-axis arm. The Lorentz analysis works if $V_y = 0$ so that $\gamma_y = 1$. In general, $V_y \neq 0$ so that $L_x = \gamma_y L_x'$, which undermines the Lorentz analysis that requires the x-axis arm to remain at length L_x, not the shorter L_x'. Comparing the unequal roundtrip paths over both arms and the assumed constant speed of light, special relativity would predict destructive interference, contrary to the observations [4].

The most sensitive version of the Michelson-Morley interferometer is the Laser Interferometer Gravitational-Wave Observatory (LIGO), which two observatories are located near Hanford, Washington, and Livingston, Louisiana. Both have 4 km long arms within nearly perfect vacuum chambers allowing laser beams to detect gravity waves. Virgo is a similar observatory in Italy that has recently joined the search for gravitational waves. LIGO uses a continuous laser beam that is amplified from 40 watts to 750 watts with power reflecting mirrors. LIGO has enhanced vibration absorption mechanisms to remove ground vibrations, tremors, solid Earth tides, etc. to isolate the signals. To increase the arm lengths from 4 km, Fabry-Perot cavities are installed near the beam splitter and near the hanging reflection mirror at the end of each arm so that 300 reflections inside the cavities increase the effective arm length to almost 1200 km. A virtually perfect vacuum is maintained so that any gaseous molecule is removed promptly to avoid

interference or extraneous reflections with the light beams. Also, one of the split signals is inverted to create complete destructive interference when recombining the two beams [5]. The original Michelson-Morley interferometer produced constructive interference, but this enhancement allows far easier detection of any light against an absolute black background, while it is hard to detect any light variation against a bright background, much like the inability to see sunspots when looking at the Sun. "At its most sensitive state, LIGO will be able to detect a change in distance between its mirrors 1/10,000th the width of a proton." [5]

The following table lists the locations in latitude and longitude of each observatory and the azimuths of each observatory's x-axis and y-axis relative to due east in a counterclockwise direction [6]. No altitude was listed, and no map datum was defined. So, a precise calculation to determine the actual radius of latitude for each arm end is not possible.

Table 1: Directional Azimuths of LIGO Axes.

Observatory	Latitude	Longitude	Azimuth (x-axis)	Azimuth (y-axis)
Hanford	46°27′19″N	119°24′28″W	126°	216°
Livingston	30°33′46″N	90°46′27″W	198°	288°
Virgo	43°37′53″N	10°30′16″E	71°	161°

At each observatory, the x-axis and y-axis arms are joined at a common point where the laser light is split. The reflecting mirror at the opposite end of either arm is suspended on cables. Designate A for the common point of the arms, B for the end of the x-axis arm, and C for the end of the y-axis arm. The LIGO observatories are stationary in the Earth-Centered, Earth-Fixed (ECEF) frame. Consider a sufficiently inertial frame that is freely falling with Earth's center of mass, but without rotation. Let R_A, R_B, and R_C be the radii of the latitude circles through the respective A, B, and C points of the arms. The Earth's rotation, ω, imparts a tangential velocity to the ends of the arms that is ωR_i in the falling frame. The event of splitting the light beam at point A, the event of light touching and reflecting off the mirror at point B, the event of light touching and reflecting off the mirror at point C, and the event of combining the two beams at point A occur at different instances of time. These are four separate simultaneous events seen by the ECEF observer on Earth's surface and by the observer fixed in the falling frame.

The combined beams arrived simultaneously at A with complete synchronization (i.e., destructive interference due to one beam being inverted). The output is witnessed by both observers to be the same. All LIGO observatories are currently in the northern hemisphere. Note that the ECEF observations are accelerated due to Earth's rotation, but the output is the same as if the ECEF frame was nonrotating. Photons emitted by atoms at points A, B, and C travel at their initial speed, due to nearly perfect vacuum in the tunnels. Any arm with an azimuth less than 180 degrees will have point A as the southernmost point and B or C as the northernmost. If the azimuth is between 180 and 360 degrees, then B or C is the southernmost and A is the northernmost point. Each arm is displaced eastward due to Earth's rotation. As derived in equations (1′) and (2′) for the moving rod, the endpoints of the arm are displaced by the cosine projection of the tangential velocity multiplied by the time of transmission of light over the arm. In the freely falling frame, the photons traverse the arm in the one-way distance of $cL/[c \mp \omega R_i \cos(\text{azimuth})]$ where i represents A, B, or C for the photons emitted at A, B, or C, and $\mp$ is chosen as photons move parallel or antiparallel in the arm. The light speed can not be a constant c in the falling frame for the LIGO observatories and still combine light beams at A to be synchronized with equal times of roundtrip transmission. All one-way distances for both x-axis and y-axis arms are unequal in the nonrotating frame and the tangential velocities are unequal (i.e., $\omega R_A \neq \omega R_B$, $\omega R_B \neq \omega R_C$, and $\omega R_A \neq \omega R_C$ because the latitudes of the endpoints are different). The theory only agrees with the observed complete synchronization of the merged beams at A when light speed obeys addition of vector velocities where photon velocity equals the

standard velocity of light plus the velocity of the light source (i.e., $c' = c \pm v$ in (1′) and (2′)).

If light obeys vector velocity addition, then a different interpretation of the Sagnac effect is needed. Light is inserted into a ring interferometer and splits in opposite directions at entry. The beams exit the ring at the entry point and undergo interference. The destructive interference determines how much the ring interferometer rotated after the beams were split. The diagram on the left of Figure 1 [7] shows a nonrotating ring of radius R would output constructive interference as each beam would travel the same length of $2\pi R$ and exit at the same time. If the ring interferometer rotated as shown on the right side of Figure 1, one beam would travel further than the other, so both beams would exit with destructive interference.

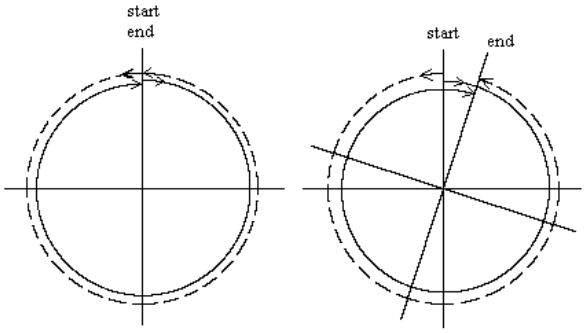

Figure 1: Sagnac effect in circular loops

It is easy to see as an external observer that one beam takes a longer trip than the oppositely traveling beam when the interferometer rotates. The rotating interferometer is a frame that is sufficiently inertial when comparing the constant angular velocity ω with the speed of light. The ring is a conduit, which is accomplished with fiber optics, that bends both beams to traverse in a circular path. A perpendicular acceleration is required to force the light beams to traverse a circle in the rotating interferometer. Such an acceleration is no different than the perpendicular gravity that exists for the Mickelson-Morley interferometer, as any acceleration to the linear paths will be equal to both beams, so the gravitational effects cancel out when combining the two beams.

One common application of the Sagnac effect is found in inertial navigation systems where the interference measurement device is fixed at the exit or end of the rotating ring gyroscope. If an observer is fixed with the rotating ring, special relativity requires that each beam originates with the same constant light speed, c, and each beam travels the circumference of $2\pi R$ inside the inertial rotating frame. This set of assumptions of special relativity for the ring's rotation undergoing constant angular velocity, ω, would predict both beams exit simultaneously (i.e., constructive interference in the output), but reality contradicts that theoretical prediction.

In an external frame, the beams are bent in circles, and the difference in distance is (4). Externally, light speed is c, and the time difference between the exiting beams in the external frame when substituting $L = 2\pi R$ and $v = \omega R$ into (4) is [7]:

$$\Delta t = \frac{2\pi R}{c}\left[\left(\frac{c}{c-\omega R}\right) - \left(\frac{c}{c+\omega R}\right)\right] = \frac{4\pi\omega R^2}{c^2-\omega^2 R^2} \quad (7)$$

Inside the interferometer, the two beams traverse identical distances of $2\pi R$ in the internal frame, and the output must be identical as (7). The speed of the corotating beam is $c-\omega R$, and the speed of the counterrotating beam is $c+\omega R$ by (7). The identical observed interference [7] of output is witnessed in both inertial rotation frames (i.e., $\omega = 0$ in the stationary rotation frame and a constant $\omega > 0$ for the rotating frame that is fixed with the rotating ring interferometer). Even internally, an observer fixed to an inertial rotation frame can detect rotations via the output. Thus, light obeys vector velocity addition in both linear and rotational frames.

IV. RAMIFICATIONS

It will take time for others to verify the results of this research, but if the velocity of photons does obey vector velocity addition, then several concepts of physics must be addressed. The finding that light's speed in a vacuum can vary generalizes light's behavior to be the same in a vacuum and in transparent materials. The speed of light in a vacuum is faster than in any

transparent material medium, and the index of refraction is the ratio of light's speed in a vacuum compared to the medium. The frequency of light in the medium is the same frequency of light in a vacuum when light enters or exits the medium. The number of waves passing through the material is the same as the number arriving at its surface. Waves cannot pile up and collect anywhere. If light's speed depends on the velocity of the emitting atoms, then $c' = c + v = f\lambda'$. The vast cosmos consists of empty space that is virtually a vacuum. The observed wavelength, λ, could well indicate the opposite that Doppler shifts would predict when assuming light in a vacuum is always the constant c. Since no medium is involved in the transmission of light through a vacuum, the principle of relativity asserts that it can be only the relative velocity of an approaching light source, v, that reduces the Doppler formulas when $c \gg v$ to $\Delta f = (v/c)f$ and $\Delta\lambda = -(v/c)\lambda$. For example, if the spectral lines of hydrogen in a star are longer in wavelength making $\Delta\lambda > 0$, then the standard Doppler formula implies $v < 0$, indicating that star is receding. If c' can vary in outer space and $\lambda' > \lambda$ with no change in frequency, this causes $c' > c$ and $v > 0$, which indicates the star is approaching. This means that all observed galaxies have reversed velocities, which will affect all cosmological models.

Readers will recall that most textbooks state that no particle travels faster than the speed of light in a vacuum. Countless electromagnetic experiments seem to demonstrate this. One of the best videos of a rigorous test using a linear accelerator demonstrated that electromagnetic fields do not accelerate free electrons faster than c [8]. As the electromagnetic energy was increased to accelerate the free electrons, the velocity of the electrons approached an asymptote of c. The film verified the timing cables were calibrated. It also showed that the colliding electrons did impart heat to the target that nearly equaled the total energy given to the electrons, but the speed of the electrons approached c. The test is just as valid today as then. Unfortunately, the conclusion has been overgeneralized to state that nothing can go faster than the speed of light. Photons generated by electromagnetic fields are limited to the standard light speed as emitted from the molecules to impart increases in momentum to the charged electrons. The free electrons can be nudged forward by momentum transfer if slower than the moving photons. Once free electrons obtain the limit of the standard light speed, the photons can no longer transfer momentum to nudge the free electrons any faster, although more energy can be given to the electrons. Such tests prove that an electrodynamic force alone does not accelerate charged particles faster than the standard light speed in a vacuum relative to the electromagnetic source. Note that the electromagnetic field produced by the linear accelerator, and the timing devices were stationary relative to each other in the laboratory frame. In this case as demonstrated by the video [8], the electrons can not be accelerated any faster than the standard light speed when the accelerator, the electromagnetic field, the timing sensors, and the target are fixed at the same distances throughout the test.

This paper demonstrates that the measured speed of light will be the standard speed when light sources and detection equipment are mutually fixed. However, when the source has an additional velocity relative to the detector, then Maxwell's equations must be modified to allow c to vary outside of the laboratory frame. This means that Einstein's assumptions for the axioms of special relativity theory are indeed excellent approximations, but not exactly accurate. For example, the last section of Einstein's 1905 paper contained the dynamics of the slowly accelerated electron [1, §10]. He derived that longitudinal mass would differ from transverse mass. No test has confirmed this even exists—directly or indirectly. No one has shown Einstein's derivation has any mathematical flaw concerning this subject. This unverified topic should have raised doubts about the accuracy of these two postulates of relativity. Most electrodynamic experiments do not approach the precision in significant digits to test Maxwell's equations when the sources are moving independent of the detectors.

Some may argue that prior tests measured the same standard speed of light emitted by moving stars external to Earth. In one case, Brecher [9]

took the pulses observed from binary x-ray sources to test whether light speed $c' = c + v$. Brecher wrote "The projected radial velocity (toward the observer) will then vary with time as $v(t') = v \cos\omega t'$, where t' is measured in the source frame. Now consider a pulse emitted at the time t' in the source frame." In that paper's equation (2), the denominator is $(c + kv \cos\omega t')$, which means ω as $\omega(t')$ and v as $v(t')$ are in the star's source units, else one is mixing units in the cosine argument. Brecher should have used primed terms in the equations to represent variables and units in the source frame, instead of mixing the variables between the Earth and the source frames. In that paper, a total derivative was attempted, not a partial derivative, of the time t' that the pulse would arrive in Earth time t. The derivative, equation (4) in that paper, ignored any differentials of $d\omega(t')$ and $dv(t')$, and the star's speed of light $c(t')$ in its time unit was treated identically in the derivative as $c(t)$ in the Earth frame. Brecher's proof is flawed with an incorrect differentiation, and it assumes beforehand in that paper's equation (4) what is eventually claimed that $c' = c$ in only time t units.

Tests have been made to measure emitted photons from high-speed particles by laboratory devices. For example, γ rays from the decay of π^o mesons with more than 6 GeV were detected with lead converters, a scintillator, and a lead-glass Cerenkov counter. [10]. The test was intended to measure $c + kv$, and the result was $k = (-3\pm13)\text{x}10^{-5}$ for mesons moving near light speed (γ>45). The team used two light detectors spaced 31.450 m and two additional detectors spaced 4.5 m from the other detectors for verification to measure the time interval the γ rays traveled. Photons are absorbed initially and emitted by the atoms of the material. The first detector absorbed the photons from high-speed γ rays and then emitted new photons at the standard speed of light. The measured speed recorded by the second detector after photons were emitted by the first detector was the standard light speed with a fixed distance between the detectors. This and similar tests must be reexamined carefully to ensure that the photon speeds were directly measured without interception to eliminate misinterpretations of the results.

Others may recall that Ives and Stillwell [11] measured a transverse Doppler effect with canal rays of hydrogen in the parallel and antiparallel directions to see if the average of the blue and red shifted lines were equally spaced from the normal emission line. The shifted lines were equally distant from the center emission line and measured within experimental limits as predicted by the relativistic transverse Doppler effect. The cathode ray tube and the detector were stationary in the experiment, forcing any measurement of light speed to be the standard light speed, c, by the analysis in the earlier section. From a classical treatment using geometry only, the full classical transverse Doppler effect will be the same as the relativistic derivation. Assume the moving hydrogen ions in the laboratory emit light perpendicular to their velocity in Figure 2 with $L = c\ \Delta t$ over the length L marked as AB. In the external 'stationary' frame, the light traverses the hypotenuse $A'B$ where $D = c'\Delta\tau$. The perpendicular length AB moves constantly to the right in Figure 2 to create the triangle $AA'B$. The light originates at point A' and the perpendicular length moves sideways to the right at a constant velocity V. Light reaches the end at B. In the laboratory frame, light could travel the length AB in the time interval of Δt, but light actually travels the longer distance of the hypotenuse in $c'\Delta\tau$. Light reaches B when the base A' is directly below B at point A after the time interval $\Delta\tau$. The Pythagorean theorem [12] produces the equation:

$$\Delta\tau = \frac{\Delta t}{\sqrt{\left(\frac{c}{c}\right)^2 - \left(\frac{v}{c}\right)^2}} \qquad (8)$$

Immediately, $c' = c \Leftrightarrow \Delta\tau = \Delta t/\sqrt{1 - v^2/c^2}$. This is a classical derivation valid in three dimensions without length contraction. Length contraction is unnecessary, but if included, the total relativistic effect will be increased to γ^2, similarly as (6) shows. This derivation shows that the time dilation effect must be included in the classical transverse Doppler effect if the speed of light is assumed to be the standard speed c, which Ives and Stillwell assumed in their derivation [11].

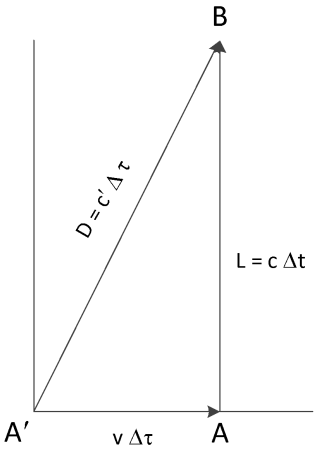

Figure 2: Constancy of light and time dilation.

Some standards of physics will need to be restored. The meter is now defined in terms of the time span it takes light to traverse a meter. This paper shows that photon velocity is affected by the velocity of the light source, and acceleration, such as gravity, can alter that additional velocity at emission. The International System (SI) definition does not define the environment that the meter is calibrated when using the speed of photons, but it states "The metre is the length of the path travelled by light in vacuum during a time interval of 1/299792458 of a second. It follows that the speed of light in vacuum is exactly 299792458 metres per second, c_o = 299792458 m/s." [13]. One problem is this is a circular definition, which renders it useless. The definition of light speed does not change even if one can repeatedly measure light speed to more precision than 9 significant digits. As a meter is now defined as a time unit, all displacements, velocities, and accelerations are reduced into time units. Philosophically, the universe is collapsed into one dimension instead of four dimensions. This is at best bizarre and illogical at worst as time has no known vector direction to set spatial axes perpendicular to the time axis and is impossible to revisit the starting point or epoch in a time scale for recalibrations or setting the origin of a reference frame by time alone. It is impractical when replacing a length as a time unit, which converts velocities into unitless numbers with unit vectors, making a velocity indistinguishable and equivalent to a position in a reference frame. Such definitions solidify mistaken concepts by changing the original definition with the intention of improving accuracy. For example, the nautical mile is defined now as exactly 1852 meters [13], but the original nautical mile was defined as 1 arcminute on the equator. Since 1984, the International Union of Geodesy and Geophysics (IUGG) [14] and the Global Positioning System (GPS) [15] have accepted the equatorial radius as 6378137 meters, which would make the nautical mile to be 1855.328 meters as an arcminute. This SI definition is almost 40 years old, illustrating that erroneous definitions are not readily updated or verified against the original definitions. A varying light speed should reestablish the physical meter standard as the international unit of length. Some other standards may need similar reexamination.

General relativity shows that gravity waves and light waves have the same universal speed [16, chapter 5]. "The existence of gravitational waves is an immediate consequence of special relativity and, to some extent, the experimental discovery of gravitational waves would merely confirm the obvious." [16, p. 242] If photons can move at different speeds in a vacuum, then gravity waves could have different speeds than the universal *c* speed. This may explain why the LIGO collaboration observes 10 to 100 daily detections with no physical explanation for most of these data. LIGO observations have been made in 3 long runs, and about 50 detections of gravitational waves have been announced. Maintenance and upgrades of the detectors are made between runs. The first run, O1, which ran from 12 September 2015 to 19 January 2016, made the first 3 detections—all black hole mergers. The second run, O2, ran from 30 November 2016 to 25 August 2017, which made 8 detections—7 black hole mergers, and 1 neutron star merger. The third run, O3, began on 1 April 2019 to 30 September 2019, and resumed from 1 November 2019 to 27 March 2020 until stopped due to the COVID-19 pandemic. At the time of this writing, LIGO had made 56 candidate detections, which may well change after this publication [17, 18].

By 2 November 2019, 41 events were announced (8 were later retracted) with 10 identified as neutron star-neutron star mergers or neutron

star-black hole mergers [19]. Such events should have some type of electromagnetic emission, but no independent telescopic observation has confirmed any LIGO announcement. Ignoring or discarding the 10 to 100 daily detections as glitches without explanation is not the best science, which concerns a few relativists [19]. Adding the Virgo observatory and other similar facilities into the LIGO collaboration, three-dimensional gravity wave detections should locate the electromagnetic sources in the cosmos. This is straightforward when implementing in reverse the Very Long Baseline Interferometry (VLBI) method for Earth orientation relative to pulsars using concurrent observations. As galaxies move independently to Earth, any observed gravitational waves are probably not at the standard light speed. The actual detections between LIGO observatories may have different time delays than expected, because the speed of light associated for each gravity wave may be a nonstandard speed.

If photons have velocities other than c, then the standard model for particle physics may need to be updated. According to special relativity, energy, E, is related to mass, m, of a particle to the speed of light, c, in a vacuum through Einstein's energy equation $E = mc^2$. In the standard model, the electron, the muon, and the tau particles are identical in all properties except mass, according to the energy equation. If c can vary and increase, then m may be unchanging while E increases in distinct steps. In the standard model, each higher member of a generation has greater mass than the corresponding particles of lower generations. A single particle type would simplify the standard model, but it still leaves an unanswered question: Why are there three generations for each type of particle? It could be that particles are emitted at three discrete energy levels, which may be like Planck's discovery that black body radiation is emitted in discrete quanta.

If energy in particle physics can vary in discrete quanta, then the constants that incorporate energy units may not be constant when the energy source and the detectors move independently of each other. For example, Planck's constant, h, has units of Joule second (Js), and Boltzmann's constant, k, is in units of Joule/Kelvin degree (J/K). Consider the burst of a solar flare, which consists mostly of hydrogen and some helium, heading toward Earth. Does the spectral radiation change as light speed is increased due to the kinetic velocity of the emitting atoms in the flare approaching Earth? For example, Planck's spectral radiation law gives power P_λ in W/m^2 per $m\mu$ for the wavelength, λ, and temperature, T, as

$$P_\lambda = \frac{2\pi hc^2}{\lambda^5(e^{hc/\lambda kT} - 1)}$$

In some references, the term hc^2 is referred as the 'first radiation constant' and hc/k as the 'second radiation constant' [20]. If c can change due to the motion of the photon emitter, some 'constants' are no longer constant. The unit J is defined in terms of $kg\ m^2/s^2$, and if light velocity in m/s can change its numerical quantity, which would affect the photon energy in J, then it may be possible that Planck's constant and Boltzmann's constant would be affected as well. If the speed of light in a vacuum, c, can vary in general, then either the fine structure constant, a, or Plank's constant, h, or both, must vary.

A varying light speed would imply that the Lorentz time dilation is incorrect for many precise timing applications. Hafele and Keating claimed they demonstrated time dilation precisely using four atomic clocks flown in commercial aircraft in westward (275±21 ns) and eastward (40±23 ns) circumnavigation of the world [21]. Essen, one of two horologists at the National Physical Laboratory (NPL) who operated the original cesium clock in the 1955-1958 calibration effort that defined the current atomic second, had reviewed the Hafele-Keating report and concluded the alterations in drift rates of the atomic clocks were useless [22].

The author examined the clock rates in Tables 1 and 2 [23] of the Hafele-Keating report released in 1972. The drift rates of 3 of the clocks varied significantly before and after each circumnavigation in that paper's Table 1, This

completely casts doubt that any average of the ensemble demonstrated relativistic time changes, as 3 of 4 clocks did not individually drift according to relativistic predictions. Table 2 of their paper proves the stability of those 3 clocks was not maintained throughout the test. Hafele had released his results at a 1971 conference, which Hafele even doubted his own test. He admitted, "Most people (myself included) would be reluctant to agree that the time gained by any one of these clocks is indicative of anything…." [24, p.273]. By averaging the time gain with 4 clocks, Hafele did get the average eastward circumnavigation with error bounds to agree with the predicted theoretical result, but there was no such fit between theory and the westward time gain [24, p. 282]. Keating later worked with Hafele to write the second report with claims that they verified time dilation [21], but careful examination uncovers many discrepancies.

The author's numerical findings on the Hafele-Keating drift rates were duplicated earlier by A. G. Kelly [25]. Kelly obtained the original raw data from the US Naval Observatory (USNO) to review against the published 1972 report and found several data in the tables differed significantly from raw data with no explanation. Kelly determined Clock #120 performed very irregularly. He wrote, "Discounting this one totally unreliable clock, the results would have been within 5ns and 28ns of zero on the Eastward and Westward tests, respectively. This is a result that could not be interpreted as proving any difference whatever between the two directions of flight". Kelly was not condemning relativity, but he was critical that the flight tests were not rigorous, and the claims were unverifiable based on the actual USNO raw data. If light speed is not a universal constant, then clocks may exhibit different time effects than the Lorentz time dilation, which would warrant a more rigorous retesting.

This is an incomplete list of possible ramifications if light speed is not a universal constant. In any case, it will take time to review the results of this paper.

V. CONCLUSION

Einstein stipulated the conditions to synchronize clocks in his definition, which were the distance between clocks must be fixed during the process and that the time interval to transmit electromagnetically is the same in either direction between the clocks, which is known as the Einstein time synchronization convention. However, no evidence was offered to support it. Einstein often interchanged the terms of simultaneity and synchronization, which are not identical. Simultaneous events occur when two or more phenomena separate or combine at one point at one instant of time. Synchronized events occur at separate points at the same coordinate time, which is maintained by separate clocks within acceptable neighborhoods around each location that have been synchronized by Einstein's convention to a master clock and that are stationary relative to that master.

Einstein further required that the speed of light be a universal constant based on experience, which is valid for the laboratory observer fixed to a uniformly moving rod and measuring light speed along the rod in either direction. It is shown that this leads to a contradiction with an external inertial observer viewing a uniformly moving rod of length L with clocks attached to both ends of the rod. By two separate techniques, the distance that light traverses to overtake the receding end of the moving rod is greater than L, and the distance to intercept the approaching end is less than L, but the sum of both legs is greater than $2L$. Assuming the same constant light speed for the external inertial observer will produce unequal time spans of transmission, contradicting Einstein's time synchronization convention. The requirement for a universal constant light speed is an excellent approximation due to the high speed of light compared to other typical velocities in physics. However, the laboratory observer, who is fixed relative to the rod, records equal lengths of L for the parallel and antiparallel traverses and predicts equal time intervals of transmission with a constant light speed. The events of light emission from end A, absorption and emission by reflection at B, and final absorption at A are all individual points occurring at separate time

instants, which require that the laboratory and stationary observers witness each point simultaneously in concurrent measurements. This means that the external, stationary observer must also record equal time spans of transmission between A and B by the time synchronization convention.

In his 1905 paper, Einstein obtained two ratios describing the time transmission intervals between the two clocks previously synchronized on each rod's end for the external stationary observer relative to the moving rod. In the translation, he wrote, "Observers moving with the moving rod would thus find that the two clocks were not synchronous, while observers in the resting system would declare the clocks to be synchronous." [1, §2, lines 53-54].

If Einstein equated the two intervals for the two one-way transmissions as required by his time synchronization convention, he would have obtained (5), which reveals that the velocity of light obeys vector addition of velocity. Instead, Einstein stated the two time spans showed simultaneity in one inertial frame, but nonsimultaneity in another inertial frame. This directly contradicts his stipulations of the time synchronization convention. There is no velocity between the rod and the laboratory observer, so the ratios reduce to L/c in either direction. Equation (5) reveals that light speed must vary precisely for the external observer as $c_{\rightarrow} = c + v$ for the parallel beam and $c_{\leftarrow} = c - v$ for the antiparallel beam, which (5) obtains $(c + v) - v = c = (c - v) + v$. Thus, light speed appears to be a constant in all directions for both observers when the light source and light detector are at a fixed distance relative to each other and when light's velocity obeys vector addition of velocities.

The LIGO consortium provides evidence that light obeys vector addition of velocity. The observatories are giant versions of the Michelson-Morley interferometer that have two perpendicular arms of four km lengths with virtually pure vacuum chambers containing the beams, so that no free molecule interferes with the beam transmissions between the ends. Each observatory is at a different latitude, and the arms are oriented uniquely in azimuth relative to the local east direction. Relative to a freely falling Earth frame that is not rotating (e.g., an inertial frame with its origin at Earth's center of gravity), each arm end is located at different latitudes. The northernmost end is moving slower than the southernmost end from Earth's rotation in this inertial frame. The cosine projection of velocity parallel to an arm displaces each arm like a moving rod in the inertial frame. Let V_A be the rotational velocity at the combination point A for both arms, V_B for the endpoint B of the x-axis arm and V_C for the endpoint C of the y-axis arm. Equations (1′) and (2′) give the one-way distances the photons traverse, but the sum of the distances for the x-axis and y-axis are not equal since $V_C \neq V_B$. If light's velocity is a universal constant, the output of the merged beams would not be synchronized. The output of LIGO observatories is always synchronized after months of continuous operations over three extended periods (excluding the data detections). The principle of concurrent observation requires all observers in the accelerated observatory frame, in the ECEF frame, and the freely falling, nonrotational frame must witness the same synchronization. Einstein's synchronization convention requires that (5) is mandated, so that all time spans for light to traverse between mutually fixed pairs of points must be equal. This means $c_{\rightarrow} = c + v$ and $c_{\leftarrow} = c - v$, which demonstrates that light obeys addition of vector velocities.

It was shown that the Sagnac effect [7] using a ring laser gyroscope in the form of a circular interferometer operates according to (7). An external observer easily sees a constant rotation of the gyroscope causes the corotating beam to travel a longer distance than the counterrotating beam. The output of destructive interference measures the angular distance the gyroscope rotated. The same output is observed by an internal observer fixed with the gyroscopic frame, but the circumference is preserved, so that the internal observer concludes the corotating light beam went slower by $c-\omega R$ and the counterrotating beam by $c+\omega R$ according to (7). This makes the theoretical predictions between external and internal observers consistent. Thus, light's velocity obeys

vector addition of velocities in both linear and rotational frames, where c is the standard light velocity.

To obtain very precise measurements of light speed to eight or more significant figures, the light source and the light detector are stationary relative to each other in a laboratory. To employ only one ultraprecise timing device, a roundtrip test of a light emission is standard [2]. This restricted linear testing will produce the standard light speed, but it is not universal. With this new interpretation of light velocity, light now behaves the same in a transparent medium and in a pure vacuum with unchanged frequency (i.e., $c' = c \pm v = f\lambda' = c/n$).

If others verify that light obeys vector velocity addition, then several physics concepts will need to be revised. Previous test results should be reviewed to determine if updates are necessary, but the precision in significant figures will generally not change most results. Several ramifications have been listed in the paper, such as old standards would need to be reestablished, such as the physical meter in the current SI standards, if light speed is not a fixed, exact numerical constant in all reference frames or external environments.

Other axioms of physics, concepts, or physical models may need future revisions. In particular, the definitions and implementations involving time and clock synchronization may well require an overhaul since light speed in a vacuum is not a constant in general applications and the distance between the source and receiver is not usually fixed during the synchronization. Thus, this research indicates more updates in physics.

Appendix: Errata for Previous Papers

In five previously published papers, the author erroneously assumed that light speed moving antiparallel to the direction of the observer, rod, conduit, or racetrack does not affect the ratio of v^n/c^n in the series derivation. Unfortunately, in vector mathematics, the ratios are $(-1)^n v^n/c^n$ in the series when using speed for the velocity magnitude, which the author discovered in this writing. The derivation of equation (2) reveals the error, and the roundtrip distance in (3) makes the total distance longer than $2L$. Thus, corrections to the relevant equations and conclusions in those papers are given in this section.

A.1: Timing in Simultaneity, Einstein's Test Scenario, and Precise Clock Synchronization [26]

Replace (2) with (2) from this paper so that $L_{BP} = Lc/(c+v)$. Then, replace (4) with $\Delta T_{BP} = L_{BP}/c = L/(c+v)$ when dividing by c. Then, $c_{AP} = c-v$ and $c_{BP} = c+v$ without invoking $v<<c$. Replace (7) with (3) in this paper to establish that the roundtrip distance in the stationary frame is greater than $2L$.

The summary needs revision stating that the speed of light does vary by vector velocity addition when the observer or detector is not fixed relative to the light source. The total roundtrip that light traverses for an external observer is greater than $2L$. The roundtrip distance is $2L$ as perceived by the observer fixed with the light source, When the distance is fixed between the source and detector, the time interval for light to traverse either leg is the same, because the speed of light obeys vector velocity addition to precisely compensate for the difference in the light paths within the reference frame that the roundtrip test is conducted.

Two Way Satellite Time and Frequency Transfer (TWSTFT) may be improved to validate precise times between timing laboratories under 1 ns by including the one-way speed of light between the ground stations and the satellite in common view of the stations. The one-way light speed must account for the motion of the satellite's velocity along the cosine projection of the transmitted signal along the line of sight of each transmission. Currently, the Sagnac effect is employed to account for the changing distance between the monitoring equipment and the satellite during transmission using only the standard light speed.

A.2: Generalized Equations for the Collinear Doppler Effect [27]

Several equations must be updated due to equations (2) and (3) derived in this paper. Although the diagrams are correct, too many changes are needed, which would be hard to

logically follow. This text will be a terse recapitulation and summary.

For simplicity, vibrations of still air are considered with horizontal propagation to avoid changes in density from altitude. The generalized Doppler equation will be developed in the collinear direction. Any transverse effect can be derived with trigonometry to get a perpendicular propagation.

The source produces waves of frequency, f, and wavelength, λ, with a positive speed of $V = f\lambda$. If the source moves at a uniform velocity, V_s, on the positive x-axis, the wavelength is shorter, but not the wave speed, so that $(V-V_s) = f\lambda_s$. An observer collects waves in one time unit by $1(V-V_o) = f_o\,\lambda$. Then, $f_o = (V-V_o)/\lambda = f_s\,(V-V_o)/(V-V_s)$, which is the standard Doppler equation found in introductory physics textbooks, but the velocities are positive parallel to the positive x-axis. The observed wavelength, $\lambda_o = (V-V_o)/f_o = (V-V_o)/(V-V_s) = (V-V_o)(V-V_s)/((V-V_o)f_s) = (V-V_s)/f_s$. The standard Doppler equation leads to the incorrect conclusion that the observed wavelength is only determined by the source's velocity and transmitted frequency. Any test of a stationary siren with still air would have a broadcast of $f = f_s$ and λ, but a moving observer with velocity, V_o, would collect fewer waves per unit time and would stretch out the observed wavelength. Although adequate, the standard Doppler equation needs to be updated.

Equation (3) is correct for the parallel propagation along the x-axis, which is $\lambda_o = \lambda\, V/(V-V_o)$. Based on (2) in this paper, the correct formula for the antiparallel propagation for Equation (4) is now $\lambda_o = \lambda\, V/(V+V_o)$ when V_o is in the negative x-axis direction. Keeping the velocity direction as a vector, the + sign in Equation (4) can be replaced, making Equation (3) the general form. For the moving source through the medium, $\lambda_s = \lambda = (V-V_s)/f_s$. As the observed λ is modified by the motion of the source and observer and using V_s and V_o as vector velocities parallel to the x-axis, the general Equation (5) is $\lambda_o = \lambda\, V/(V-V_o) = V(V-V_s)/((f_s(V-V_o))$. As $f_o = (V-V_o)/\lambda_o$, then insert λ_o into (5) to get (6) as $f_o = f_s\,(V-V_o)^2/((V(V-V_s))$. Equation (6) is the general collinear Doppler effect. Note that in a constant wind, $V = V_{propagation} + V_{wind}$ can be inserted into (5) or (6). If both the source and observer move with the same speed, (i.e., $V_o = V_s$), then (5) reveals the transmitted wavelength is preserved (i.e., $\lambda_o = \lambda_s$). If both the source and observer are stationary (i.e., $V_o = o = V_s$), then $f_o = f_s$, even in the presence of a wind, which Figures 4 and 5 indicate. Equation (6) reduces to the standard Doppler equation if the observer's velocity is significantly less than the wave's total speed (i.e., $V_o << V = V_{propagation} + V_{wind}$).

A.3: Simultaneity, Chronometrology, and the Two Postulates of Relativity [28]

Replace (2) with (2) in this paper, so that $L_{BP} = Lc/(c+v)$. Also, $L_{AP} = Lc/(c-v)$, and $\Delta T_{AP} = L_{AP}$ /c $= L/(c-v)$. Replace (4) with the updated ΔT_{BP} so that $\Delta T_{BP} = L_{BP}$ /c $= L/(c+v)$. Then, the light speed $c_{AP} = L/\Delta T_{AP} = c-v$ in the original (5). Equation (6) is updated as $c_{BP} = L/\Delta T_{BP} = c+v$ without having to invoke $v<<c$. Replace (7) with (3) in this paper where $L_{\rightarrow} + L_{\leftarrow} = 2Lc^2/(c^2-v^2) > 2L$, because the original (4) is incorrect. The conclusion needs to be updated that the roundtrip distance of the moving rod of length L is greater than $2L$, but $2L$ in the inertial frame fixed with the uniformly moving rod. The speed of light obeys the addition of vector velocity according to (5) in this paper, which adjusts the transmission intervals in either direction to be the same.

A.4: Vector Addition of Light's Velocity Versus the Hafele-Keating Time Dilation Test [23]

Relace (4) with (2) in this paper, which would make $L_{C'A''} = Lc/(c+v)$. This will change (6) to be $\Delta T_{C'A''} = L/(c+v)$ and the roundtrip time as $\Delta T_{A'C'A''} = \Delta T_{A'C'} + \Delta T_{C'A''} = 2Tc^2/(c^2-v^2)$ with $T = L/c$ for the stationary frame, but 2T for the inertial frame fixed with the interferometer.

Replace (9) with $c_{C'A''} = L/\Delta T_{C'A''} = c+v$ without the need to use v << c. This analysis shows that the velocity of light obeys vector velocity addition. The comments concerning the Hafele report of 1971 and the Hafele-Keating report of 1972 remain unaltered.

A.5: Measuring Velocity of Moving Inertial Frames with Light Transmissions [29]

After making the needed changes in key equations, one retraction is made. The experimental setup will accomplish the one-way measurement of light's velocity, but it will produce the standard light speed, c, in all horizontal directions. The vertical direction will vary light speed as previously determined by the Pound-Rebka experiment [30] with $v \approx gL/c$ where g is the local gravity of Earth, L is the vertical length, and v is ± if L and g are parallel or antiparallel, respectively.

The one-way time span of light traversing a uniformly moving rod of length L in a stationary frame in either parallel or antiparallel direction of movement is exactly the same one-way time span in the moving inertial frame fixed with that rod. The reason is the distance between the light source and detector remains fixed during the test. Replace (2) with (2) in this paper so that $L_{BA} = Lc/(c+v)$. This change will revise (4) to be $\Delta T_{BA} = Tc/(c+v)$ where $T = L/c$. Also, (6) is updated with $c_{BA} = L/\Delta T_{BA} = c-v$ without requiring $v<<c$. Both (5) and (6) verify that light's velocity obeys vector velocity addition. However, one cannot use either (3) or the updated (4) to measure a different time interval for light to traverse the horizontal length L in parallel or antiparallel directions, because $\Delta T_{BA} = \Delta T_{AB}$ for the external observer as shown by (5) in this paper. The author had not considered $c_{\rightarrow} = c + v$ and $c_{\leftarrow} = c - v$ in a generalized version of (3) and (4), which would be $\Delta T_{AB} = L_{AB}/c_{\rightarrow} = Lc_{\rightarrow}/[c_{\rightarrow}(c_{\rightarrow}-v)] = L/c$ and $\Delta T_{BA} = L_{BA}/c_{\leftarrow} = Lc_{\leftarrow}/[c_{\leftarrow}(c_{\leftarrow}+v)] = L/c$. This shows that a one-way light speed will be the standard value when distance is fixed between the light source and detector even though the apparatus moves inertially in outer space, because light velocity obeys vector addition of velocity.

REFERENCES

1. Miller, A. I. (1981) Albert Einstein's Special Theory of Relativity: Emergence (1905) and Early Interpretation(1905-1911), Addison-Wesley Publishing Co., Inc., Reading, Mass., Miller's English translation is enumerated in its appendix. Muller, D., (October 21, 2020) "Why the Speed of Light Can't Be Measured", Veritasium videocast on YouTube.
2. Einstein, A., (1961) Relativity: The Special and the General Theory, Three Rivers Press, New York, 15th ed., ISBN 0-517-88441-0. Deines S. D., (2018) "Dichotomy Between Null Results from All Interferometer Experiments versus Special Relativity Expectations", *London Journal of Research in Science*, 20(3)1, DOI 1017472/LJRS.
3. LIGO.caltech.edu website (operated by Caltech and MIT), Facts subpage lists the extreme engineering to construct LIGO and its operation.
4. www.ligo.org/scientists/GW100916/GW100916-geometry.html
5. Brown, K. (2011) Reflections on Relativity, Section 2.7 "The Sagnac Effect", ISBN 978-1-257-03302-7.
6. Bertozzi, W., "The ultimate speed: and exploration with high energy electrons", Educational Development Center, Newton, Mass.
7. Becher, K. (1977) "Is the Speed of Light Independent of the Velocity of the Source?" Phys. Rev. Lett., 39 (17), p. 1051-1064
8. Alväger, T. A., Farley, F. J. M., Kjellman, J., and Waller, I (1964) "Test of the Second Postulate of Special Relativity in the GeV Region", Physics Letters, 12 (3): 260-262.
9. Hils, D., and Hall, J. L. (1990) "Improved Kennedy-Thorndike experiment to test relativity", *Phys. Rev. Lett.* 64, (15): 1967.
10. Euclid, Elements, Book 1, Proposition 47.
11. BIPM (2006) The International System of Units (SI), 8th ed.
12. The Astronomical Almanac (1984), US Government Printing Office, Washington, D.C.
13. NIMA (1 Jan 2000) "Department of Defense World Geodetic System 1984", National Imagery and Mapping Agency Technical Report TR 8350.2, 3rd ed., Amendment 1.
14. Ohanian, H. C. and Ruffini, R. (1994) Gravitation and Spacetime, 2nd ed, W. W. Norton and Co., New York.
15. Wikipedia, "List of gravitational wave observations".

16. LIGO Scientific Collaboration (02 Feb 2021) ligo.org/news.php
17. Hossenfelde, S. (2 Nov 2019) videocast, "Have we really measured gravitational waves?" backreaction.blogspot.com/2019/11/have-we-really-measured-gravitational.html
18. Deeson, E. (2009) Collins Internet-Linked Dictionary of Physics, Harper Collins Publishers, Ltd., London, p. 350.
19. Hafele, J. C. and Keating, R. E., (1972) "Around-the-World Atomic Clocks: Predicted Relativistic Time Gains", *Science*, 177: 166-177.
20. Essen, L., Creation Res. Society Quarterly, (1977) 14: 46.
21. Deines, S. D. (2017a) 'Vector Addition of Light's Velocity Versus the Hafele-Keating Time Dilation Test', *Int. J. App. Math. and T. Phys.,* 3(3):50-55, DOI 10.11648/j.ijamtp.20170303.12.
22. Hafele, J. C., (1971) "Performance and Results of Portable Clocks in Aircraft", Third Annual Department of Defense (DOD) Precise Time and Time Interval (PTTI) Strategic Planning Meeting, 16-18 Nov 1971, Washington, DC, p. 261-288
23. Kelly, A. G., (2000) "Hafele and Keating Tests: Did They Prove Anything?", *Physics Essays*, 13(4): 616, DOI: 10.4006/1.3025451.
24. Deines, S. D. (2016a) 'Timing in Simultaneity, Einstein's Test Scenario, and Precise Clock Synchronization', *Int. J. App. Math. and T. Phys.,* 2(4):31-40, DOI 10.11648/j.ijamtp. 20160204.12
25. Deines, S. D. (2016b) 'Generalized Equations for the Collinear Doppler Effect', *Int. J. App. Math. and T. Phys.,* 2(4):46-51, DOI 10.11648/j.ijamtp. 20160204.14.
26. Deines, S. D. (2017b) 'Simultaneity, Chrono metrology, and the Two Postulates of Relativity', *Int. J. App. Math. and T. Phys.,* 3(3):43-49, DOI 10.11648/j.ijamtp. 20170303.11.
27. Deines, S. D. (2017b) 'Measuring Velocity of Moving Inertial Frames with Light Transmissions', *Int. J. App. Math. and T. Phys.,* 3(3):56-60, DOI 10.11648/j.ijamtp.20170303.13.
28. Pound, R. V., Rebka Jr., G. A., (1959) "Gravitational Red-Shift in Nuclear Resonance", *Phys Rev. Let.*, 3(9), 439-444.

Effect of Different Floor Types on Growth Performance of Pigs and Carcass Back-Fat Thickness

K. Kidega, T. Aliro, B. Mugonola, E. K. Ndyomugyenyi & I. Okello-Uma

ABSTRACT

Pig production (Sus scrofa domesticus) amongst smallholder farmers is constrained by poor growth performances in terms of feed intake (FI), weight gain (WG) and feed conversion ratio (FCR) and, high proportion of carcass back-fat thickness to lean meat. This study investigated the effect of floor types on growth performance of pigs and carcass back-fat thickness of pigs raised on IMO treated deep litter floor, untreated deep litter floor and concrete floor.Three-month old pigs (Large White x Landrace) were raised on a deep litter floor and concrete floor (control); one type of deep litter floor was treated with IMO solution and one type not treated. No significant (P≥0.05) difference were observed in feed conversion ratio (FCR), carcass back-fat thickness at the back from the 15th rib to the last Lumbar vertebrae, at gluteus medius muscle and the thigh of pigs raised on both concrete floor, IMO treated and untreated deep litter floor.

Keywords: feed intake; feed conversion ratio; weight gain; back-fat thickness.

Classification: FOR CODE: 070799

Language: English

London Journals Press

LJP Copyright ID: 925652
Print ISSN: 2631-8490
Online ISSN: 2631-8504

London Journal of Research in Science: Natural and Formal

Volume 21 | Issue 2 | Compilation 1.0

Effect of Different Floor Types on Growth Performance of Pigs and Carcass Back-Fat Thickness

K. Kidega[α], T. Aliro[σ], B. Mugonola[ρ], E. K. Ndyomugyenyi[ω] & I. Okello-Uma[¥]

ABSTRACT

Pig production (Sus scrofa domesticus) amongst smallholder farmers is constrained by poor growth performances in terms of feed intake (FI), weight gain (WG) and feed conversion ratio (FCR) and, high proportion of carcass back-fat thickness to lean meat. This study investigated the effect of floor types on growth performance of pigs and carcass back-fat thickness of pigs raised on IMO treated deep litter floor, untreated deep litter floor and concrete floor. Three-month old pigs (Large White x Landrace) were raised on a deep litter floor and concrete floor (control); one type of deep litter floor was treated with IMO solution and one type not treated. No significant (P≥0.05) difference were observed in feed conversion ratio (FCR), carcass back-fat thickness at the back from the 15th rib to the last Lumbar vertebrae, at gluteus medius muscle and the thigh of pigs raised on both concrete floor, IMO treated and untreated deep litter floor. However, significant (P≤0.05) difference were observed in feed intake (FI), weight gain (WG), carcass back-fat thickness in the neck at 1st cervical vertebrae, over the shoulder and at the back from the 6th to the 14th rib of pigs raised on concrete floor, IMO treated and untreated deep litter floor. Therefore, IMO treatment of deep litter floors does not affect feed conversion ratio rather enhance weight gain and reduce back-fat thickness in pigs.

Keywords: feed intake; feed conversion ratio; weight gain; back-fat thickness.

Author α ¥: Department of Food Science and Post-harvest Technology, Gulu University, P. O. Box 166 Gulu, Uganda.

σ ω: Department of Animal Production and Range Management, Gulu University, P. O. Box 166 Gulu, Uganda.

ρ: Department of Rural Development and Agribusiness, Gulu University, P. O. Box 166, Gulu, Uganda.

I. INTRODUCTION

Worldwide, pig (Sus scrofa domesticus) production is the fourth among livestock with a population of 977 million pigs of which 36 million are in Africa (Gennari et al., 2015). Pig rearing is one of the fastest growing livestock enterprises in Uganda that has become attractive and has made Uganda to be the largest pork consumers in East Africa (Lagu et al., 2017). Per capita pork consumption in Uganda was estimated to be increasing at the rate of 3.4 kg/person/year and the demand is still rising amongst urban and peri-urban population (Tatwangire, 2013).

Smallholder farmers in Uganda produce nearly 3 million pigs yearly of which more than 80% are concentrated in rural areas (MAAIF, 2008). Pigs do not only provide people with pork which is a source of good quality protein but also a source of reliable income for smallholder farmers (Ikwap *et al.,* 2014). There is high potential of economic gain from pig production given its high feed conversion efficiency, prolificacy and rapid growth rate compared to other livestock which makes pigs to generate income for farmers within a short period of time and ensure food security (FAO, 2011). Regardless of the benefits and opportunities pigs offer for better livelihood of rural smallholder farmers, pig production is still hindered by poor growth performance in terms of feed conversion ratio, weight gain and high back-fat content to lean meat (Corrêa *et al.*, 2009).

Generally, conventional systems of pig production under smallholder farmer systems are associated with poor animal performance and welfare that results in deterioration of pork quality (Ngapo *et al.*, 2004). However, environmental enrichment of piggery house floor with substrates (litter) has been found to be effective in improving performance and welfare of pigs by providing more comfortable resting surfaces (Morrison *et al.,* 2007). Deep litter floor bedding materials provides pigs with adequate sources of manipulatable objects to exhibit rooting and other natural behaviours (Gentry et al., 2004).

Daily application of indigenous micro-organism (IMO) solution on deep litter floors of pig houses have been suggested to improve growth performance of pigs and reduce back-fat thickness and, it is increasingly being practiced in Uganda by smallholder pig farmers (Nistor et al., 2012; Ndyomugyenyi and Kyasimire, 2015). Implementation of pig production systems that lower environmental impact, improve animal performances, welfare and reduce carcass back-fat content is very important for smallholder farmers therefore, this study aimed to assess the growth performance and carcass back-fat thickness of pigs raised on IMO treated deep litter floor.

II. MATERIALS AND METHODS

Study area

The study was carried out in Paicho and Koro sub-counties in Gulu and Omoro Districts of Northern Uganda for a duration of three months (90 days). These districts were selected because they have the highest population of pig farmers in the region (MAAIF, 2008). The districts are located between longitudes 30° 21' east to longitude 32° east and latitude 2° north to latitude 4° north. The districts receive an average rainfall of 1,500 mm per annum with a monthly average ranging between 14 mm in January and 230 mm in August. The wet season normally extends to October with the highest rainfall in May, August and October (Nabukenya *et al.,* 2014).

2.1 Experimental treatments and design

Concrete floors and deep litter floors were used in the study where three deep litter floor units with IMO treatment as experimental units; three deep litter floor units without IMO treatment and three concrete floor units as control units. A completely randomised block design (CRBD) was used, whereby thirty six (36) three months old healthy crosses of Large White and Landrace pigs of mixed sex were purchased from the existing pig farmers within the two districts. The pigs were randomly distributed into nine piggery units within the treatments, the beddings in all deep litter floor units were laid systematically in 1 metre deep hole measuring 3x3m on bare soil ground with, charcoal as the first layer, followed by tree shoots, maize stalks, dry red soil mixed with lime and wood shavings. The IMO solution was applied on a daily basis in all the experimental units. Restricted feeding method was used and all pigs were fed on growers' mash consisting of maize bran (74 kg), fishmeal (5 kg), soybean meal (10 kg), sunflower cake (5 kg), lake shells (4 kg), bone ash (1 kg), salt (0.5 kg) and premix (0.05 kg). In general, the nutrient composition of the feed contained; energy (2971 kcal kg-1), crude protein (13.6%), lysine (0.957%), methionine + cysteine (0.685%), fats (5.1%), crude fibre (6.3%), calcium (1.97%) and phosphorus (0.74%).

2.2 Growth performance of pigs

Growth performance of pigs raised on both concrete, IMO treated and untreated deep litter floors was determined by measuring their feed intake (FI), feed conversion ratio (FCR) and weight gain (WG). To determine WG, pigs were weighed at the beginning of the experiment and after every one week for 12 weeks using a spring balance weighing scale. The FI was determined by subtracting the total feed left (refused) by pigs from the total feed given to the pigs in a week and, the ratio of FI to WG was used to calculate the FCR. Pigs in all units were fed and watered daily two times (in the morning and evening) and application of IMO solution on the deep litter floor was also done on a daily basis.

2.3 Carcass back-fat thickness determination

Carcass back-fat thickness was measured (cm) at 6 points on one of the half carcasses using a vernier caliper; in the neck at 1st cervical vertebrae, over the shoulder at the thickest point, at the beginning of the back from the 6th rib to the 14th rib, at the centre of the back from the 15th rib to the last Lumbar vertebrae, at the centre of Gluteus medius muscle and on the thigh. The average back-fat thickness of the 6 measurements was then calculated to determine the total back-fat (Duzinski *et al.,* 2015).

2.4 Data analysis

All data obtained were analysed using Statistical Package for the Social Sciences (SPSS) version 20.0 and One-way ANOVA was generated. Means were separated by Least Significant Difference (LSD) Tests at 5 % significance level ($P \leq 0.05$).

III. RESULTS

3.1 Growth performance of pigs raised on different floor types

Feed conversion ratio (FCR) of pigs raised on both concrete, IMO treated and untreated deep litter floor houses had no significant ($P \geq 0.05$) difference (Table1). However, significant ($P \leq 0.05$) differences were observed in feed intake (FI) and weight gain (WG) of pigs raised on concrete, IMO treated and untreated deep litter floors. The FI of pigs raised on concrete floor was higher by 2.4kg than those raised on IMO treated deep litter floor and 3.4kg than those raised on untreated deep litter floor. The WG of pigs raised on concrete floor was higher by 2.4kg compared to pigs raised on IMO treated deep litter floor and 9.4kg than pigs raised on untreated deep litter floor.

Table 1: Effect of floor types on growth performance of pigs

Variable	Concrete floor (Control)	Litter floor without IMO	Litter floor with IMO	LSD	*P-value*
Initial weight (kg)	17.50±13.00	15.10±3.82	19.50±5.40	0.45	0.428
Feed intake (kg)	12.10 ± 0.46^{c}	8.73 ± 1.78^{b}	9.72 ± 1.18^{a}	0.150	0.031
Weight gain (kg)	23.80 ± 4.23^{c}	14.40 ± 3.46^{b}	21.40 ± 3.52^{a}	0.183	0.051
Feed conversion ratio	0.52±0.09	0.62±0.14	0.46±0.08	0.27	0.248

Means within a row with different superscripts differ significantly ($P \leq 0.05$)

3.2 Carcass back-fat thickness of pigs raised on different floor types

Carcass back-fat thickness of pigs raised on concrete floor, IMO treated and untreated deep litter floor significantly ($P \leq 0.05$) differed over the shoulder, in the neck at the 1st cervical vertebra and, at the back from the 6th to the 14th rib. However, no significant ($P \geq 0.05$) difference was observed in carcass back-fat fat thickness at the centre of the back from the 15th rib to the last Lumbar vertebrae, at gluteus medius muscle and thigh of pigs raised on both concrete floor, IMO treated and untreated deep litter floor. Carcass back-fat thickness of pigs raised on concrete floor was higher in the neck at the 1st cervical vertebrae by 1.7cm than of pigs raised on IMO treated deep litter floor and, by 0.9cm compared to pigs raised on untreated deep litter floor. Over the shoulder, it was higher by 1.8cm compared to pigs raised on IMO treated deep litter floors and, by 1cm than pigs raised on untreated deep litter floors. At the back from the 6th rib to the 14th rib, carcass back-fat thickness of pigs raised on concrete floor was higher by 1.6cm than of pigs raised on IMO treated deep litter floor and, by 1cm compared to pigs raised on untreated deep litter floors.

Table 2: Effects of floor types on carcass back-fat thickness

Variables (cm)	Concrete floor	Litter floor without IMO	Litter floor with IMO	LSD	*P-value*
Neck 1st cervical vertebra	3.63± 0.61^{c}	2.70± 0.46^{b}	1.93± 0.29^{a}	0.031	0.004
Over the shoulder	3.63±0.35^{c}	2.60±0.46^{b}	1.87±0.32^{a}	0.016	0.001
Beginning of the back (6th rib to the 14th rib)	2.67± 0.64^{c}	1.70± 0.53^{b}	1.10± 0.00^{a}	0.045	0.005
Centre of the back (15th rib to the last Lumbar vertebrae)	1.67± 0.65	0.97± 0.55	0.90± 0.26	0.349	0.202
Gluteus medius muscle	2.10± 1.31	1.17± 0.86	1.17± 0.21	0.459	0.430
Thigh	1.93± 0.83	1.23± 0.74	1.10± 0.36	0.376	0.346

Means within a row with different superscripts differ significantly ($P \leq 0.05$)

IV. DISCUSSION

4.1 Effect of different floor types on growth performance of pigs

The significant difference ($P \leq 0.05$) in FI and WG of pigs raised on concrete, IMO treated and untreated deep litter floor (Table 1) suggests that it is worth for smallholder farmers to adopt the IMO technology for pig production putting its costs and value under consideration as compared to conventional system (concrete floor). The costs and labour involved in making IMO solution included; boiling a carbohydrates source food, cooling and burying it in the soil for five days to trap the micro-organisms, making the IMO solution and applying it daily on the deep litter floor to achieve its better results. The increased FI of pigs raised on concrete floors could be due to increased energy requirements because they were more susceptible to heat (higher temperatures) stress and much of their energy were used in body temperature regulation and manipulative behaviour in stress conditions than pigs raised on deep litter floors. The more the FI, the higher the WG and this explains why pigs raised on concrete floors had higher WG compared to those raised on deep litter floors.

This suggestion concurs with Morrison *et al.* (2007) who reported that, weight gain in pigs was not influenced by housing treatment for pigs raised on deep litter (straw bedding) floor and conventional (slatted concrete floor) housing system. In addition, Correa *et al.* (2009) and Sheen et al. (2005) also reported that weight gain and feed conversion ratio of pigs raised on deep litter floor housing systems to be equal to those raised in conventional concrete floor pig houses.

However, our findings disagree with Corrêa et al. (2009) who reported no significant difference in weight gain of pigs raised on solid concrete floor and deep litter (rice husk) floor. In addition, Zhou *et al.* (2011) and Peeters et al. (2006) also reported that pigs raised on fermented bedding (sawdust, paddy husk, dry soil, charcoal, dried tree leaves, extract of fermented bamboo shoot, black salt, water, and active culture of (Lactobacillus brevis) had higher weight gain of 8.49% than those raised conventionally on cemented concrete floor which justify that deep litter bed had obvious effect on improving growth performance in pigs. In a similar study, Gentry *et al.* (2002); Johnston and Morrison (2004) also reported that pigs raised on deep-litter (Wheat straw) floor, large group systems are fatter and consumed more feed than conventionally housed pigs on concrete-slatted floor and this increased in feed intake was partly attributed to the cooler ambient temperatures experienced. Furthermore, Lebret *et al.* (2006a) reported that pigs reared on an enriched environment (sawdust bedding) floor exhibited higher feed consumption and increased growth rate than those raised conventionally on fully slatted floor and the increase could be due to the lower ambient temperature. Our findings also disagree with Honeyman and Harmon (2003) who found out that there was an increase in feed

intake of 2.54kg/day and weight gain of 834g/day for pigs reared on straw beddings (cornstalks) compared to those kept on slatted floor.

4.2 Carcass back-fat thickness of pigs raised on different floor types

Reduced carcass back-fat thickness of pigs raised on IMO treated deep litter in comparison with pigs raised on concrete floor and untreated deep litter floor (Table 2) suggests that, there was a high proportion of lean meat in pork of pigs raised on IMO treated deep litter floor. This could be due to the fact that, the daily application of IMO solution on the deep litter floors on which pigs were resting most of the time cooled down their body temperature and this could have facilitated the assimilation of back-fat into the muscle to form Intramuscular fats (IMF). This suggestion concurs with Dooremalen and Ellers (2010), who reported that when temperature increases, the composition of membrane lipids (phospholipid fatty acids) become more saturated to be able to maintain homeo viscosity.

In addition, Kidega et al. 2020 also reported a high composition of saturated fatty acids in the back-fat of pigs raised on deep litter floors without IMO treatment where temperature was slightly higher than IMO treated deep litter floored. Furthermore, Lu et al., 2007 also reported that, improved external fat deposition is probably an adaptive regulation under hot conditions; the more dietary energy stored as fat, the lower heat produced thus, less heat needed to be dispersed. In addition, Kouba et al. (2001) also reported that exposure to high ambient temperature increased back-fat deposition in pigs and increased amounts of external fat in pigs could increase thermal insulation which is useful to adapt to high ambient temperature.

However, our study disagrees with Morrison *et al.* (2007) who reported no significant difference in back-fat depth of 23.7 (mm) and 23.4 (mm) of pigs raised on deep litter (straw bedding) floor and conventional (totally slatted concrete floor) housing system. In addition, Millet et al., (2004) also reported a lower muscle thickness and higher back-fat thickness in the carcass of pigs raised on organic stable (straw bedding) than those reared on conventional stable (concrete floor). In a similar study, Olsson et al. (2003) reported that organic pigs reared outdoors on free range land had lower lean meat percentages and higher carcass back-fat thickness than conventionally raised pigs indoor on concrete floor.

V. CONCLUSIONS

Daily application of IMO solution on deep litter floors (wood shavings) neither reduces feed intake nor enhance weight gain of pigs but rather reduces back-fat thickness.

VI. RECOMMENDATIONS

Further research should be conducted to compare back-fat thickness of pigs raised on different deep litter floor bedding materials treated with IMO solution.

ACKNOWLEDGEMENT

The authors acknowledge the support of MASTERCARD foundation (MCF) through the Regional Universities Forum for Capacity Building in Agriculture (RUFORUM) for funding the study. Further regards go to Dr. Solomon Olum, Mr. Samuel Elolu, Mr. Junior Kasima Senyonga and Asso Prof. Duncan Ongeng whose outstanding comments contributed in stimulating suggestions and encouragement that motivated me to coordinate this study effectively.

Conflicts of Interest

The authors declare no conflicts of interest concerning the publication of this paper.

REFERENCES

1. Corrêa, E. K., Bianchi, I., Ulguim, R. R., Corrêa, M. N., Gil-Turnes, C. and Júnior, T. L. (2009). Effects of different litter depths on enviro- nmental parameters and growth performance of growing finishing pigs. Ciência Rural, Santa Maria , 39 (3) 838-843.
2. Dooremalen, C.V. and Ellers, J. 2010. A moderate change in temperature induces changes in fatty acid composition of storage

and membrane lipids in a soil arthropod. Journal of Insect Physiology 56:178-184.
3. Duzinski, K., Lisiak, D., Knecht, D. and Srodon, S. (2015). The estimation of pork carcass primal cuts value based on backfat thickness. Journal of Central European Agriculture, 16 (1): 112-121.
4. FAO. (2011). World Livestock 2011-Livestock in food security. Rome, Italy. FAO.
5. Gennari, P., Heyman, A. and Kainu, M. (2015). FAO Statistical pocket book. World Food and Agriculture, Food and Agricultural Organization of United nations, Rome, Italy.
6. Gentry, J. G., McGlone, J. J., Blanton, J. R. and Miller, M. F. (2002). Alternative housing systems for pigs: Influence on growth, composition and pork quality. Journal of Animal of Sciences., 80:1781-1790.
7. Gentry, J.G., McGlone, J.J., Miller, M.F. and Blanton, Jr., J.R. (2004), Environmental effects on pig performance, meat quality, and muscle characteristics. Journal of Animal Sciences.82: 209-217.
8. Honeyman, M. S. and Harmon, J. D. (2003). Performance of finishing pigs in hoop structures and confinement during winter and summer. Journal of Animal Science, 8:1663–1670.
9. Ikwap, K., Jacobson, M., Lundeheim, N., Owiny, D. O., Nasinyama, G. W., Fellstrom, C. and Erume, J. (2014). Characterization of pig production in Gulu and Soroti districts in northern and eastern Uganda. Livestock Research for Rural Development , 26(4):8-24.
10. Johnson, L. J. and Morrison, R. S. (2004). Growth performance and carcass quality of pigs housed in deep-litter barns fed diets containing alternative ingredients. Minnesota: Final report to Minnesota Pork Producers. Minnesota Pork Producers, MN, USA.
11. Kidega, K., Ndyomugyenyi, E.K. and Okello -Uma, I. (2020). Effect of indigenous microorganism treatment of deep litter floor on nutrient content of pork. African Crop Science Journal, Vol. 28 Issue Supplement, s1 pp. 247 - 254
12. Kouba, M., Hermier, D. and Le Dividich, J. (2001). Influence of a high ambient temperature on lipid metabolism in the growing pig. Journal of Animal Science. 79:81–87.
13. Lagu, C., Andama, M., Lee, S., Park, M., Ainomugisha, A., Ariho, A., Weisheit, A. and Tusingwire, S. (2017). Prevalence and intensity of internal parasites in pigs under indigenous micro-organism (IMO) and conventional piggery farms, greater Mbarara, Uganda. Livestock Research for Rural Development, 29 (6).
14. Lebret, B., Meunier-Salaun, M.C., Foury, A., Mormede, P., Dransfield, E. and Dourmad, J.Y. (2006) Influence of rearing conditions on performance, behavioural, and physiological responses of pigs to pre slaughter handling, carcass traits, and meat quality. Journal of Animal Sciences, 84: 2436-2447.
15. Lu, Q., Wen, J. and Zhang, H. (2007). Effect of Chronic Heat Exposure on Fat Deposition and Meat Quality in Two Genetic Types of Chicken. Poultry Science, 86: 1059-1064
16. MAAIF. (2008). The National Livestock Census Report 2008. UBOS, Uganda Bureau of Statistics. Ministry of Finance, Planning and Economic Development, Kampala, Uganda.
17. Millet, S., Hestaa, M., Seynaeveb, M., Ongenae, E., DeSmet, S., Debraekeleer, J. and Janssens, G. P. J. (2004). Performance, meat and carcass traits of fattening pigs with organic versus conventional housing and nutrition. Livestock Production Science, 87;109 – 119 .
18. Morrison, S. R., Johnston, J. L. and Hilbrands, A. M. (2007). The behaviour, welfare, growth performance and meat quality of pigs housed in deep litter, large group housing system compared to a conventional confined housing system.Applied Animal Behaviour Science , 103:12-24.
19. Nabukenya, I., Akiiki, C.R., Olila, D., Ikwap, K., and Höglund, J. (2014). Ethnopharmacological practices by livestock farmers in Uganda: Survey experiences from Mpigi and Gulu districts. Journal of Ethnobiology and Ethnomedicine, 10:1-14.
20. Ndyomugyenyi, E. K. and Kyasimire, J.(2015). Pig production in Kichwamba Sub-county,

Rubirizi district, Uganda . Livestock Research for Rural Development 27(10):1-13.
21. Ngapo, T.M., Dransfield, E., Martin, Magnusson, M., Bredahl, L. and Nute, G.R. (2004) Consumer perceptions: Pork and pig production. Insights from France, England, Sweden, and Denmark. Meat Science, 66:125-134.
22. Nistor, E., Bampidis, V., Pentea, M., Prundeanu, H. and Ciolac, V. (2012). Nutritional Quality of Pork Produced by Mangalitsa Breed. Scientific Papers: Animal Science and Biotechnologies 45 (2):386-389.
23. Olsson, V., Andersson, K., Hansson, I. and Lundström, K. (2003). Differences in meat quality between organically and conventionally produced pigs. Meat Science, 64 (3) : 287–297.
24. Peeters, E., Driessen, B., Moons, C. P. H., Ödberg, F. O. and Geers, R. (2006). Effect of temporary straw bedding on pigs' behaviour, performance, cortisol and meat quality. Applied Animal Behaviour Science, 98 : 234–248.
25. Sheen, S.Y., Su, C.C., Lee, M.S., Chang, H.L. and Hong, C.M. (2005). Study on the management model of litter bedded pig houses. Livestock Research, 34(2): 69-78.
26. Tatwangire, A. (2013). Successes and failures of institutional innovations to improve access to services, input and output markets for smallholder pig production systems and value chains in Uganda. CGIAR.
27. Zhou, Y. G., Wen, A. Y., Ning, K. J. N., Xu, B. N., Xie, J. L., Tang, H. and Liu, S. Q. (2011). Effects of biological fermentation bed on growth performance and pork quality of growing-finishing pigs. Journal of Anhui Science Technology University 25(1), 9-12.

This page is intentionally left blank

Supreme Theory of Everything: The Open Hysteresis in Place of Inverse-Square Law

Ulaanbaatar Tarzad

Mongolian University of Science and Technology

ABSTRACT

The inverse-square law (ISL) is used widely in physics, astronomy, celestial mechanics, cosmology, and other branches of sciences from the very beginning of classic physics up to date. But the development of modern physics and cosmology reveals that ISL becomes a big source of two problems. First, crucial cosmic-scale problems concerning gravity such as the accelerating expansion of the universe, the anomaly in galaxy rotation speed, the missing baryon problem, and dark matter remain unsolved. Second, Coulomb's electrostatic law, DLVO theory, Lennard-Jones 12-6 potential, and Yukawa potential were described imperfectly the nature at the scale of atoms and subatomic particles. The reasons connect to the ISL and the inverse-proportional law (IPL) consequence of which these laws will be deducted slowly from scientific and practical applications. In this paper, a possibility using the open hysteresis instead of ISL and IPL is proposed. The open hysteresis law can work from particle physics to cosmology.

Keywords: inverse-square law, inverse- proportional law, coulomb's law, dlvo theory, l-j 12-6 potential, yukawa potential, hysteresis-law in place of the inverse-square law.

Classification: FOR CODE: 010599p

Language: English

London Journals Press

LJP Copyright ID: 925652
Print ISSN: 2631-8490
Online ISSN: 2631-8504

London Journal of Research in Science: Natural and Formal

Volume 21 | Issue 2 | Compilation 1.0

Supreme Theory of Everything: The Open Hysteresis in Place of Inverse-Square Law

Ulaanbaatar Tarzad

ABSTRACT

The inverse-square law (ISL) is used widely in physics, astronomy, celestial mechanics, cosmology, and other branches of sciences from the very beginning of classic physics up to date. But the development of modern physics and cosmology reveals that ISL becomes a big source of two problems. First, crucial cosmic-scale problems concerning gravity such as the accelerating expansion of the universe, the anomaly in galaxy rotation speed, the missing baryon problem, and dark matter remain unsolved. Second, Coulomb's electrostatic law, DLVO theory, Lennard-Jones 12-6 potential, and Yukawa potential were described imperfectly the nature at the scale of atoms and subatomic particles. The reasons connect to the ISL and the inverse-proportional law (IPL) consequence of which these laws will be deducted slowly from scientific and practical applications. In this paper, a possibility using the open hysteresis instead of ISL and IPL is proposed. The open hysteresis law can work from particle physics to cosmology.

Keywords: inverse-square law, inverse- proportional law, coulomb's law, dlvo theory, l-j 12-6 potential, yukawa potential, hysteresis-law in place of the inverse-square law.

Author: Department of Physics, School of Applied Sciences Mongolian University of Science and Technology.

I. INTRODUCTION

In science, an inverse-square law is any scientific law stating that a specified physical quantity is inversely proportional to the square of the distance from the source of that physical quantity. The fundamental cause for this can be understood as geometric dilution corresponding to point-source radiation into three-dimensional space. It indicates the intensity of the radiation (I) decreases in proportion to the square of the change in distance (d) and is writing as follows [1]:

$$LIGHT\ INTENSITY\ (I) = \frac{1}{(DISTANCE\ (d))^2} \tag{1}$$

Since it describes the intensity of light at different distances from a light source:

$$\frac{I_1}{I_2} = \frac{(d_2)^2}{(d_1)^2} \tag{2}$$

Where I_1 is the initial intensity of radiation, I_2 is the final intensity, d_1 is the initial distance, d_2 is the final distance.

The base of the ISL is the inverse-proportional law (IPL). People used widely to measure speed, calculate time, keep calendars, and plan work in ancient times.

The majority of physical laws have been described based on ISL and IPL. Since IPL may be the most common law in the universe.

Here I would like fearlessly to show the applications of ISL and IPL based on the famous physical laws of genius scientists. These laws are so popular that the question is rarely asked whether they are fit for purposes.

1. Isaac Newton (1687)

$$F = G \cdot \frac{m_1 \cdot m_2}{r^2} \qquad \leftarrow \frac{1}{r^2}$$

2. Charles-Augustin de Coulomb (1785)

$$F = k \cdot \frac{q_1 \cdot q_2}{r^2} \qquad \leftarrow \frac{1}{r^2}$$

3. Georg Simon Ohm (1827)

$$I = \frac{U}{R} \qquad \leftarrow \frac{1}{R}$$

4. Wilhelm Carl Werner Otto Fritz Franz Wien (1896)

$$\lambda_{max} = \frac{b}{T} \qquad \leftarrow \frac{1}{T} \; and \; \frac{1}{\lambda}$$

5. Max Carl Ernst Ludwig Planck (1900)

$$B_\nu(\nu, T) = \frac{2hc^2}{\lambda^5} \cdot \frac{1}{e^{\frac{hc}{\lambda k_B T}}} \qquad \leftarrow \frac{1}{\lambda} \text{ and } \frac{1}{T}$$

6. Pierre Curie and Marie Curie (1903)

$$\mathrm{M} = \chi \cdot H = \frac{c}{T} \cdot H \qquad \leftarrow \frac{1}{T}$$

7. Albert Einstein (1915)

$$ds^2 = -\left(1 - \frac{r_s}{r}\right)\Delta t^2 - \frac{1}{\left(1 - \frac{r_s}{r}\right)} dr^2 \leftarrow r_s = r$$

   a. Relativistic momentum:

$$\mathrm{p} = \frac{mV}{\sqrt{1 - \left(\frac{v}{c}\right)^2}} \qquad \leftarrow \mathrm{v} \approx c$$

   b. Time dilation:

$$\Delta t = \frac{\Delta t_0}{\sqrt{1 - \left(\frac{v}{c}\right)^2}} \qquad \leftarrow v \approx c$$

8. Louis Victor Pierre Raymond de Broglie (1929)

$$\lambda = \frac{h}{mV} \qquad \leftarrow \frac{1}{m} \; and \; \frac{1}{V}$$

9. Edwin Powell Hubble (1929):

$$\text{Hubble constant} \rightarrow \text{Hubble flow} \rightarrow \text{Hubble} - \text{Lema}\hat{i}tre\ law$$

10. Werner Karl Heisenberg (1932)

$$\Delta x \geq \frac{h}{2 \cdot \Delta y} \qquad \leftarrow \Delta y \approx 0; \qquad \Delta y \geq \frac{h}{2 \cdot \Delta x} \qquad \leftarrow \Delta x$$
$$\approx 0$$

11. Erwin Rudolf Josef Alexander Schrödinger (1933)

$$\mathrm{i}\hbar \cdot \frac{\partial \psi}{\partial t} = -\frac{\hbar^2}{2m} \cdot \frac{d^2\psi}{dx^2} + \mathrm{U}\psi \qquad \leftarrow \frac{1}{m}$$

12. Hideki Yukawa (1949)

$$V_{Yukawa}(r) = -g^2 \frac{e^{-\alpha m r}}{r} \qquad \leftarrow \frac{1}{r}$$

13. Speed and speed limit

$$V = \frac{S}{t} \left[\frac{m}{sec}\right] \qquad \leftarrow \frac{1}{t}$$

The limit of speed is the limit of time. Since $\mathrm{t} \approx 0.000000003\ \mathrm{sec} = 3.33 \cdot 10^{-9}\ \mathrm{sec}$.

14. Pressure

$$\mathrm{P} = \frac{F}{S} \qquad \leftarrow \frac{1}{S}$$

15. Propagation of sound

$$\mathrm{p} \approx \frac{1}{r} \qquad \leftarrow \frac{1}{r}$$

$$\mathrm{v} \approx \frac{1}{r} \qquad \leftarrow \frac{1}{r}$$

$$\mathrm{I} = \mathrm{p} \cdot r = \frac{1}{r^2} \qquad \leftarrow \frac{1}{r^2}$$

So forth. We can list a long series.

Do you think the above laws of nature are perfect? If so, we don't have to think or do anything. If not, what are their shortcomings and reasons? Can we solve them?

In my opinion, it is possible if we do it in the exact opposite direction, that is, from infinity to infinitesimal smallness.

II. THE ISL AND IPL

Newton's law of universal gravitation is usually stated as that every particle attracts every other particle in the universe with a force that is directly proportional to the product of their masses and inversely proportional to the square of the distance between their centers [2].

This is a general physical law derived from empirical observations by what Isaac Newton called inductive reasoning [3].

What are the backgrounds of gravity or electromagnetic interaction that take two quantities (two masses or two charges) on the unit surface (over the square)?

The law of gravity is equal to the product of the masses divided by the square of the distance.

It looks like the weight of a body. Does it mean gravity or attraction?

Like it, the electric charges also lie over a square according to Coulomb's law.

The origin and the mathematical description of the inverse-square law are unclear. Its author maybe Isaac Newton or Robert Hooke.

It is a part of classical mechanics and was formulated in Newton's work Philosophiæ Naturalis Principia Mathematica ("the Principia"), first published on 5 July 1687. When Newton presented Book 1 of the unpublished text in April 1686 to the Royal Society, Robert Hooke claimed that Newton had obtained the inverse square law from him [3].

Above mentioned theories and formulas include the singularities by expression 1/x. This expression lurks in the shadow of ISL because we only give attention to ISL but apply mainly to the IPL.

$$y(x) = \frac{1}{x} \quad \text{and} \quad y1(x) = \frac{1}{x^2} \tag{3}$$

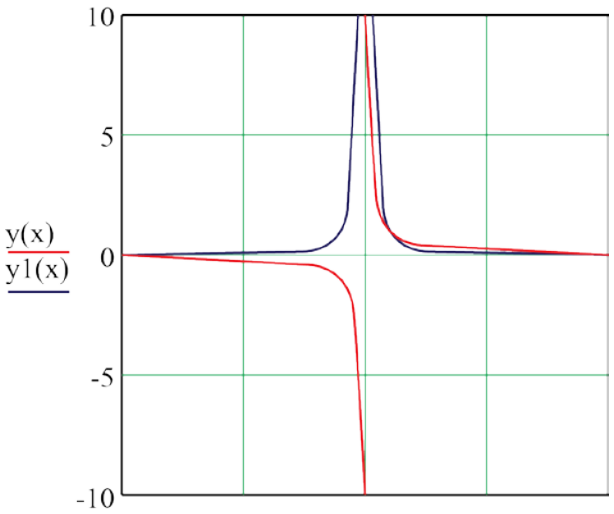

Figure 1: Graphs of ISL and IPL

Figure 1 illustrates the graphs of the continuity to plus and minus infinity. The ISL is written by a mathematical equation, which is infinite (Equation (4) and Equation (5)) for short-range:

$$F_{gravity} = Gm_1m_2 \cdot \lim_{r\to 0} \frac{1}{r^2} = \infty \tag{4}$$

$$F_{coulomb} = k_e q_1 q_2 \cdot \lim_{r\to 0} \frac{1}{r^2} = \infty \tag{5}$$

The results of the physical (or biological, chemical, economic, and so on) processes calculated by ISL and IPL have not any saturates. It means that the magnitudes of forces, the strength, the intensity, and so on have infinite. Since, all forces as gravity, mechanical, electromagnetic, seismic, acoustic, and thermal become infinite. Consequently, everything cannot exist in the universe. Indeed, these laws

include always somewhat imperfections and finally remained unsolved. The ISL and IPL cause trouble in science because they have a common error, which is infinite. Consequently, plus and minus values of physical parameters lose the meaning of nature.

What if a violation of the 1/r2 law were observed? [4] This problem is mathematical, not physical. What we do if mathematics works wrong? If the ISL is wrong, so many laws become wrong too.

The development of modern physics and cosmology reveals that ISL becomes a big source of two problems.

A) On cosmic scales it becomes a source to the serious problems in cosmology and modern physics:

1. *Anomalous rotation of galaxies.* If the force of gravity is a lot messier than Newton and Einstein thought, then it could account for the speedy rotation of spiral galaxies without requiring dark matter. For gravity to speed up stars on a galaxy's edge, it must deviate from the "inverse-square law" — the rule that gravity decreases by the square of the distance away from something — at galactic distances [5].

   Galactic rotation curves of about 1000 Galaxies [6] have provided by far the strongest evidence for the disagreement of 'dynamical' and visible mass. Assuming that all mass of a spiral galaxy is contained within its optical radius, one expects due to

$$v^2 = \frac{GM}{r} \tag{6}$$

   a radial dependency $v \sim r^{-\frac{1}{2}}$ in the velocity profile of clouds that can be measured by Doppler shifts. Interestingly, up to multiples of the optical radius, practically all galaxies show rather constant ('flat') velocities than the expected Keplerian behavior. Usually, an explanation with 'dark matter' is given, though this requires a particular distribution. While the deviation is already visible within the optical radius, in the outer regions the ratios of dark and luminous matter up to 1000 are required [7]. The form of the galactic rotation curves seems to depend just on the size of the galaxy [7], [8] a fact that is hard to explain by the properties of any dark matter candidate. Many precision profiles ~~are~~ conflict with the standard model [9], among these the most extended velocity profile of NGC 3741 [10]. While many questions are still open [11], [12], the anomaly itself is beyond any experimental doubt (see overviews [13], [14]). There are clear hints that the morphology of galaxies is dominated by systematics we do not understand yet [15], [16].

1. *Weak gravitation*. One of the big puzzles about gravity is the fact that it is so much weaker than the other forces: it is a factor of about 10^{40} times weaker than the electrostatic and magnetic forces [17]
2. *Limit in Earth's magnetotail.* At the night side of the earth, the magnetic field is stretched far downstream to form the magnetic tail. The diameter of the tail is between 40 and 60 earth radii; its length exceeds 1000 earth radii [18].
   It means that the charged particles of the earth magnetic field don't go to infinity, but more than 1000 earth radii and then come back to the earth pole. The magnetic field extensions of the stars and galaxies exceed more and more far distance, but not to infinity. The nature of everything is cyclical. In other words, everything goes and comes back to the initial point.
3. *The accelerating expansion of the universe* is the observation that the expansion of the universe is such that the velocity at which a distant galaxy is receding from the observer is continuously increasing with time [19], [20], [21]. So, the expansion of the universe has not been slowing due to gravity, as everyone thought, it has been accelerating. No one expected this, no one knew how to explain it. But something was causing it. Eventually, theorists came up with three sorts of

explanations. Maybe it was a result of a long-discarded version of Einstein's theory of gravity, one that contained what was called a "cosmological constant." Maybe there was some strange kind of energy-fluid that filled space. Maybe there is something wrong with Einstein's theory of gravity and a new theory could include some kind of field that creates this cosmic acceleration. Theorists still don't know what the correct explanation is, but they have given the solution a name. It is called dark energy [22].

B) At short interparticle distances the ISL and IPL cannot work perfectly:

1. *Coulomb's inverse-square law* is an experimental law [23] of physics that quantifies the amount of force between two stationaries, electrically charged particles. The electric force between charged bodies at rest is conventionally called electrostatic force or Coulomb force.[24] Coulomb's law was essential to the development of the theory of electromagnetism, maybe even its starting point,[23] as it made it possible to discuss the quantity of electric charge in a meaningful way.[25] The law states that the magnitude of the electrostatic force of attraction or repulsion between two point charges is directly proportional to the product of the magnitudes of charges and inversely proportional to the square of the distance between them,[26]

$$|F| = k_e \cdot \frac{|q_1 q_2|}{r^2} \tag{7}$$

Here, k_e is Coulomb's constant ($k_e \approx 8.988 \times 10^9\ \mathrm{N \cdot m^2 \cdot C^{-2}}$), [23] q_1 and q_2 are the signed magnitudes of the charges, and the scalar r is the distance between the charges.

2. *Van der Waals Interactions*

In molecular physics, the Van der Waals force is a distance-dependent interaction between atoms or molecules. Unlike ionic or covalent bonds, these attractions do not result from a chemical electronic bond; they are comparatively weak and therefore more susceptible to disturbance. The Van der Waals force quickly vanishes at longer distances between interacting molecules.

Van der Waals force plays a fundamental role in fields as diverse as supramolecular chemistry, structural biology, polymer science, nanotechnology, surface science, and condensed matter physics. It also underlies many properties of organic compounds and molecular solids, including their solubility in polar and non-polar media.

If no other force is present, the distance between atoms at which the force becomes repulsive rather than attractive as the atoms approach one another is called the Van der Waals contact distance; this phenomenon results from the mutual repulsion between the atoms' electron clouds.[27] The Van der Waals force has the same origin as the Casimir effect, which arises from quantum interactions with the zero-point field.[28]

The Van der Waals forces [29] are usually described as a combination of the London dispersion forces between "instantaneous~~ly~~ induced dipoles" [30], Debye forces between permanent dipoles and induced dipoles, and the Keesom force between permanent molecular dipoles whose rotational orientations are dynamically averaged over time.

3. *The Lennard-Jones (L-J) 12-6 potential (Nanoparticle Attraction Force)*

The common way to describe intermolecular forces is to use the so-called Lennard-Jones potential which is an expression for the interaction energy of the pair potential (r) of two molecules at a distance r:

$$W(D) = \frac{B}{r^{12}} + \frac{C}{r^6} \tag{8}$$

with the constants C and B for the attractive Van der Waals and repulsive Born repulsion, respectively. At first, the second term (Born repulsion) will be neglected [31], [32]. This law is in many respects DLVO-like interaction energy

The Lennard-Jones potential models soft repulsive and attractive interactions. Hence, the Lennard-Jones potential describes electronically neutral atoms or molecules. The potential equation accounts for the difference between attractive forces (dipole-dipole, dipole-induced dipole, and London interactions) and repulsive forces [32]. The L-J potential is arguably the most widely used pair potential in molecular simulations. It is so popular that the question is rarely asked whether it is fit for purpose. In this paper, we argue that whilst the LJ potential was designed for noble gases such as argon, it is often used for systems where it is not expected to be particularly realistic. Under those circumstances, the disadvantages of the LJ potential become relevant: most important among these is that in simulations the LJ potential is always modified such that it has a finite range. More seriously, there is by now a whole family of different potentials that are all called Lennard-Jones 12-6, and that are all different – and that may have very different macroscopic properties. [33]

$$\upsilon(r) = 4\epsilon\left[\left(\frac{\sigma}{r}\right)^{12} - \left(\frac{\sigma}{r}\right)^{6}\right]$$

Is this famous potential ever used in simulations?

Figure 2: Lennard-Jones potential in simulations

4. Yukawa potential.

In particle, atomic, and condensed matter physics, a Yukawa potential (also called a screened Coulomb potential) is a potential of the form:

$$V_{Yukawa}(r) = -g^2\frac{e^{-\alpha m r}}{r} \tag{9}$$

Where g is a magnitude scaling constant i.e. is the amplitude of potential, m is the mass of the particle, r is the radial distance to the particle, and α is another scaling constant so that $r \approx \frac{1}{\alpha m}$ is the approximate range. The potential is monotonically increasing in r and it is negative, implying the force is attractive. In the SI system, the unit of the Yukawa potential is (1/meters) [34].

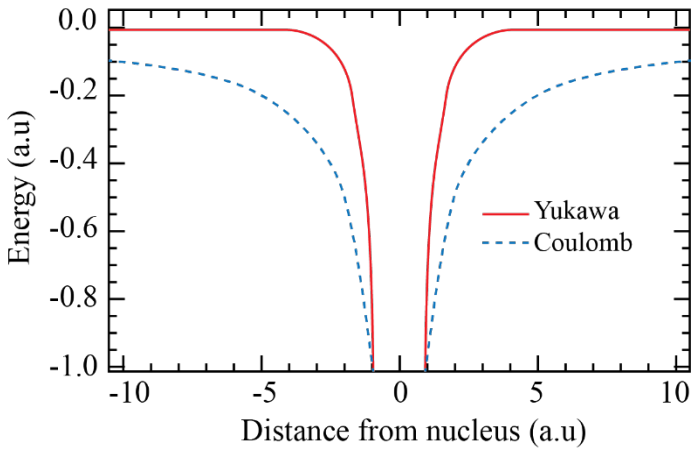

Figure 3: A short-range Yukawa potential in relation with Coulomb's potential [35]

From Figure 3 we see that the distance from the nucleus goes to 0, the energy also becomes infinite as Coulomb's potential (Equation (5)).

5. *The DLVO theory [36] explains that the interaction energy between the Coulomb repulsion and the Van der Waals attraction.*

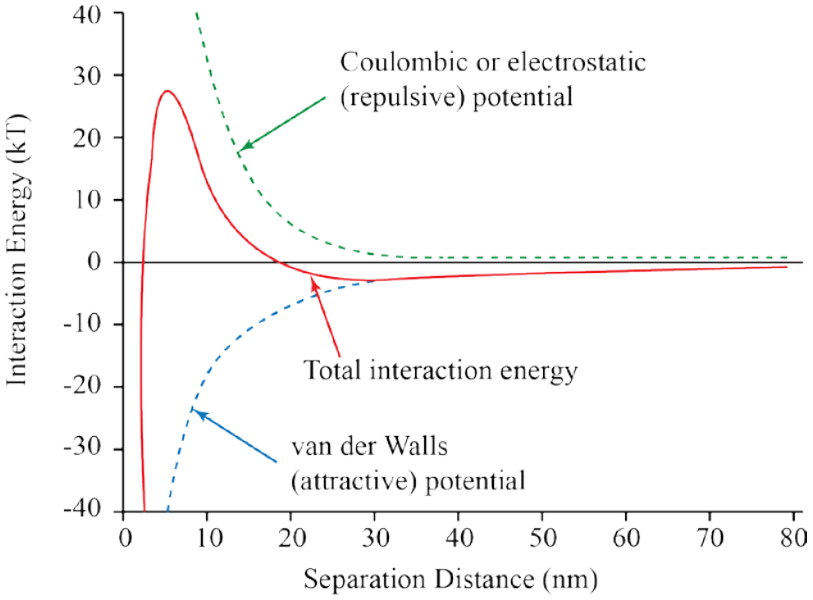

Figure 4: Schematic interaction energy versus distance profiles of DLVO

According to the DLVO theory, Coulomb's repulsion, Van der Waals attraction, and their interaction energy go to plus and minus infinities. Is it right?

6. *Modified Newtonian dynamics (MOND)* is a hypothesis that proposes a modification of Newton's laws to account for observed properties of galaxies [37]. For elliptical galaxies, galaxy groups, galaxy clusters, and larger-scale structures, the theory doesn't quite fit observations, and so it requires that extra matter — i.e., dark matter — be invoked once again. "So instead of just using an undiscovered particle to explain our observations of structures in the universe, MOND requires both an undiscovered particle and a modification to the gravitational-force law" [5].

The infinity of ISL seems also in the DLVO theory. The IPL also cannot explain the physical nature of being. Because the term "infinity" is only a mathematical trick.

Why do we Still Believe in Inverse-Square Law? [38]. Yes, it is right. This kind of a sign that we might be missing something kind of fundamental. So maybe one way to attack this problem is to go back to first principles. Nature is very simple and perfect with nothing to repair. Natural laws are only possible to comprehend. To err is human. "You've been making things unnecessarily complicated" by mathematics as said Hugh Everett (1957).

III. OPEN HYSTERESIS INSTEAD OF INVERSE-SQUARE LAW

...The measurements suggest that the anomalous phenomena have a common origin [38]. What is a common origin? It was the ISL, particularly the IPL to date. Instead of them, open hysteresis would be more suitable.

"We review recent experimental tests of the gravitational inverse-square law and the wide variety of theoretical considerations that suggest the law may break down in experimentally accessible regions." [4]

We compare the modulations of the open hysteresis and ISL. The comparison indicates the open hysteresis can be used in place of ISL (Figure 5).

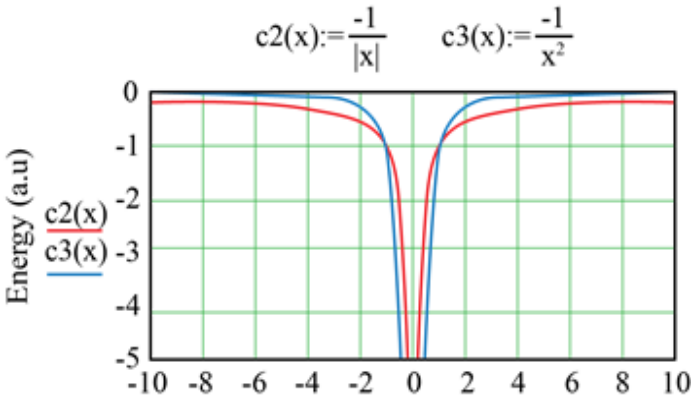

Figure 5: Distance from the nucleus (a.u.)

The c3(x) is the base of the Coulomb interaction (blue) and c2(x) is the base of the open hysteresis (red). The base of the open hysteresis indicates the only accuracy, but the result of which goes to infinite.

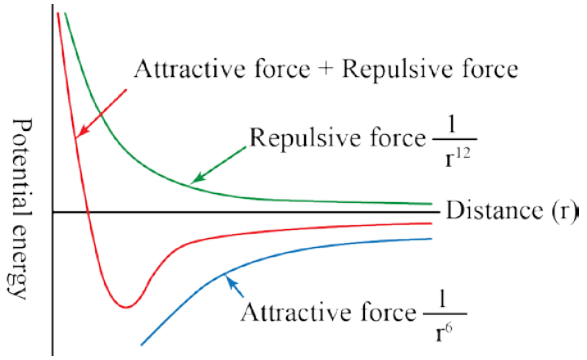

Figure 6: The potential energy between the Coulomb repulsion and Van der Waals attraction by the inverse-square law [39]

Figure 6 is calculated by the Lennard-Jones potential, the potential energy of which flies exponentially to infinity. It must be limited by interaction energy. For this reason, I show the change of the picture of the interaction of the electric charges in Figure 7b.

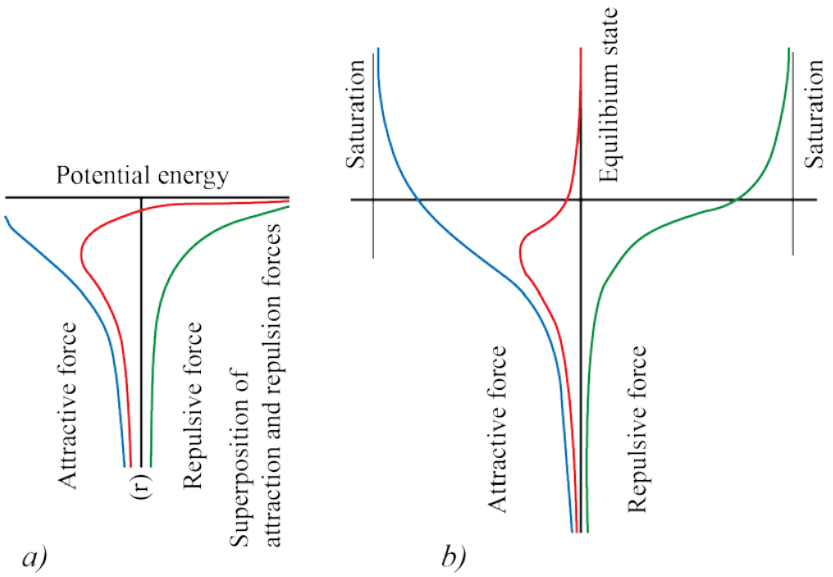

Figure 7: Interaction of the electrical charges

a) Superposition of potential energy (yellow curve), b) Open hysteresis

(Note: Distance and relative sizes are shown not to scale)

Opposite charges attract and like charges repel because doing so lowers their potential energy (energy of interaction). Energy is a force exerted through a distance ($E = Fr$). Consequently, the potential energy of two charged particles separated by a distance r. ΔE, which is referred to as the energy of interaction, is the potential energy of the two particles separated by a distance r relative to their potential energy when they are separated by an infinite distance (i.e., not interacting).

The energy change is negative (the energy decreases) as r decreases when q_1 and q_2 have opposite signs, therefore particles of opposite charge lower their energy as they get closer. Systems strive to lower their energy, so particles of opposite signs are attracted. However, the energy change is positive (the energy increases) when q_1 and q_2 have the same sign, which means that the energy of two particles of the same sign increases as they get closer. Consequently, particles of the same charge move apart to lower their energy; i.e., particles of like charge are repelled [40].

The total energy of a system is the sum of the attracting and repelling forces. The exchange interaction forces the spins of electrons to align either parallel (ferromagnetic exchange interaction) or antiparallel (antiferromagnetic exchange interaction). The origin of the exchange interaction is the spin-dependent Coulomb interaction. There are three contributions to exchange interaction between localized electrons: 1) spin-dependent electron-electron Coulomb repulsion at a short distance (antiferromagnetic); (2) spin-dependent electron-nuclear Coulomb attraction (ferromagnetic); 3) spin-dependent electron-electron Coulomb repulsion at a longer distance (ferromagnetic) [41].

The exchange interaction of quantum mechanics is the superposition of two forces (Figure 7a and Figure 7b). The interaction of two forces is described by the open hysteresis in Supreme Theory of Everything [42], [43] (Figure 7b). In other words, the equilibrium state originates from the superposition of both energy states.

In any case, the attractive and repulsive forces have saturation limits of potential energy and the system strives for their equilibrium state (Figure 7).

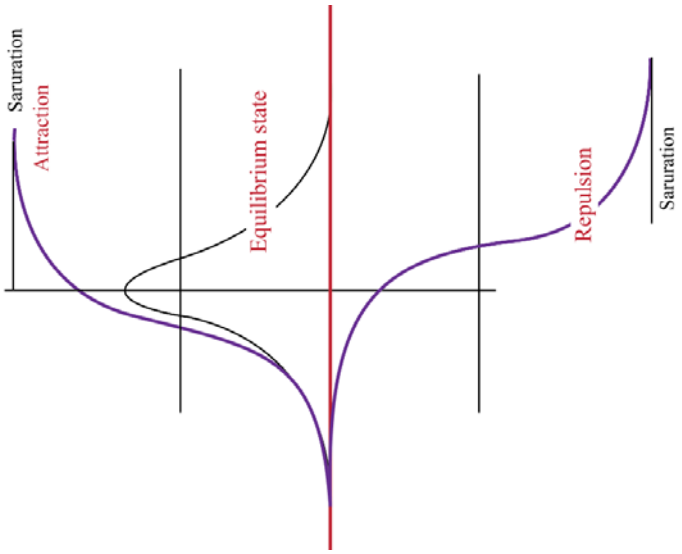

Figure 8: The open hysteresis [44] instead of "inverse-square law" shown in Figure 6.

As shown in Figure 8, everything has a limit of v saturation. For instance, the abovementioned Earth's magnetotail comes back into the north pole after traveling more than 8 million kilometers. Nothing blocks the continuous outflow of the magnetotail, but it comes back. So, its reason lies in the expression the answer is "infinity" of calculation results by ISL.

IV. THE FIRST ATTEMPT TO DETERMINE ELECTROSTATIC INTERACTIONS BY OPEN HYSTERESIS

We need to understand that open hysteresis gives the general picture of anything that looks like the ISL and IPL. In other words, it is independent of physical, chemical, biological, and other factors. Since the open hysteresis is valid not only in electromagnetism but everything else. All the forces blend harmonically with everything.

To avoid the difficulties of ISL we need to use open hysteresis. The problem becomes more and more quantum mechanical. To do this I think presently to show interactions of electrical charges (Figure 9).

The K border is the equilibrium boundary of electromagnetic forces and separates two different mediums (Figure 9).

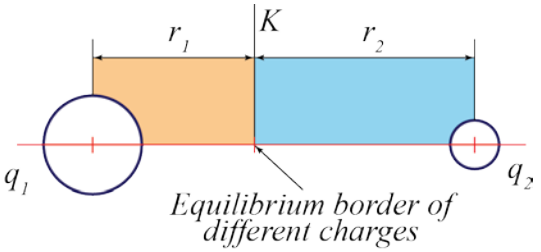

Figure 9: The two charges in equilibrium

The distance between electrons has possible to determine by the ratio:

$$q_1 r_1 = q_2 r_2 \tag{10}$$

$$\frac{r_1}{r_2} = \frac{q_2}{q_1} \tag{11}$$

In case that r_1 and r_2 are little, we can use $\sin r \approx r$

$$\frac{\sin r_1}{\sin r_2} = \frac{q_2}{q_1} \tag{12}$$

It is Snell's law, which gives the hysteresis formula:

$$F_e = \mathrm{Q} \cdot \frac{sin(r_1 - r_2)}{|cos(r_2)|} \tag{13}$$

Where r_1 is the influence radius of q_1 electric charge, r_2 is the radius of q_2.

$$Q = Q(q_1, q_2), \textit{ which needs to determine by experiments}$$

The interaction force between the electric charges is displayed by Figure 10.

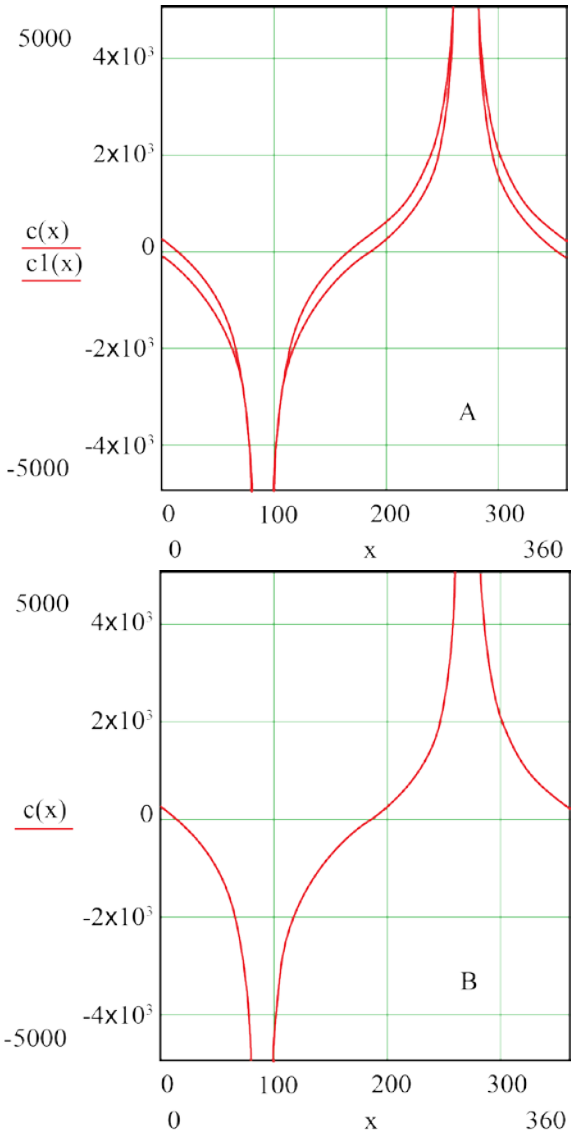

Figure 10: The hysteresis of the electric interaction of charges
(For simplicity $Y = 1000$ *and* $r_1 = 10$)
(Note: Distance and relative sizes are shown not to scale)

In Figure 10 A is the closed hysteresis and B is the open hysteresis. So, I would like to ask that excuse me because it is my first attempt to use open hysteresis in electromagnetism. I truly appreciate your critical review, comments, feedback, and questions.

The theory is valid only as long as it is not disproved by experiments. However, 'the great tragedy of science – the slaying of a beautiful hypothesis by an ugly fact.' - Thomas H. Huxley. And 'No theory should fit all data, because some data are surely wrong' [38].

If we use the open hysteresis in a general application, the vertical axis shows the force, intensity, magnitude, and the horizontal axis shows the repeated processes such as distance and period (Figure 10).

I imagine that if we use the open hysteresis instead of ISL, it may make big progress in science because the open hysteresis has a memory that causes the output value to depend on the history of the input [45], [46]. It also has periodicity, saturation and it also works in all scales.

V. CONCLUSION

1. The inverse square law can work neither on a cosmic scale nor on the subatomic scale. A lot of physical laws have been described based on the ISL,which has generated a large discrepancy between the results of theory and observation.
2. When the variable (r) of the inverse-square law and inverse-proportional formula goes to 0, the results become infinite. All the potential energy as van der Waals attraction potential, Coulombic repulsion potential, and their interaction have limits or saturations. Everything has a saturation. Nothing continues to infinity.
3. Instead of the ISL and IPL, the applications of open hysteresis are more suitable in practice due to open hysteresis having periodicity, saturation, and memory and it works in all scales.
4. The open hysteresis describes the general picture of the geometrical entity of everything that looks like the ISL and IPL. It is independent of physical, chemical, biological, and other factors. Since the open hysteresis is valid not only in electromagnetism but everything else.

REFERENCES

1. Inverse-square law, https://en.wikipedia.org/wiki/Inverse-square_law
2. Newton's law of universal gravitation, https://en.wikipedia.org/wiki/Newton%27s_law_of_universal_gravitation
3. Isaac Newton, "In [experimental] philosophy particular propositions are inferred from the Phenomena and afterward rendered general by induction": "Principia", Book #, General Scholium, at p.392 in Volume 2 of Andrew Motte's English translation published 1729.
4. Adelberger, E.G., B.R. Heckel, A.E. Nelson, Tests of the gravitational inverse-square law, Annual Review of Nuclear and particle Science, Vol. 53:77-121 (Volume publication date December 2003), https://doi.org/10.1146/annurev.nucl.53.041002.110503arXiv:hep-ph/030728a4,(or arXiv:hep-ph/0307284v1)https://arxiv.org/pdf/hep-ph/0307284.pdf
5. If Not Dark Matter, Then What? https://www.livescience.com/19796-dark-matter- alternatives. html.
6. M. Persic and P. Salucci. Rotation curves of 967 spiral galaxies. arXiv, astro-ph/9502091,1995.
7. M. Persic, P. Salucci, and F. Stel. The universal rotation curve of spiral galaxies - I. The dark matter connection. Monthly Notices of the Roy. Astr. Soc., 281:27–47, 1996, astro-ph/9506004
8. P. Salucci, A. Lapi, C. Tonini, G. Gentile, I. Yegorova, and U. Klein. The Universal Rotation The curve of Spiral Galaxies. II The Dark Matter Distribution out to the Virial Radius.ArXiv: astro-ph/0703115, 2007.
9. G. Gentile, P. Salucci, U. Klein, D. Vergani, and P. Kalberla]. The cored distribution of dark matter in spiral galaxies. Monthly Notices of the Royal Astronomical Society, 2004, astro-ph/0403154.

10. G. Gentile, P. Salucci, U. Klein, and G. L. Granato. NGC 3741: the dark halo profile from the most extended rotation curve. Monthly Notices of the Roy. Astr. Soc., 375:199–212,2007, arXiv:astro-ph/0611355.
11. P. Salucci and A. Borriello. Cold Dark Matter Halos Must Burn. In M. Gilfanov, R. Sunyaev, and E. Churazov, editors, Lighthouses of the Universe: The Most Luminous Celestial Objects and Their Use for Cosmology: Proceedings of the PA/ESO/MPE/USM, pages 534–+, 2002, astro-ph/0106251,
12. P. Salucci and A. Borriello. The Intriguing Distribution of Dark Matter in Galaxies. In J. Trampeti and J. Wess, editors, Particle Physics in the New Millennium, volume 616 of Lecture Notes in Physics, Berlin Springer Verlag, pages 66–77, 2003, astro-ph/0203457.
13. Aguirre, C. P. Burgess, A. Friedland, and D. Nolte. TOPICAL REVIEW: Astrophysical constraints on modifying gravity at large distances. Classical and Quantum Gravity,18:223–+, December 2001, hep-ph/0105083.
14. Bosma. Dark Matter in Disc Galaxies. ArXiv Astrophysics e-prints, astro-ph/9812013 1998. Y. Sofue and V. Rubin. Rotation Curves of Spiral Galaxies. Annual Review of Astronomy and Astrophysics, 39:137–174, 2001, astro-ph/0010594]
15. M. J. Disney et. al. Galaxies appear simpler than expected. Nature, 455:1082–1084, October 2008.
16. S. van den Bergh. Astrophysics: How do galaxies form? Nature, 455:1049–1051, 2008.
17. Testing the gravitational inverse-square law https://physicsworld.com/a/testing-the- gravitational-inverse-square-law/
18. Edward W. Hones Jr, (1986), The Earth's magnetotail, Scientific American, Vol. 254, No. 3, pp.40-47, Scientific American, A Division of Springer Nature America, Inc. https://www.jstor.org/stable/24975910.
19. Overbye, Dennis (2017), "Cosmos Controversy: The Universe Is Expanding, But How Fast?". The New York Times. https://astronomy.com/news/2017/10/gravitational-waves-show-how-fast-the-universe-is-expanding.
20. Scharping, Nathaniel (18 October 2017). "Gravitational waves show how fast the universe is expanding". *Astronomy*. Retrieved 18 October 2017 https://astronomy.com/news/2017/10/gravitational-waves-show-how-fast-the-universe-is-expandin
21. Weaver, Donna; Villard, Ray (2018). "Measuring universe expansion reveals mystery – Is something unpredicted going on in the depths of space?". Earth & Sky. https://astronomy.com/news/2017/10/gravitational-waves-show-how-fast-the-universe-is-expanding
22. Dark Energy, Dark Matter, https://science.nasa.gov/astrophysics/focus-areas/ what-is- dark-energy.
23. Huray, Paul G., 1941- (2010). *Maxwell's equations*. Hoboken, N.J.: Wiley. Pp. 8, 57. ISBN 978-0-470-54991-9. OCLC 739118459.
24. Halliday, David; Resnick, Robert; Walker, Jearl (2013). *Fundamentals of Physics*. John Wiley & Sons. pp. 609, 611. ISBN 9781118230718.
25. Roller, Duane; Roller, D.H.D. (1954). *The development of the concept of electric charge: Electricity from the Greeks to Coulomb*. Cambridge, MA: Harvard University Press. p. 79.
26. Coulomb (1785) "Premier mémoire sur l'électricité et le magnétisme," *Histoire de l'Académie Royale des Sciences*, pp. 569–577.
27. Garrett, Reginald H.; Grisham, Charles M. (2016). *Biochemistry* (6th ed.). University of Virginia. pp. 12–13.
28. Klimchitskaya, G. L.; Mostepanenko, V. M. (July 2015). "Casimir and Van der Waals Forces: Advances and Problems". *Proceedings of Peter the Great St. Petersburg Polytechnic University* (517): 41–65. arXiv:1507.02393. doi:10.5862/PROC.516.4. S2CID 119270219.
29. Tschumper, Gregory S. (20 October 2008). "Reliable Electronic Structure Computations for Weak Noncovalent Interactions in Clusters". In Lipkowitz, Kenny B.; Cundari, Thomas R. (eds.). *Reviews*

in Computational Chemistry. 26. John Wiley & Sons. pp. 39–90. doi:10.1002/9780470399545.ch2. ISBN 9780470399545.
30. Mahan, Gerald D. (2009). *Quantum mechanics in a nutshell*. Princeton: Princeton University Press. ISBN 0-691-13713-7. OCLC 226037727.
31. Jörg Polte, Supplementary Information Fundamental Growth Principles of Colloidal Metal Nanoparticles, The Royal Society of Chemistry 2015, http://www.rsc.org/suppdata/c5/ce/c5ce01014d/c5ce01014d1.pdf
32. Lennard-Jones potential, https://en.wikipedia.org/wiki/Lennard-Jones_potential.
33. Xipeng Wang, Simón Ramírez-Hinestrosa, Jure Dobnikar and Daan Frenkel, The Lennard-Jones potential: when (not) to use it, Physical Chemistry Chemical Physics, Issue 19, 2020. https://pubs.rsc.org/en/content/articlelanding/2020/cp/c9cp05445f#!divAbstract
34. Yukawa potential, https://en.wikipedia.org/wiki/Yukawa_potential.
35. U. Satya Sainadh, Han Xu, Xiaoshan Wang, Atia-Tul-Noor, William C. Wallace, Nicolas Douguet, Alexander W. Bray, Igor Ivanov, Klaus Bartschat, Anatoli Kheifets, R. T. Sang1 & I. V. Litvinyuk, Attosecond angular streaking and tunneling time in atomic hydrogen. https://www.researchgate.net/publication/318527833_Attosecond_angular_streaking_and tunnelling_time_in_atomic_hydrogen.
36. Adair, J.H., ... J. Sindel, DLVO Theory, Surface and Colloid Chemistry, in Encyclopedia of Materials: Science and Technology, 2001
37. https://www.sciencedirect.com/topics/pharmacology-toxicology-and-pharmaceutical-science/dlvo-theory DLVO theory
38. Modified Newtonian dynamics, htpp://en.wikipedia.org/wiki/Modified_Newtonian_dynamics
39. Unzicker, A., Why do we Still Believe in Newton's Law? Facts, Myths, and Methods in Gravitational Physics, https://arxiv.org/pdf/gr-qc/0702009.pdf
40. Intermolecular forces: Van der Waals forces, hydrogen bond, hydrophobic effect, Ryosuke University, https://j-tradition.com/interaction.html
41. The Early Experiments, Chapter 1, Advanced Instructional Systems, Inc. and NC State College of Sciences Foundation 2014, https://www.webassign.net/question_assets/wertzcams3/ch_1/manual.pdf
42. Vadym Zayets, Exchange Interaction: Spin and Charge Transport, *https://staff.aist.go.jp/v.zayets/*
43. Ulaanbaatar Tarzad, Supreme Theory of Everything, Advances in Theoretical & Computational Physics, Volume 2 | Issue 2 |, 1-6
44. Ulaanbaatar Tarzad, Supreme Theory of Everything: Whole Universe in a Simple Formula, London Journal of Research in Science: Natural and Formal, Volume 20 | Issue 5 | Compilation 1.0, p. 73-90.
45. Ulaanbaatar Tarzad, Formula Extraction in Supreme Theory of Everything, Advances in Theoretical & Computational Physics, Volume 2 | Issue 4 | 1 of 3Hysteresis, https://en.wikipedia.org/wiki/Hysteresis
46. Positive feedback, https://en.wikipedia.org/wiki/Positive_feedback#/media/File: Hysteresis sharp_curve.svg

This page is intentionally left blank

Joint Geophysical Methods and Hydro Physicochemical Analyses for Environmental and Criminal Geoforensics Investigations of Leachate Plume Migration in Third Cemetery, Edo State, Nigeria

Idehen, O & Airen, O. J

ABSTRACT

Health concern about possible impact of the cemeteries in Nigeria on the water supply has prompted this research. The research engaged Vertical Electrical Sounding (VES), 2-Dimensional and 3-Dimensional imaging (tomography) to investigate the presence and migration of leachate plumes in the cemetery, hydro physicochemical analysis of water samples (for multivariate analysis) and computation of time- lapse to detect the time rate of migration in both the vertical and horizontal directions.

The field work covered a time – lapse of six months (June 2017 to December 2017). Three sites at the peripheral of the cemetery and a reference site were used as water sample sources. Groundwater samples were collected and analyzed. The electrical resistivity data collected in parallel equidistant lines was processed to obtain geoelectric models using Res2dinv and the second survey data was also merged and inverted as a single 3-D data set using Res3dinv software and Voxler 4.0 to give 3-D block model and volumetric analysis of the leachate plume. Multivariate analysis involving Principle Component Analysis, Cluster Analysis and computation of Water Quality Index, was also carried out to identify the major contaminants and their levels of contamination.

Keywords: groundwater, contamination, cemetery, hydro-physicochemical, geophysical.

Classification: FOR CODE: 040499p

Language: English

London Journals Press

LJP Copyright ID: 925652
Print ISSN: 2631-8490
Online ISSN: 2631-8504

London Journal of Research in Science: Natural and Formal

Volume 21 | Issue 2 | Compilation 1.0

Joint Geophysical Methods and Hydro Physicochemical Analyses for Environmental and Criminal Geoforensics Investigations of Leachate Plume Migration in Third Cemetery, Edo State, Nigeria

Idehen, O [α] & Airen, O. J [σ]

ABSTRACT

Health concern about possible impact of the cemeteries in Nigeria on the water supply has prompted this research. The research engaged Vertical Electrical Sounding (VES), 2-Dimensional and 3-Dimensional imaging (tomography) to investigate the presence and migration of leachate plumes in the cemetery, hydro physicochemical analysis of water samples (for multivariate analysis) and computation of time- lapse to detect the time rate of migration in both the vertical and horizontal directions.

The field work covered a time – lapse of six months (June 2017 to December 2017). Three sites at the peripheral of the cemetery and a reference site were used as water sample sources. Groundwater samples were collected and analyzed. The electrical resistivity data collected in parallel equidistant lines was processed to obtain geoelectric models using Res2dinv and the second survey data was also merged and inverted as a single 3-D data set using Res3dinv software and Voxler 4.0 to give 3-D block model and volumetric analysis of the leachate plume. Multivariate analysis involving Principle Component Analysis, Cluster Analysis and computation of Water Quality Index, was also carried out to identify the major contaminants and their levels of contamination.

The study showed that the status of the groundwater at the vicinity of the cemetery is fit for drinking and other domestic purposes though with some degree of contaminations. The main parameters constituting the contaminants include pH, EC, Cl, NO_3, SO_4 and Na, which are mostly influenced by the on-site activities in the cemetery. The leachate plumes in the cemetery migrate vertically and horizontally at different rates. The research also showed that repeated ERT surveys can track movement of leachate plume emanating from decomposed dead bodies over time in active cemetery.

Keywords: groundwater, contamination, cemetery, hydro-physicochemical, geophysical.

I. INTRODUCTION

The investigation of cemeteries is always difficult and challenging task in geoforensic prospective. The identification of individual graves through geophysical techniques is relatively problematic and thus in the prospection of cemeteries and graves there are no rules or specific guidelines. The success of such a survey depends on the conservation of the graves, the various artifacts that may accompany a burial, the depth and dimensions of the burial, the environmental noise, the geology, etc.

Geoforensic, which simply means Forensic Geology, is defined as the gathering and analysis of geological evidence of a crime. It is the study of evidence relating to minerals, oil, petroleum, and other materials found in the earth, used to answer questions raised by the legal system (Murray and Tedrow 1975). However, the implications of land utilization for burial of dead human bodies in the form of cemeteries and many cases associated with coffin and caskets used for interment of

remains has received no consideration in Nigeria. Interment of bodies in cemeteries remains a widespread practice and the only alternative endpoint to dead bodies in Nigeria. In Nigeria, this practice had not been perceived as having a significant potential contaminant effect in the environment and especially the groundwater component as search of literature attracted no such study to the country. In Benin City and Nigeria in general, the major cemeteries are located close to human residential areas and virtually all the populace within this locality depends on groundwater as the primary water source for various domestic purposes Idehen, O and Ezenwa,I. M (2019). According to DOC (2016), cemetery sites/graveyards have the potential to result in impact on the local water environment and in particular, the groundwater underlying such sites.

Toxic chemicals that may be released into groundwater include substances that were used in embalming and burial practices as well as varnishes, sealers and preservatives and metal component of ornaments used on wooden coffins (Jonker and Olivier, 2012). Wood preservatives and paints used in coffin construction contain compounds such as copper, naphthalene and ammoniac or chromated copper arsenate (Spongberg and Becks, 2000). Paints contain lead, mercury, cadmium, and chromium; arsenic is used as a pigment, wood preservative and anti-fouling ingredient while barium is used as a pigment and a corrosion inhibitor (Katz and Salem, 2005; Huang *et al.*, 2010; Jonker and Olivier, 2012).

This underpins the importance of carrying out studies aimed at investigating the impact and attendant risks that cemeteries present to the populace living close to them. This project has been carried out to provide information on whether the cemetery located at Third Cemetery, Benin City, impacts the groundwater resources in aquifer within that zone.

Studies on the impact of cemeteries on the quality of groundwater in unsaturated and saturated zones are usually conducted within or at some distance from the cemeteries (Schraps, 1972; Zychowski *et al.*, 2000b). Over 40% of cemeteries in South Africa contaminate water resources (Fisher and Croukamp, 1993). Local authorities seem oblivious of the problem. Both legal regulation and the determination to act in a way which would limit the threat are lacking (Alfoldi and Croukamp, 1988). Most researchers assess the impact of interment on the environment by comparing study results from cemeteries with data from reference sites. This type of assessment is satisfactory despite some possible errors (Zychowski, 2012).

Groundwater has for many decades served as a source of drinking water and it is still relevant for same purpose till date (Radajevic and Bashkin, 1999) despite the fact that different human activities have impaired its quality in some locality.

II. STUDY AREA

This study was conducted in Benin City located in south-south geopolitical zone of Nigeria. Benin City is the capital of Edo State, bounded by latitudes 06° 06' N, 06° 30' N and longitudes 005° 30' E, 005° 45' E and an area of about 500 square kilometers. The city is located within the rain forest ecological zone with annual mean temperature of 27.5 °C (Ikhuoria, 1987, Idehen, 2019) and an annual mean rain fall of about 2095 mm (Ikhile and Olorode, 2011). Three cemeteries namely First, Second and Third cemeteries are located within this city. The Third cemetery which has existed for over 50 year was considered for this study because of its proximity to human residents. The cemetery which is the biggest among the cemeteries in Benin City covers an area of about 5.167 ha (Ibhadode *et al.*, 2017). The burial load of this cemetery could not be calculated, because the record-keeping was not always adequate regarding the number of people buried. Also there is issue where a single grave is used for multiple burials. Three sampling sites were used for the collection of water samples.

III. METHODOLOGY

Electrical resistivity imaging data was acquired twice using Pasi Earth Resistivity Meter. The

second data set was acquired six months after the first one. The data coverage was made over an area defined by rectangular loop measuring 30 m by 230 m in the first survey while in the second survey was 30 m by 200 m. The electrical resistivity data was collected in seven equidistant lines as 2-D data set using Wenner-Schlumberger Array at 5 m interval in both periods. The first survey, the inter-electrode spacing in each line was 10 m while in the second survey was 5 m .Thus, first survey used to guide planning and execution of the second. The resistance values read from the measuring instrument was then transformed to apparent resistivity using the geometrical factor each sequence of measurement.

In order to characterize the physicochemical parameters of the water and further ascertain the suitability of these groundwater resources located near the cemetery, equal replicate of water samples were collected from borehole located at the peripheral of the cemetery.

Wenner -Schlumberger spread was used. In first survey, in each line location, electrodes numbered 0- 23 were placed into the ground at intervals of 10 m along the line, while in the second survey, electrodes numbered 0-40 at 5 m interval was planted into the ground. Each time measurement, was to be taken, array of four electrodes are selected manually and connected to the PASI earth resistivity meter via single core cable.

IV. RESULTS AND DISCUSSION

The geoelectric models obtained for the first and second surveys displayed leachate plumes starting from the laterite (the burial environment) down to the sandy formation (the regional water supply source). The leachate plumes presence in the sand bed are modeled and described as shown in the 2-D and 3-D displays (Fig. 1 to Fig. 3).

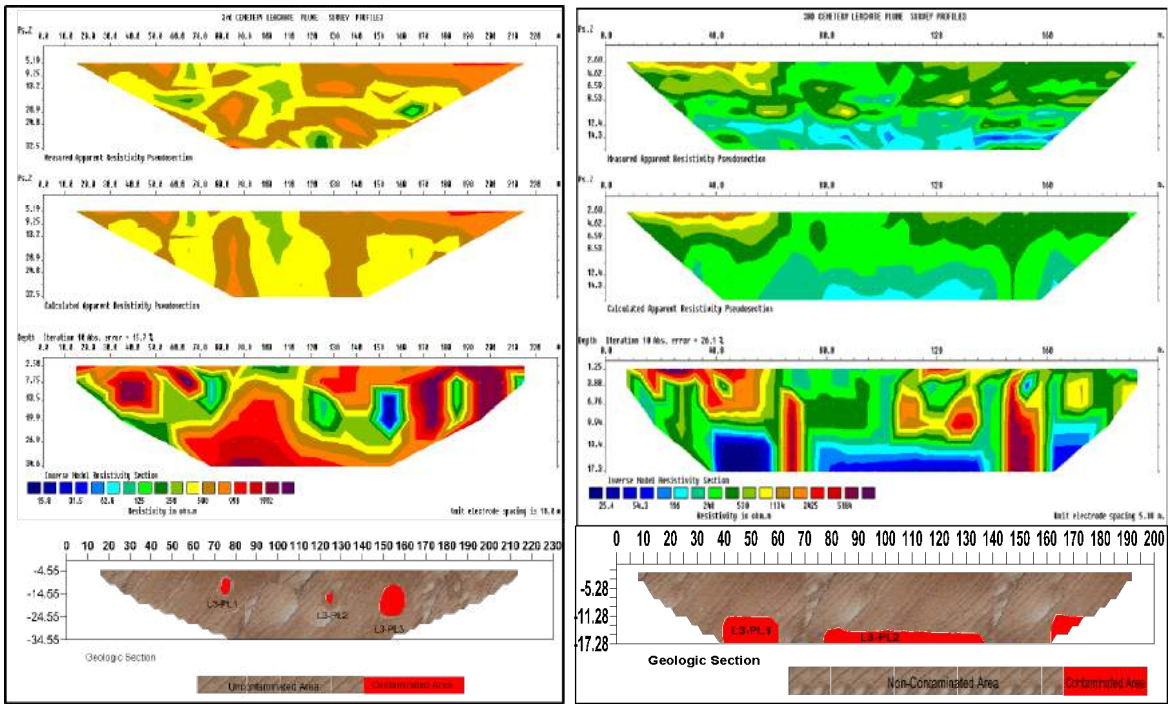

First Survey Profile3 (June, 2017) Second Survey Profile3 (Dec. 2017)

Fig. 1: 2: D Geoelectric Models of Profile3 in the First and Second Survey

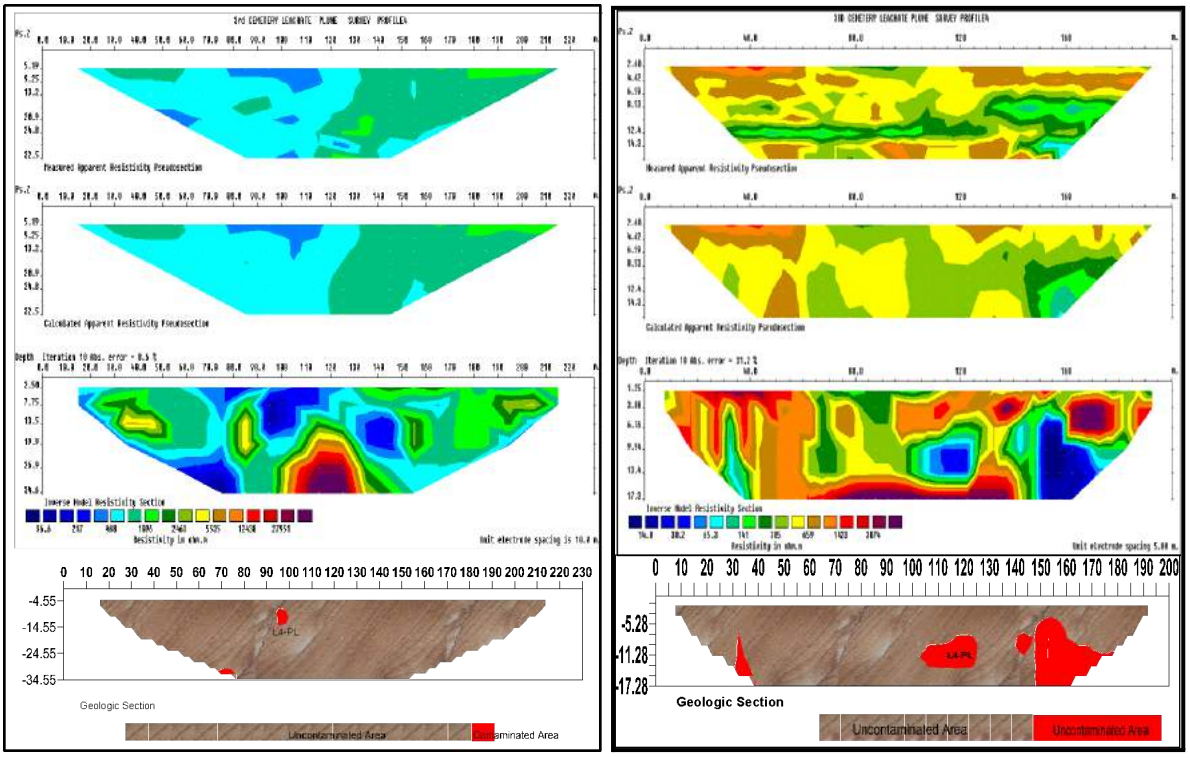

First Survey Profile 4 (June, 2017) Second Survey Profile 4(Dec. 2017)

Fig. 2: 2: D Geoelectric Models of Profile 4 in the First and Second Survey

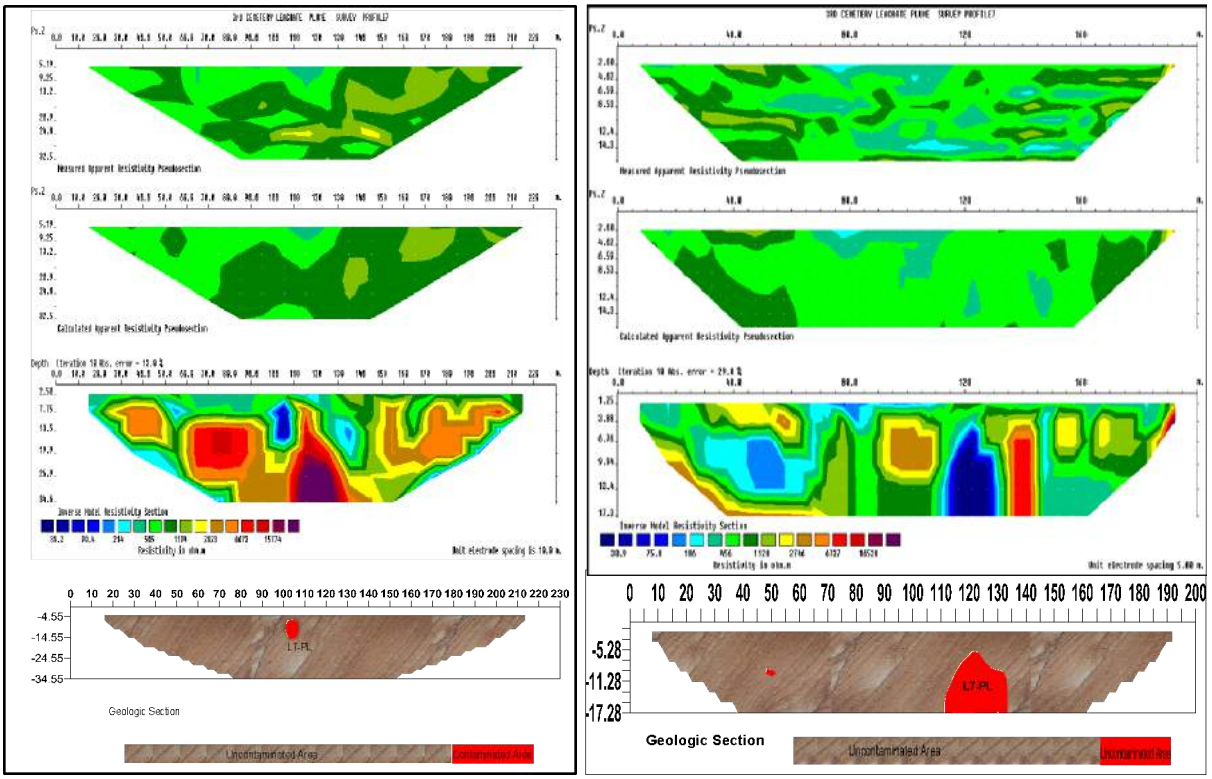

First Survey Profile 7 (June, 2017) Second Survey Profile 7 (Dec. 2017)

Fig. 3: 2: D Geoelectric Models of Profile 7 in the First and Second Survey

V. DISCUSSION

The field works were conducted in two sessions with a time interval of six (6) months. The first ERT survey was conducted in June 2017 (early period of rainy season) and the second ERT survey was conducted in December 2017 (early period of dry season) when the plumes must have been diluted with excess infiltrating water and move faster in the vertical and horizontal directions. The rate of migration depends on the permeability of the soil, incline topography, depressions created by decomposed corpses and collapsed burial materials. All these aid infiltration into the subsurface.

The rate of migration in the horizontal direction is higher than the rate of migration in the vertical direction. The maximum rate of migration in the vertical direction is 4.1 cm/day while the maximum rate of migration in the horizontal direction is 32.8 cm/day. It is observed that horizontal migration is higher than the corresponding vertical migration. The plume flows vertically and outwardly into the ground, and the horizontal permeability of sediment is found to be higher than the vertical permeability except in vertical solution fractures (Djebbar *et al.*, 2004, Idehen, 2020).

VI. PHYSICOCHEMICAL ANALYSES OF WATER SAMPLES MULTIVARIATE STATISTICAL ANALYSIS

Exploratory data analysis was performed by linear display methods (principal component analysis, PCA) and unsupervised pattern recognition techniques (hierarchical cluster analysis, CA) on experimental data. Cluster analysis allows the grouping of obtained samples on the basis of their similarities in chemical composition. Cluster analysis uses all the variance or information contained in the original data set (Razmkhah et al., 2010).

Table.1: Summary Of Variations In The Physicochemical Variables

Variables	Site 1	Site 2	Site 3	Reference	CV	NSDQW
Ph	4.96	4.34	4.05	6.80	24.51	7.50
EC	118.00	82.00	160.00	12.00	67.43	1000.00
TDS	59.00	41.00	80.00	6.30	67.04	500.00
TSS	0.58	0.07	0.66	0.00	103.80	0.00
Calcium	3.84	3.20	4.48	2.40	25.56	NA
Magnesium	1.15	2.30	3.84	3.00	44.25	0.20
Sulphate	0.17	0.25	0.00	0.43	83.75	100.00
Nitrate	0.29	1.37	1.75	0.08	93.23	50.00
Phosphate	0.64	0.83	0.33	0.24	53.65	NA
Calcium carbonate	30.50	24.40	18.60	50.80	45.11	150.00
Chloride	44.52	23.78	36.40	18.40	38.57	250.00
Sodium	37.60	16.40	32.00	2.60	71.43	200.00
Potassium	48.88	21.32	41.60	3.38	71.43	NA
Lead	0.01	0.00	0.01	0.00	115.01	0.01
Chromium	0.01	0.01	0.01	0.01	0.00	0.05
Copper	0.02	0.01	0.03	0.01	81.65	1.00
Zinc	0.02	0.01	0.02	0.02	28.57	3.00
Iron	0.04	0.02	0.03	0.08	61.88	0.30

Manganese	0.03	0.01	0.02	0.01	81.65	0.20
Cadmium	0.00	0.00	0.00	0.00	0.00	0.00
Nickel	0.01	0.01	0.02	0.01	70.71	0.02
Mercury	0.00	0.00	0.00	0.00	0.00	0.00
DO	8.80	6.20	9.80	9.20	18.68	NA
BOD_5	2.60	1.80	3.40	0.60	56.88	NA
COD	12.46	10.32	14.77	12.10	14.74	NA

NSDWQ - Nigerian Standard for Drinking Water Quality (NIS, 2007).

All variables except pH and EC were measured in mg/l; EC was measured in µS/cm.

VII. VARIATIONS IN THE PHYSICOCHEMICAL PARAMETERS

Table.1 shows the variations in the physicochemical parameters characterized in the groundwater samples obtained from the various sites. The levels of homogeneity of the levels of the variables across the sites including the reference site are represented by the coefficient of variation (CV). TSS and lead had CV values > 100; EC, TDS, sulphate, nitrate, phosphate, sodium, potassium, copper, iron, manganese, nickel and BOD_5 recorded CV values > 50 while pH, calcium, magnesium, alkalinity, chloride, zinc, DO and COD had CV values < 50. The levels of chromium, cadmium and mercury were relatively the same across the sites including the reference site thus no variation was recorded (CV = 0).

The groundwater was slightly acidic at all sites except the reference; electrical conductivity (EC), total dissolved and total suspended solids, nutrients including nitrate and phosphate, the alkali metals, heavy metals (excluding iron values which was high in the reference sites and cadmium and mercury which were not detectable in the water samples) values were low in the water samples obtained from reference site (Idehen and Ezenwa,2019). Generally chloride was the dominant anion across all the sites samples were obtained while the least of the same group were sulphate and nitrate for cemetery peripheral sites and reference site respectively.

VIII. CONCLUSION

The geoelectric models obtained for the first and second surveys displayed leachate plumes starting from the laterite (the burial environment) down to the sandy formation (the regional water supply source). The leachate plumes presence in the sand bed are modeled and described as shown in the 2-D and 3-D displays. This study showed that parts of the cemetery had been contaminated. This was evident in the attendant low resistivity values. This contamination was also observed to have infiltrated into the aquifer in the cemetery. This could pose serious health risks to the inhabitants of the study area who depend largely on boreholes for their drinking water supply.

The acquired two-dimensional electrical resistivity data covered laterite, fine sand, very coarse sand, medium sand. The sandy formation is porous and highly permeable, and hence the flow leachate through it is rapid. The study clearly revealed that the status of the groundwater at the vicinity of Third Cemetery is fit or suitable for drinking and other domestic purposes though with some degree of contaminations. Under favourable hydrological and geological conditions, the plumes delineated from the Electrical Resistivity Imaging will slowly migrate into the groundwater.

Human experience has taught that people shall continue dying and they shall continue being buried, however, we could reduce the number of people whose death could be linked to consumption of polluted groundwater by paying attention to obvious risk to residents who live close to cemeteries. This should be considered more seriously since priority must be given to the

living above the dead. Based on the data obtained in this study, we conclude that there are very clear variations between various indices of the groundwater around the cemetery at Benin City, Nigeria and the reference site. These variations could have been caused by decomposition process going on at the cemetery.

REFERENCES

1. Djebbar, T., Erle C. and Donaldson (2004). Petrophysics: theory and practice of measuring reservoir rock and fluid transport Properties.
2. DOC (2016).Cemeteries, Burials and the Water Environment;A good practice guide for applicants and planning authorities when planning cemetery developments or extensions. Practice guide. Version 1.1. NIEA Natural Heritage Division, Belfast BT7 2JA.
3. Fisher, G. J. and Croukamp, L. (1993). Ground Water Contamination and its Consequences, Resulting from the Indiscriminate Placing of Cemeteries in the Third World Context. Conference Africa Needs Groundwater. University of the Witwatersrand, Johannesburg, South Africa.
4. Huang, S. L., Yin, C. Y. and Yap, S. Y. (2010). Particle size and metals concentrations of dust from a paint manufacturing plant. J. Hazard. Mater., 174, 839-842.
5. Ibhadode, C. A. E., Dirius, A. R. and Akhimien (2017). Adequacy or otherwise of cemetery space for sustainable human body disposal in Benin City, Nigeria. Ethiopian Journal of Environmental Studies & Management, 10 (5): 566 – 571.
6. Idehen, O and Ezenwa,I. M (2019). Influence of Third Cemetery Location on the Quality of Domestic and Groundwater Resources in Benin City, Nigeria. *Journal of Applied Sciences and Environmental Management*. Vol.23(1) 05–11. ISSN 1119-8362. DOI: https://dx.doi.org/10.4314/jasem.v23i1.1
7. Idehen, O. (2019). The Impact of Typical Cemetery on Groundwater using both Geophysical Techniques and Physicochemical analyses of Water in South-South, Nigeria. *International Journal of Applied Science*; Vol.2, No. 2; 2019. ISSN 2576-7240 E-ISSN 2576-7259. https://doi.org/10.30560/ijas.v2n2p12
8. Idehen, O. (2020). A Comparative Investigation of Groundwater Contamination in Typical Dumpsites and Cemetery Using ERT and Physicochemical Analysis of Water in Benin Metropolis, Nigeria. *Journal of Geoscience and Environmental Protection, 8, 72-85*. https://doi.org/10.4236/gep.2020.81005
9. Idehen O. (2020). Volumetric Analysis of 3-D Resistivity Distribution of Leachate Plume in Third Cemetery, Benin, South-South, Nigeria. *Journal of Advances in Physics*. Vol.17. 32-40. ISSN: 2347 – 3487. DOI: https://doi.org/10.24297/jap.v17i.8486.
10. Ikhile, C. I. and Oloriode, D. O. (2011). Impact of climate change on underground-water resources development in Benin-Owena River basin, Edo State, Nigeria: case study. European Journal of Scientific Research, 63(2): 272 – 278.
11. Ikhuoria, I. A. (1987). Urban land use patterns in traditional Nigeria City: A case study of Benin City. Land use policy, Great Britain, 4 (1): 62–75.
12. Jonker, C. and Olivier, J. (2012). Mineral Contamination from Cemetery Soils: Case Study of Zandfontein Cemetery, South Africa. Int. J. Environ. Res. Public Health, 9:511-520; doi:10.3390/ijerph9020511
13. Katz, S. A. and Salem, H. (2005). Chemistry and toxicology of building timbers pressure-treated with chromated copper arsenate: a review. J. Appl. Toxicol., 25, 1-7.Loke M. H. (2014*). Electrical Imaging surveys for Environmental and Engineering Studies*. A Practical Guide to 2-D and 3-D Surveys.
14. Murray Raymond C and Tedrow John C. F (1975). Forensic Geology: Earth Sciences and Criminal Investigation.Rutgers University Press, New Brunswick, New Jersey.ISBN 978-06-8135-0794-1.
15. Nigerian Industrial Standard NIS 554: 2007. Nigerian Standard for Drinking Water Quality ICS 13, 060.20 (c) SON 2007.
16. Radajevic, M and Bashkin, V. N. (1999). Practical environmental analysis.Royal school

of chemistry, Thomas Graham house, Science Park Cambridge, UK. 645 pp.
17. Razmkhah, H., Abrishamchi, A., and Torkian, A. (2010). Evaluation of spatial and temporal variation in water quality by pattern recognition techniques: A case study on Jajrood River (Tehran, Iran). Journal of Environmental Management 91: 852–860; doi:10.1016/j.jenvman.2009.11.001
18. Schraps, W. G. (1972). The relevance of soil filtration properties for the installation of cemeteries, 16, 225-229.
19. Short K. and Stauble A. J. (1967). Outline of the Geology of Niger Delta. *Am Assoc Petroleum Geologists Bull*; 51: 761 pp.Spongberg, A. L. and Becks, P. (2000). Organic Contamination in Soils Associated with Cemeteries. Journal of Soil Contamination 9 (2), 87–97.
20. Spongberg, A. L. and Becks, P. (2000). Inorganic Soil Contamination from Cemetery Leachate. Water, Air, and Soil Pollution 117, 313–327.
21. Zychowski, J. (2012). Impact of Cemeteries on groundwater Chemistry. Elsevier (93), 29-37.
22. Zychowski, J., Lach, J. and Kolber, M. (2000). Physico-chemical features of groundwaters on cemeteries of south-eastern Poland, in Burchard, J. (ed.), State and anthropogenic changes of water quality in Poland. 1, 261-269.

Analysis of the Impact of Surface Volume Reduction on River Height Sedimentation Around Pangururan District, Samosir Regency, North Sumatra, Indonesia

Sianturi Novdin Manoktong, Mohd Khairul Amri Kamarudin, Sunardi Sudianto, Saiful Iskandar Khalit & Roslan Umar

Universitas Simalungun

ABSTRACT

This study aims to investigate the high sedimentation in riverbed of Binaga Aron Samosir Regency, North Sumatra Indonesia. The investigation was carried out on identification of types sediment materials, sediment distribution, soil texture and sediment statistics based on USDA. Sediment sampling was performed in range points of 300 meters along the 1500 meters of the sampling area. The laboratory tests were carried out to determine the type of grain, sediment distribution, soil texture and sediment statistics. The results of the study shown four types of sedimentary materials, namely rock, sand, silt and clay. The average percentage of sediment grain types in the river bed of Binanga Aron River are: rocky 7.0%, rocky sand 3.50%, sand 18.43%, sandy silt 23.09%, silt 22.07%, silty clay 22.07% and clay 12.82% scattered in each points. The soil texture class for the bottom sediment of the Binanga Aron river is rocky sand. The sediment statistical value of sediment sorting results are poorly sorted, the sedimentary skewness is coarse and sedimentary kurtosis is blunt.

Keywords: river, basic sediment, usda.

Classification: FOR CODE: 040699

Language: English

London Journals Press

LJP Copyright ID: 925652
Print ISSN: 2631-8490
Online ISSN: 2631-8504

London Journal of Research in Science: Natural and Formal

Volume 21 | Issue 2 | Compilation 1.0

Analysis of the Impact of Surface Volume Reduction on River Height Sedimentation Around Pangururan District, Samosir Regency, North Sumatra, Indonesia

Sianturi Novdin Manoktong[α], Mohd Khairul Amri Kamarudin[σ], Sunardi Sudianto[ρ], Saiful Iskandar Khalit[ↀ] & Roslan Umar[¥]

ABSTRACT

This study aims to investigate the high sedimentation in riverbed of Binaga Aron Samosir Regency, North Sumatra Indonesia. The investigation was carried out on identification of types sediment materials, sediment distribution, soil texture and sediment statistics based on USDA. Sediment sampling was performed in range points of 300 meters along the 1500 meters of the sampling area. The laboratory tests were carried out to determine the type of grain, sediment distribution, soil texture and sediment statistics. The results of the study shown four types of sedimentary materials, namely rock, sand, silt and clay. The average percentage of sediment grain types in the river bed of Binanga Aron River are: rocky 7.0%, rocky sand 3.50%, sand 18.43%, sandy silt 23.09%, silt 22.07%, silty clay 22.07% and clay 12.82% scattered in each points. The soil texture class for the bottom sediment of the Binanga Aron river is rocky sand. The sediment statistical value of sediment sorting results are poorly sorted, the sedimentary skewness is coarse and sedimentary kurtosis is blunt.

Keywords: river, basic sediment, usda.

Author

α σ: Civil Engineering, Faculty of Engineering, Universitas Simalungun, North Sumatra, Indonesia.

σ ρ ¥: East Coast Environmental Research Institute (ESERI), Universiti Sultan Zainal Abidin, Gong Badak Campus, 21300 Terengganu, Malaysia.

σ: Faculty of Applied Social Sciences, Universiti Sultan Zainal Abidin, Gong Badak Campus, Malaysia.

ρ: Post Graduate School Universitas Padjadjaran, Bandung, West Java, Indonesia.

ↀ: Fakulti Biosumber dan Insdustri Makanan, Universiti Sultan Zainal Abidin, Kampus Besut, Terengganu, Malaysia.

I. INTRODUCTION

Geographically, the river around Samosir Regency, North Sumatra Indonesia, is crossed by several rivers, one of them is Binanga Aron river. The Binanga Aron was used as a means of transportation and a source of livelihood. After decades, the quality of water has decreased and in recent years has extreme silting to drought. Today, in several parts, the deserts and rocks are formed due to the clogged materials of deforestation around the river. The high base sediment material occurs by erosion [1,2,5,6,8,10,11].

The previous studies related to bed sedimentary materials have been carried out in the same basin. The sediment materials of Binaga Aron river are rock (7.0%), sandy rock (3.50%), sand (18.43%), sandy silt (23.09%), (silt 22.07%), silt clay (22.07%), clay (12.82%), sand (85. 99%), gravel (11.08%) and mud (2.93%). [1,2,6,10,11]. The dominant sedimentary materials on the coast of the river are rock, sand, and clay. Related to trapped sediment, it was found the dominant average sediment balance in the cross-river direction with an average mass of 28.00 grams [1,3,5.9,10,11]. Based on these previous findings, the sedimentation study will be carried out to identify the type of bed sediment materials. The sampling will be conducted for every 300 meters of the river along the 1500 meters of Binanga Aron. This is due to the lunge of drought along the

London Journal of Research in Science: Natural and Formal

1500 meter of Binanga Aron. This research is aimed to provide information about the sediment distribution and riverbed sediment material of Binanga Aron river.

1.1 Objective

The objective of this study is to investigate types sediment materials, sediment distribution, soil texture that related as impact of decreasing of Binanga Aron river water surface.

Literature Review

II. METHOD

2.1 Time and site of the study

This study was conducted from November 2017 to November 2018 in the Binanga Aron River, Samosir Regency. Sampling was performed at three points with each points are 300 meters along the 1500 meter of river. Figure 1 and 2 shows the site of study and sampling location.

Figure 1: The site of study

Figure 2: Sampling location

2.2 Tools and Materials

Tools and materials used in this study are: 1) sample bag to store sample research data; 2) distance binoculars to find out the width of the river; 3) stopwatch to find out the length of time used; 4) gauge; 5) digital scale to determine the weight of the sediment sample; 6) depth meter to measure the depth; 7) cloth as a container for drying sediment; 8) GPS to determine the coordinates of the research location; 9) Digital cameras are used to take photos of the research location situation and when conducting research; 10) Sediment grab is used to collect sediment data at the research location.

2.3 Laboratory Testing

The laboratory testing was carried out using these equipments: 1) oven with an adjustable temperature at 105 – 1100 C; 2) ASTM 152 H hydrometer; 3) distilled water; 4) measuring cup tube 1000 ml; 5) calgon (NaPO3) as reagent materials; 6) thermometer; 7) stopwatch; 8) vacuum or stove; 9) suspense mixer; 10) the scale with accuracy up to 0.01 grams; 11) Porcelain cup with pastel to break the clods into grains without damaging the granules; and 12). filter consisting of top and bottom covers.

III. DATA COLLECTION

3.1 Sediment Sampling

Sediment sampling was carried out in predetermined locations as shown in Figure 2. Sampling was taken in 6 points, namely Points 1a, 1b, and 1d; Points 2a, 2b, 2c and 2d; Points 3a, 3b and 3c; Points 4a, 4b and 4c; Points 5a, 5b, and 5c; and Points 6a, 6b, and 6c The distance between points is determined based on the width of the river then divided into 6 points. Sampling was performing along the 1500 meters of the river due to the erosion was high and more sediment was deposited [1,4.5,10.11]. The relationship between erosion and sediment is the accumulation of sedimentary materials in a location caused by erosion [4,5,9.10,11].

3.2 Treatment of sediment samples

3.2.1 Preparation

Samples were dried using an oven for about 24 hours. The dried sediment samples were filtered using a sieve number 10. The escaped grain of the

sieve is separated by 50 grams. Five grams of reagent is put into a container that contains water. Then, the samples are put into water and reagent. The sample is left for ± 24 hours so that the sediment grains are broken down. Then, the sediment samples were shaken using a mixer for 10 minutes. The mixed sample was transferred to a measuring tube/glass and poured the rinsing water into the tube and added water until the volume became 1000 cm. The tube is closed and then shaken by turning the tube vertically 60 times. After shaking, the tube is placed on the table then runs the stopwatch, and is the deposition of T = 0.

The hydrometer is read when T = 2, T = 5, T = 30, T = 60, T = 250 and T = 1440. After hydrometer measurements of all samples, the samples contained in the tube is refiltered using a wet sieve number 200 until the clay content contained in the sample is completely filtered out. The sample left on filtered number 200 is transferred into a cup/container to be heated for ± 24 hours and cooled.

3.2.2 Determination of sediment grain types

The type of sediment grain is identified in the sieving results. The remaining sediment in the filter numbers 20, 40, 60, 80, 120, and number 200 are recorded and weighed. The grains left in the filter were recorded into the sieve analysis table. The percentage that appears on the sieve analysis chart was used as a reference for determining the type of sediment grain.

3.2.3 Determination of soil texture

The analysis of soil texture classes is classified using the USDA Soil Classification pyramid as shown in Figure 4. The percentage values for the types of sediment grains (rock, sand, silt, and clay) have been presented in Table 4 and referred to each point. The example of point 4a that reveals the silty clay texture was presented in Table 4, where the soil structure is dusty clay.

3.2.4 Statistical determination

The statistical classification of sediment (sorting, thickness and kurtosis) was determined by equations (1), (2) and 3 [5,6,10,11]:

$$\sigma_1 = \frac{\phi_{84} - \phi_{16}}{4} + \frac{\phi_{95} - \phi_5}{6.6} \quad (1)$$

$$Sk_1 = \frac{\phi_{16} - \phi_{84} - 2\phi_{50}}{2(\phi_{84} - \phi_{16})} + \frac{\phi_5 + \phi_{95} - 2\phi_{50}}{2(\phi_{95} - \phi_5)} \quad (2)$$

$$K_\sigma = \frac{\phi_{95} - \phi_5}{2.44(\phi_{7\,5} - \phi_{2\,5})} \quad (3)$$

Where :

σ_1 = sorting

Sk_1 = skewness

K_σ = kurtosis

In line with the formula, the phi value at a frequency of 84% is transformed into the form of particle diameter, and so forth. After calculating, sediment statistics can be classified using a standard deviation table [1,2,5,6,10,11]. Table 1 is the classification of the value of sediment sorting. Table 2 is the classification of the value of sediment thickness and Table 3 is the value of sediment kurtosis.

Table 1: Sediment sorting, Skeweness and Kurtosis classification [1,2,3,7]

Sorting Classification		Skewness Classification		Kurtosis Classification	
Values	Categories	Values	Categories	Values	Categories
< 0.35	Very well sorted	+ 1 s/d + 0.3	Strongly fine skewed	< 0.67	Very platykurtic

0.35-0.50	Well sorted	+ 0.3 s/d + 0.1	Fine skewed	0.67 - 0.9	Platykurtic
0.50-0.71	Moderately well sorted	+ 0.1 s/d - 0.1	Nearly symmetrical	0.9 - 0.11	Mesokurtic
0.71-1.00	Moderately sorted	- 0.1 s/d - 0.3	Coarse skewed	1.11 - 1.5	Leptokurtic
1.00-2.00	Poorly sorted	- 0.3 s/d – 1	Strongly coarse skewed	1.5 - 3	Very leptokurtic
2.00-4.00	Very poorly sorted			> 3	More leptokurtic
>4.00	Extremely poorly sorted				

IV. RESULTS AND DISCUSSION

4.1 General analysis on baseline sediment grain percentage and sediment distribution

The clay type sediment has the smallest diameter and sedimentation rate compared to sand and silt. Based on the results of the study, it was found that the river bed sediment material was of rock, sand, silt, and clay. The percentages of the four types of sediment include rock 8% to 10%, sand 20% to 30%, silt 30% to 40% and clay 30% to 40%.

The average percentage of stone and sand for each section is more or less the same. Silt type sediment is the sediment that has the highest percentage compared to rock, sand, and clay types. It can be seen that the four types of sediment are scattered every 300 meters along the 1500 meters of the river. However, the percentage of scattered material is dissimilar, where the composition is rock 7%, sand 21.93%, silt 46.18% and clay 34.89%.

4.2 Sediment analysis based on soil texture class

The analysis of soil texture classes is classified using the USDA gradation concept using a soil classification pyramid. Based on the results of the study, there are two types of soil texture, namely dusty clay, and clayey clay dust. Table 4 shows the results of the soil texture. in the Binanga Aron River, is mostly sandy and silty rock. Unlike the others, points 2c, 4c, 5b, 4b, and 4a have dusty clayey clay textured soil. This is because at that point the percentage of stones, sand, clay is less than 30%, while the other points have a percentage of clay type material ranging from 30% to 40%. Of the 12 sampling points, the type of soil texture tends to be the same, namely dusty clay. The average percentage of sand for each section is approximately the same.

It was found that the silt type sediment is the highest percentage compared to sand and clay types. Those three types of sediment are scattered in every distance of every 300 meters along the 1500 meters of the Binaga Aron River. However, the material percentage is various, the silt was 30%, and clay and sand was 34%.

The sediment analysis based on class Analysis of soil texture class is classified using the USDA (United States Department of Agriculture) gradation concept, namely the USDA soil classification point 4a). From the results of the study, there are two types of soil texture, namely sandy sand and clay located in the Binanga Aron River, Samosir Regency. Unlike the other points, points 2c, 4c, 3b, 4b, and 4a have silty clay sand. This is because at that point the percentage is less than 30%, while the other points have a specific material percentage between 30% to 40%.

4.3 Sediment Statistical Analysis

Sediment statistical analysis was carried out to derive the sediment statistical classification as presented in Table 5. The value of the sampling sorting was dominated by the condition of the sediment in a less sorted state. It was said to be less unsorted because the grain size of the sediments was not uniform.

Based on the skewness value, the station has roughly skewness due to the most of dominant are fine and the sediment is deposited during low current conditions [6,7,8,11,12]. The strongly

skewness was resulted due to the fine grains fill the spaces among the large grains. Based on the results of sediment processing, a kurtosis value of 0.8 was also obtained, with the range categories are blunt to quite blunt. It can be concluded in 1 that the overall average value of sediment kurtosis of Binaga Aron River is 0.79 that was fell in the blunt category. Table 1 also shows that the results of the sediment statistical analysis (sorting, skewness, and kurtosis) tend to be uniform.

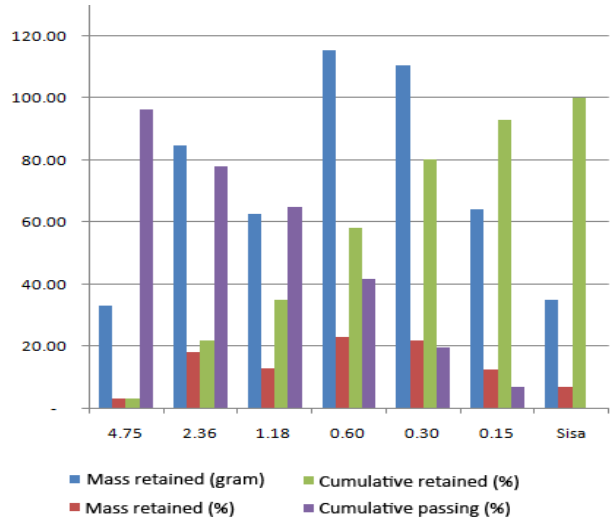

Figure 3: The percentage of basic sediment at the sampling point and the the type of soil texture

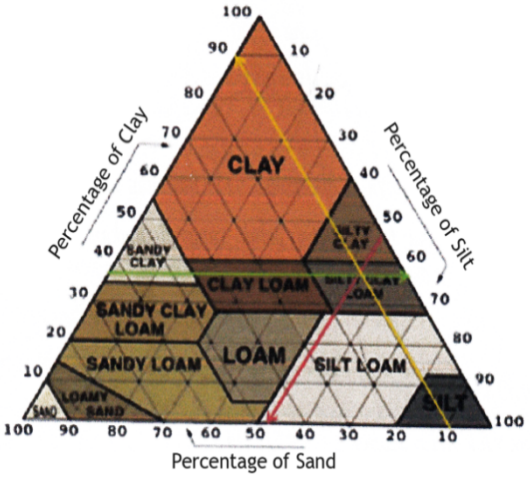

Figure 4: Soil classification

V. SEDIMENT STATISTICAL ANALYSIS

Based on sediment statistical classification, it was found that the sampling stations dominated by poorly sorted, because the size of the sediment grains was not uniform. Based on the skewness value, the average skewness was coarse because the sediment was more dominant in size and the sediment is deposited when the current conditions are low [1,2,5,6,8]. It is very coarse causing the fine grains to fill a large space based on the processing results. Sediment statistical data also obtained a kurtosis value between 0.7s.d 0.8 which is in the blunt to quite a blunt category. As shown in Table 10, it can be concluded that the overall average value of the sediment kurtosis value of the Binanga Aron River is 0.79. Moreover, the results of the sediment statistical analysis found that the sorting, skewness, and kurtosis tend to be uniform.

Based on the soil classification as shown in Figure 4, it was concluded that the residual samples are rocks due to retained on the filter. The 4.75 size filter is concluded as rocky sand, the filter size is 2.36 sand, the filter size 1.18 is called silt sand, the filter size 0.60 is called silt, the 0.30 size sieve is called silty clay and the 0.15 size sieve is called clay, below is the aggregate sieve analysis table obtained from the field, among others:

Table 2: Aggregate Sieve Analysis of Binaga Aron River 000 Meter Sample weight = 1000 grams

Sieve size (mm)	Mass retained (gram)	Mass retained (%)	Cumulative retained (%)	Cumulative Passing (%)
Sample I				
4.75	33.20	3.32	3.32	96.68
2.36	184.80	18.48	21.80	78.20
1.18	129.70	12.97	34.77	65.23
0.60	233.20	23.32	58.09	41.91
0.30	219.50	21.95	80.04	19.96
0.15	128.00	12.80	92.84	7.16
Residual	71.60	7.16	100.00	0.00

Total	1,000.00	100.00		
		MHB		
Sample II				
4.75	33.40	3.34	3.34	96.66
2.36	183.80	18.38	21.72	78.28
1.18	131.30	13.13	34.85	65.15
0.6	225.30	22.53	57.38	42.62
0.3	221.40	22.14	79.52	20.48
0.15	127.50	12.75	92.27	7.73
residual	77.30	7.73	100.00	0.00
Total	1,000.00	100.00		
		MHB		
Sample III				
4.75	33.20	3.32	3.32	96.68
2.36	184.80	18.48	21.80	78.20
1.18	129.70	12.97	34.77	65.23
0.60	233.20	23.32	58.09	41.91
0.30	219.50	21.95	80.04	19.96
0.15	128.00	12.80	92.84	7.16
Residual	71.60	7.16	100.00	0.00
Total	1,000.00	100.00		
		MHB		

** 1000 um (micro-meters) = 1 mm*

Table 3: Aggregate Sieve Analysis of Binaga Aron River 300 Meters Sample weight = 1000 gram

Sieve size (mm)	Mass retained (gram)	Mass retained (%)	Cumulative renained (%)	Cumulative Passing (%)
Sample I				
4.75	4.60	3.46	3.46	96.54
2.36	85.50	18.55	22.01	77.99
1.18	31.90	13.19	35.20	64.80
0.60	226.30	22.63	57.83	42.17
0.30	222.90	22.29	80.12	19.88
0.15	128.50	12.85	92.97	7.03
Residual	70.30	7.03	100.00	0.00
Total	1,000.00	100.00		
Sample II				
Sieve size (mm)	Mass retained (gram)	Mass retained (%)	Cumulative retained (%)	Cumulative Passing (%)
4.75	36.00	3.60	3.60	96.40
2.36	186.00	18.60	22.20	77.80
1.18	129.70	12.97	35.17	64.83
0.60	233.20	23.32	58.49	41.51
0.30	219.50	21.95	80.44	19.56
0.15	128.00	12.80	93.24	6.76
Residual	67.60	6.76	100.00	0.00
Total	1,000.00	100.00		
Sample III				

4.75	35.20	3.52	3.52	96.48
2.36	184.00	18.40	21.92	78.08
1.18	133.10	13.31	35.23	64.77
0.60	235.30	23.53	58.76	41.24
0.30	224.30	22.43	81.19	18.81
0.15	129.00	12.90	94.09	5.91
Residual	59.10	5.91	100.00	0.00
Total	1,000.00	100.00		

** 1000 um (micro-meters) = 1 mm*

Table 4: Aggregate Sieve Analysis of Binaga Aron River 600 Meters Sample weight = 1000 gram

Sieve size (mm)	Mass retained (gram)	Mass retained (%)	Cumulative retained (%)	Cumulative Passing (%)
Sample I				
4.75	33.00	3.30	3.30	96.70
2.36	183.00	18.30	21.60	78.40
1.18	129.70	12.97	34.57	65.43
0.60	233.20	23.32	57.89	42.11
0.30	219.50	21.95	79.84	20.16
0.15	128.00	12.80	92.64	7.36
Residual	73.60	7.36	100.00	0.00
Total	1,000.00	100.00		
Sampe II				
4.75	34.10	3.41	3.41	96.59
2.36	182.00	18.20	21.61	78.39
1.18	130.10	13.01	34.62	65.38
0.60	233.30	23.33	57.95	42.05
0.30	220.30	22.03	79.98	20.02
0.15	129.00	12.90	92.88	7.12
Residual	71.20	7.12	100.00	0.00
Total	1,000.00	100.00		
Sample III				
4.75	38.30	3.83	3.83	96.17
2.36	184.00	18.40	22.23	77.77
1.18	130.90	13.09	35.32	64.68
0.6	225.30	22.53	57.85	42.15
0.3	221.40	22.14	79.99	20.01
0.15	127.50	12.75	92.74	7.26
Residual	72.60	7.26	100.00	0.00
Total	1,000.00	100.00		

** 1000 um (micro-meters) = 1 mm*

Table 5: Aggregate Sieve Analysis of Binaga Aron River 900 Meters Sample weight = 1000 grams

Sieve size (mm)	Mass retained (gram)	Mass retained (%)	Cumulative retained (%)	Cumulative Passing (%)
Sample 1				
4.75	33.30	3.33	3.33	96.67
2.36	186.20	18.62	21.95	78.05
1.18	129.30	12.93	34.88	65.12
0.60	236.20	23.62	58.50	41.50
0.30	219.40	21.94	80.44	19.56
0.15	128.20	12.82	93.26	6.74
Residual	67.40	6.74	100.00	0.00
Total	1,000.00	100.00		
Sample II				
4.75	37.60	3.76	3.76	96.24
2.36	185.20	18.52	22.28	77.72
1.18	137.90	13.79	36.07	63.93
0.6	222.80	22.28	58.35	41.65
0.3	222.40	22.24	80.59	19.41
0.15	127.50	12.75	93.34	6.66
Residual	66.60	6.66	100.00	0.00
Total	1,000.00	100.00		
Sample III				
4.75	40.20	4.02	4.02	95.98
2.36	182.00	18.20	22.22	77.78
1.18	130.10	13.01	35.23	64.77
0.60	234.30	23.43	58.66	41.34
0.30	220.30	22.03	80.69	19.31
0.15	129.00	12.90	93.59	6.41
Residual	64.10	6.41	100.00	0.00
Total	1,000.00	100.00		

** 1000 um (micro-meters) = 1 mm*

Table 6: Aggregate Sieve Analysis of Binaga Aron River 1200 Meters Sample weight = 1000 grams

Sieve size (mm)	Mass retained (gram)	Mass retained (%)	Cumulative retained (%)	Cumulative Passing (%)
Sample I				
4.75	37.00	3.70	3.70	96.30
2.36	185.00	18.50	22.20	77.80
1.18	129.70	12.97	35.17	64.83
0.60	233.20	23.32	58.49	41.51
0.30	219.50	21.95	80.44	19.56
0.15	128.00	12.80	93.24	6.76
Residual	67.60	6.76	100.00	0.00
Total	1,000.00	100.00		
Sample II				
4.75	36.20	3.62	3.62	96.38
2.36	185.00	18.50	22.12	77.88

1.18	130.10	13.01	35.13	64.87
0.60	234.10	23.41	58.54	41.46
0.30	220.30	22.03	80.57	19.43
0.15	129.00	12.90	93.47	6.53
Residual	65.30	6.53	100.00	0.00
Total	1,000.00	100.00		
Sample III				
4.75	33.60	3.36	3.36	96.64
2.36	184.00	18.40	21.76	78.24
1.18	131.90	13.19	34.95	65.05
0.6	225.30	22.53	57.48	42.52
0.3	221.40	22.14	79.62	20.38
0.15	127.50	12.75	92.37	7.63
Residual	76.30	7.63	100.00	0.00
Total	1,000.00	100.00		
		MHB		

** 1000 um (micro-meters) = 1 mm*

Table 7: Aggregate Sieve Analysis of Binaga Aron River 1500 Meters Sample weight = 1000 gram

Sieve size (mm)	Mass retained (gram)	Mass retained (%)	Cumulative retained (%)	Cumulative Passing (%)
Sample I				
4.75	33.60	3.36	3.36	96.64
2.36	184.00	18.40	21.76	78.24
1.18	130.90	13.09	34.85	65.15
0.60	225.30	22.53	57.38	42.62
0.30	221.40	22.14	79.52	20.48
0.15	127.50	12.75	92.27	7.73
Residual	77.30	7.73	100.00	0.00
Total	1,000.00	100.00		
Sample II				
4.75	33.00	3.30	3.30	96.70
2.36	185.00	18.50	21.80	78.20
1.18	129.70	12.97	34.77	65.23
0.60	233.20	23.32	58.09	41.91
0.30	219.50	21.95	80.04	19.96
0.15	128.00	12.80	92.84	7.16
Residual	71.60	7.16	100.00	0.00
Total	1,000.00	100.00		
Sample III				
4.75	34.20	3.42	3.42	96.58
2.36	183.00	18.30	21.72	78.28
1.18	130.10	13.01	34.73	65.27
0.60	234.30	23.43	58.16	41.84
0.30	220.30	22.03	80.19	19.81
0.15	129.00	12.90	93.09	6.91
Residual	69.10	6.91	100.00	0.00
Total	1,000.00	100.00		

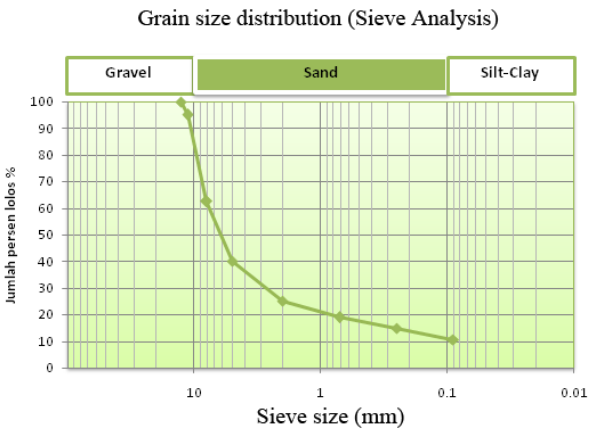

Grain size (mm)

Name of organization	Gravel	Sand	Silt	Clay
Massachusetts Institute of Technology (MIT)	>2	2 to 0.06	0.06 to 0.002	<0.002
U.S. Department of Agriculture (USDA)	>2	2 to 0.05	0.05 to 0.002	<0.002
American Association of State Highway and Transportation Officials (AASHTO)	76.2 to 2	2 to 0.075	0.075 to 0.002	<0.002
Unified Soil Classification System (U.S. Army Corps of Engineers, U.S. Bureau of Reclamation)	76.2 to 4.75	4.75 to 0.075	Fines (i.e., silts and clays) <0.075	

The average values of sieve sizes analysis is as follows:

Sieve size (mm)	Mass retained (gram)	Mass retained (%)	Cumulative retained (%)	Cumulative Passing (%)
4.75	33.32	3.50	3.50	96.50
2.36	84.82	18.43	21.93	78.07
1.18	62.66	13.09	35.02	64.98
0.60	115.47	23.09	58.11	41.89
0.30	110.36	22.07	80.18	19.82
0.15	64.09	12.82	93.00	7.00
Residual	35.01	7.00	100.00	-
Total	1,000.00	100.00		

** 1000 um (micro-meters) = 1 mm*

Standar Sieve Designation (ASTME 11)		Nominal Sieve Opening	
		mm	in
Coaurse Sieves			
Standard	Alternatif		
75.0 mm	3 in	75.00	3.000
63.0 mm	2-1/2 in	63.00	2.500
50.0 mm	2 in	50.00	2.000
37.5 mm	1-1/2 in	37.50	1.500
25.0 mm	1 in	25.00	1.000
19.0 mm	3/4 in	19.00	0.750
12.5 mm	1/2 in	12.50	0.500
9.5 mm	3/8 in	9.50	0.375
Fine Sieves			
4.75 mm	No. 4	4.750	0.1870
2.36 mm	No. 8	2.360	0.0937
1.18 mm	No. 16	1.180	0.0464
600 um*	No. 30	0.600	0.0234
300 um	No. 50	0.300	0.0117
150 um	No. 100	0.150	0.0059
Finest Sieve Normally used for aggregates			
75 um	No. 200	0.075	0.0029

Based on Table above, the classification of soils texture is ranging from clay to rock with the thickness as presented in Table4.

Table 8: Soil texture based on the percentage of sand, silt and clay in Binanga Aron River

Station/ Distance	Rock (%)	Sand (%)	Silt (%)	Clay (%)	Soil classification
1a	7,16	21.80	36,29	34.75	RSS
lb	7.73	21.72	35.66	34.89	RSS
lc	7.16	21.80	36.29	34.75	RSS
2a	7.03	22.01	35.82	35.14	RSS
2b	6.76	22.20	36.25	34.75	SSC
2c	5.91	21.92	36.84	35.33	SSC
3a	7.36	21.60	36.29	34.75	RSS
3b	7.12	21.61	36.34	34.93	RSS
3c	7.26	22.23	35.62	34.89	RSS
4a	6.74	21.95	36.55	34.76	SSC
4b	6.66	22.28	36.07	34.99	SSC
4c	6.41	22.22	36.44	34.93	SSC
5a	6.76	22.20	36.29	34.75	SSC
5b	6.53	22.12	36.42	34.93	SSC
5c	7.63	21.76	35.72	34.89	RSS
6a	7.73	21,76	35.62	34.89	RSS
6b	7.16	21.80	36.29	34.75	RSS
6c	6.91	21.72	36.44	34.93	RSS

Description: RSS = Rock Sand Silt; SSC = Sand Silt Clay

Table 9: Sediment classification based on the degree of sorting, skewness and kurtosis

Station/ Distance	Point	Sorting	Skewness	Kurtosis
0	1a	KT	FS	blunt
	1b	KT	CS	blunt
	1c	KT	SCS	blunt
300	2a	KT	SCS	blunt
	2b	KT	CS	blunt
	2c	KT	FS	blunt
600	3a	KT	SFS	blunt
	3b	KT	CS	blunt
	3c	KT	SCS	blunt
900	4a	KT	CS	blunt
	4b	KT	SCS	blunt
	4c	KT	CS	blunt
1200	5a	KT	SCS	blunt
	5b	KT	CS	blunt
	5c	KT	SCS	blunt
1500	6a	KT	CS	blunt
	6b	KT	SCS	blunt
	6c	KT	CS	blunt

Description: PS= Poorly sorted; CS= Coarse skewed; SCS= Strongly coarse skewed; FS= Fine skewed; SFS= Strongly fine skewed.

VI. CONCLUSION

The type of sedimentary materials found in Binanga Aron river is rock, sand, silt, and clay. The four types of material are scattered in a range of 300 meters along the 1500 meter of the sampling area, with a rock percentage of 7.0%. rocky sand 3.50%, sand 18.43%, sandy silt 23.09%, silt 22.07%, silty clay 22.07% and clay 12.82%. The average soil texture class of the Binanga Aron River is rock, sand, and dusty clay. Moreover, it was found that the sediment sorting value was classified as poorly sorted, while the slope of the sediment was categorized as strongly coarse to coarse skewness and sedimentary kurtosis tends to be blunt.

REFERENCES

1. Anonim, 2011, Laporan Model DAS Mikro Sungai Duri DAS Muntok SWPDAS Mancang, BPDAS Baturusa-Cerucuk, Pangkalpinang.
2. ASTM D 422, 2007, Standard Test Method for Particle-Size Analysis of Soils.
3. Anwas, M, 1994, Bentuk Muka Bumi,http://elcom.umy.ac. id/elschool /muallimin muhammadiyah/file.php/1/materi/Geografi/ Bentuk mukabumi. Pdf, diakses pada tanggal 20 April 2015.
4. Abdul Ghani. N.A.A., Othman. N., Baharudin. M.K.H, 2012, Study on Characteristics of Sediment and Sedimentation Rate at Sungai Lembing, Kuantan, Pahang, Precedia Engineering of Malaysian Technical Universities Conference on Engineering & Technology 2012, MUCET 2012 Part 3 -Civil and Chemical Engineering.
5. Dermina R.S Damanik, Novdin.M. Sianturi, Evaluasi Kegunaan Ilmu Teknik Sipil dan Manajemen Dalam Kebutuhan Air Bersih Pada Masyarakat Kabupaten Simalungun, Jurnal Ilmiah SP Stindo Protesional, Jilid 4, 2018, Hal 106-112.
6. Ira Modifa Tarigan, Novdin M Sianturi, Evaluasi Manajemen Debit Air Pada Skema Jaringan Irigasi Pada Daerah Irigasi Semangat Baris Kecamatan Siantar Kabupaten Simalungun, Jurnal Ilmiah SP Stindo Profesional, Jilid 4, 2018, Hal 104-112
7. Ikoniko YJ. Analisis Jenisdan Laju Angkutan Sedimen Dasar pada Sungai Sebalo di Kecamatan Bengka yang (Skripsi S1) Pontianak: Universitas Tanjungpura; 2011.
8. Kataresada Ketaren, Novdin M Sianturi,, 2017, Decision Making Modelling with Logistic Regression Approach, Internasional Journal of Applied Engineering Research 12 (19) (2017),pp9067-9073.
9. Purnawan, Syahrul., Setiawan, Ichsan., Marwantim, 2012, Studi sebaran sedimen berdasarkan ukuran butir di perairan Kuala Gigieng, Kabupaten Aceh Besar, Provinsi Aceh, Jurnal Depik Vol 1 Nomor 1, Hal31-36.
10. Sianturi, N. M., Kamarudin, M. K. A., Wahab, N. A., Mohd Saudi, A. S. (2019). The Hydraulic Modelling on Sediments Ponds in Binanga Aron River, North Sumatera Indonesia. *International Journal of Recent Technology and Engineering, 8*(2): 392-404.
11. Sianturi, N.M, Kamarudin, M. K. A., Toriman, M. E., Wahab, N. A., Hakparn, S., Lertbunchardwong, K., Potikengrith, T., Islam, M. S., Harith, H. (2018). Assessment of Environmental Management in Lake Toba, Samosir Regency, North Sumatera Province, Indonesia. *International Journal of Engineering & Technology, 7* (3.14): 337-343.
12. Sulvina. Analisis Kecepatan Anus dan Pola Angkutan Sedimen pada Pantai di Daerah Sungai Dua Kecamatan Sungai Kunyit Kabupaten Pontianak (Skripsi S1) Pontianak: Universitas Tanjungpura; 2009.
13. Purnawan, Syahrul., Setiawan, Ichsan., Marwantim, 2012, Studi sebaran sedimen berdasarkan ukuran butir di perairan Kuala Gigieng, Kabupaten Aceh Besar, Provinsi Aceh, Jurnal Depik Vol 1 Nomor 1, Hal31-36.
14. SNI 1964:2008, Cara Uji Berat Jenis Tanah, Badan Standarisasi Nasional.
15. Sya'rani L, H. Penentuan Sumber Sedimen Dasar Perairan Berdasarkan Analisis Minerologi dan Kandungan Karbonat. Ilmu Kelautan. 2006; 3(1).
16. Yanti D. Panduan Praktikum Teknik Konservasi Tanah dan Air Padang: Universitas Andalas; 2016.
17. NM Sianturi, Kajian Terhadap Sistem Drainase Jalan Merdeka Dan HOS

Cokroaminoto Kecamatan Siantar Utara Pematangsiantar, Jurnal Teknik Sipil Volume 9 Nomor 2, Oktober 2013 : 85-171
18. NM Sianturi, Deardo Saragih, Evaluasi Pembangunan Ringroad Pangururan-Tomok STA 32.000 s/d STA 38.000 Di Kabupaten Samosir, Jurnal Santeksipil, Vol. I No. 1, April 2020 : Hal 54-67.

London Journal Press Membership

For Authors, subscribers, Boards and organizations

London Journals Press membership is an elite community of scholars, researchers, scientists, professionals and institutions associated with all the major disciplines. London Journals Press memberships are for individuals, research institutions, and universities. Authors, subscribers, Editorial Board members, Advisory Board members, and organizations are all part of member network.

Read more and apply for membership here:
https://journalspress.com/journals/membership

For Authors

Author Membership provide access to scientific innovation, next generation tools, access to conferences/seminars /symposiums/webinars, networking opportunities, and privileged benefits.
Authors may submit research manuscript or paper without being an existing member of LJP. Once a non-member author submits a research paper he/she becomes a part of "Provisional Author Membership".

For Institutions

Society flourish when two institutions come together." Organizations, research institutes, and universities can join LJP Subscription membership or privileged "Fellow Membership" membership facilitating researchers to publish their work with us, become peer reviewers and join us on Advisory Board.

For Subscribers

Subscribe to distinguished STM (scientific, technical, and medical) publisher. Subscription membership is available for individuals universities and institutions (print & online). Subscribers can access journals from our libraries, published in different formats like Printed Hardcopy, Interactive PDFs, EPUBs, eBooks, indexable documents and the author managed dynamic live web page articles, LaTeX, PDFs etc.

GO GREEN AND HELP
SAVE THE ENVIRONMENT

JOURNAL AVAILABLE IN

PRINTED VERSION, INTERACTIVE PDFS, EPUBS, EBOOKS, INDEXABLE DOCUMENTS AND THE AUTHOR MANAGED DYNAMIC LIVE WEB PAGE ARTICLES, LATEX, PDFS, RESTRUCTURED TEXT, TEXTILE, HTML, DOCBOOK, MEDIAWIKI MARKUP, TWIKI MARKUP, OPML, EMACS ORG-MODE & OTHER

SCAN TO KNOW MORE

support@journalspress.com
www.journalspress.com

*THIS JOURNAL SUPPORT AUGMENTED REALITY APPS AND SOFTWARES